O'Brien, P.E., Cooper, A.K., Richter, C., et al., 2001
Proceedings of the Ocean Drilling Program, Initial Reports Volume 188

1. Leg 188 Summary: Prydz Bay–Cooperation Sea, Antarctica[1]

Shipboard Scientific Party[2]

ABSTRACT

Ocean Drilling Program (ODP) Leg 188 was drilled based on one of five linked proposals to decipher the Cenozoic glacial history and paleoenvironments of Antarctica by drilling transects across the continental margin in five different regions. ODP Leg 178 (Antarctic Peninsula) was the first such proposal to be drilled. Three sites were drilled during Leg 188, with one each on the Prydz Bay continental shelf, slope, and rise. These sites document the paleoenvironments for select periods during Cenozoic and older times as Antarctica transformed from a temperate to a polar setting. The sites provide records of the transition from East Antarctic preglacial to glacial conditions on the shelf (Site 1166); the variability of ice sheet extent, sediment source areas, and glaciomarine depositional processes during latest Neogene glacial–interglacial periods on the slope (Site 1167); and the long-term lower to upper Miocene transition from a temperate climate to cold-climate glaciation, with superimposed short-term glacier fluctuations since early Miocene time (Site 1165).

INTRODUCTION

The Antarctic Ice Sheet and the surrounding ocean are key components in the global climate regime from the early Cenozoic to the present. The steep latitudinal climatic gradient generates the vigorous atmospheric and oceanic circulation of the Southern Hemisphere. Antarctic sea ice formation promotes bottom-water formation, which ventilates and provides nutrients to much of the world's oceans and acts as a major sink for atmospheric carbon dioxide. The ice sheet is also the

[1] Examples of how to reference the whole or part of this volume.
[2] Shipboard Scientific Party addresses.

Ms 188IR-101

most likely governor of rapid eustatic sea-level change (Barrett, 1999). As part of the effort to understand the mechanics of Antarctic climate and its likely response to change, the Scientific Committee for Antarctic Research (SCAR) Working Groups on Geology and Solid Earth Geophysics have supported the Antarctic Offshore Stratigraphy Project (ANTOSTRAT), which has developed a series of Ocean Drilling Program (ODP) proposals for drilling on the Antarctic margin.

Because of its long history of sedimentation, Prydz Bay was seen as a place to investigate the long-term record of Antarctic glaciation. The size of the Lambert Glacier–Amery Ice Shelf system that enters the bay in relation to the total drainage from East Antarctica (~20%) makes it a potential indicator of processes operating in the East Antarctic interior. It complements other ANTOSTRAT-identified regions that record fast-responding coastal ice centers (Antarctic Peninsula), the West Antarctic Ice Sheet (Ross Sea), and coastal East Antarctica (Wilkes Land) (Barker et al., 1998). Leg 188 was designed to build on the results of Leg 119 by investigating the history of the Lambert-Amery system during key periods of the Cenozoic. In particular, the proposal aimed at dating the earliest arrival of glacier ice on the shelf, documenting the number and timing of late Neogene expansions of ice to the shelf edge, and extracting a climate record from the interbedding of continent-derived siliciclastics and marine biogenic sediments on the continental rise.

Investigations of Antarctic Cenozoic Climate History

Antarctic climate history has largely been deduced from oceanic proxy records, from fragmentary onshore outcrops, and from several drilling campaigns around the margin. Modeling of ice sheet development has been used to extend this patchy record and to provide a guide for further work, but it needs continual calibration with the geological record.

Common proxy records from marine sediments include eustatic sea level curves, oxygen isotope ($\delta^{18}O$) stratigraphy, and ice-rafted debris (IRD) records. Sea-level curves are probably the most controversial; some workers claim a record of ice expansion extending back to the Mesozoic (Miller et al., 1999), whereas others doubt the validity of global correlation based on eustacy because of regional tectonic influences and a lack of precision in correlation (e.g., Miall, 1986). Short-term global eustatic changes during the Pleistocene are generally recognized as driven by ice volume changes, but the role of the Antarctic Ice Sheet, even for the Pleistocene, is not clear. The initial assumption that Antarctica ice extended to the shelf edge during the last glacial maximum (LGM) (Denton and Hughes, 1981) and was used in modeling postglacial sea-level rise has been shown to be inaccurate in the Ross Sea (Licht et al., 1996), some coastal oases (Goodwin, 1992), and Prydz Bay (Domack et al., 1998).

IRD indicates the presence of floating debris-charged icebergs or sea ice at a particular site, but its interpretation in terms of climate and glacial history is extremely complex due to the many poorly understood factors influencing the discharge and dispersal of debris-rich icebergs. IRD records can set a minimum age for the arrival of calving glaciers at the coast and the increase of icebergs associated with climatic cooling.

Oxygen isotope variations are the only measurements of global ice volume that are relatively continuous for the Cenozoic, with curves

published and interpreted back to the Paleocene (e.g., Abreu and Anderson, 1998; Flower, 1999). Some researchers have used isotope curves to argue for the onset of glaciation in Antarctica as early as the Paleocene (Denton et al., 1991), whereas others argue for glacial onset in the early to middle Eocene (Abreu and Anderson, 1998). Major ice expansions have been inferred at 33.6 Ma (Eocene/Oligocene boundary), 23.7 Ma (Oligocene–Miocene), 12 to 16 Ma (middle Miocene), and 2.7 Ma (late Pliocene), which marked the onset of Northern Hemisphere glaciation (Flower, 1999). For all the value of $\delta^{18}O$ curves, they are a function of both temperature and global ice volume, making for ambiguity in the detailed interpretation of the record (Wise et al., 1992; Barker et al., 1998). Also, oxygen isotope curves record global ice volume and therefore cannot provide information on the distribution of ice between the hemispheres during periods of bipolar glaciation. Neither can they indicate the distribution and interplay of ice and ocean around different parts of Antarctica, information necessary for calibrating models of glaciation.

Deposits and landforms on the Antarctic continent provide a direct window into Antarctic climate history that can be very detailed (e.g., Quilty, 1991) but, by their nature, are fragmentary and difficult to correlate. Difficulties in the correlation of sediments in the Transantarctic Mountains have led to disagreements over the extent of ice retreat during the Pliocene (Webb et al., 1984; Denton et al., 1991; Warnke et al., 1996). However, outcrops and landforms also indicate the possible complexities of responses by ice to climate change, with out-of-phase expansion of valley glaciers and the ice sheets first reported by Scott (1905).

Drilling of continental shelf sediments can provide a record of ice expansion onto the shelf and the evolution of shelf environments but must be considered in the light of both (1) facies depositional models and (2) sequence stratigraphic models of facies stacking patterns and preservation (Fielding et al., 1998). Such concepts need to be applied to drilling of sections on the continental shelf and slope because of the strongly reciprocal nature of glacial–interglacial sedimentation on continental margins (Boulton, 1990). During major ice advances, the shelf tends to be eroded followed by the deposition of compact till, a difficult stratigraphic record to sample and interpret (Barron et al., 1991). At the same time, significant deposits are forming on the upper slope in trough mouth fans (Vorren and Laberg, 1997) or sediment is deposited on the continental rise as turbidites or contourite drifts (Rebesco et al., 1997).

A more complete picture of glacial history requires the linking of onshore outcrop data to the deep-sea record via the drilling of key locations on the Antarctic shelf, slope, and rise. Leg 188 was designed to provide such a transect, building on the work of Leg 119 (Barron, Larsen, et al., 1991) and linking studies of Cenozoic glacial sediments in the Prince Charles Mountains (Hambrey and McKelvey, 2000) and around Prydz Bay (Quilty, 1991) to the oceanic record. Linking these data sources provides a transect extending ~1000 km from the interior of East Antarctica to the continental rise along a single ice drainage system.

Aims of the Leg

Onset of Glaciation

Prydz Bay is at the downstream end of a drainage system that rises in the Gamburtsev Mountains in central East Antarctica (Fig. F1). Modeling studies of ice sheet development indicate that these mountains, if present in the Paleogene, would be the first area to develop extensive ice cover (Huybrechts, 1993). Thus, Prydz Bay could contain the first sedimentary evidence of ice in East Antarctica. Evidence on the early development of the Antarctic Ice Sheet has been interpreted as indicating initiation of ice sheet growth from as early as the early middle Eocene to the early Oligocene (Abreu and Anderson, 1998; Barron et al., 1991). As yet, there has been no section drilled in the Antarctic that clearly spans the complete transition from preglacial to glacial conditions. ODP Site 742 in eastern Prydz Bay reached glacial deposits interpreted by Barron et al. (1991) to be late middle Eocene in age. Cooper et al. (1991a) estimated that these sediments continued for 100 m below the total depth of Site 742 and rested on an erosion surface overlying older sediments. A hole drilled through this lower 100 m as well as the underlying sediments could establish the lower age limit for large-scale glaciation of Prydz Bay and potentially provide paleontological and sedimentological evidence of the preglacial environment.

F1. Lambert Glacier drainage basin, p. 29.

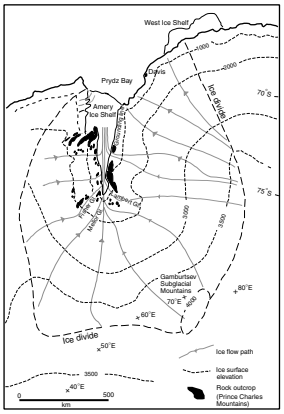

Major Events

Oxygen isotope records have been used to infer episodes of increased ice volume at 33.6 Ma, (Eocene/Oligocene boundary), 23.7 Ma (Oligocene/Miocene boundary), 12 to 16 Ma (middle Miocene), and 2.7 Ma (late Pliocene), the latter marking the onset of Northern Hemisphere glaciation (Flower, 1999). In Prydz Bay, an unconformity identified during Leg 119 (Solheim et al., 1991) may have resulted from major ice expansion during the late Miocene (Barron et al., 1991). Kuvaas and Leitchenkov (1992) studied the seismic facies of the Prydz Bay continental rise and slope and identified the initiation of drift sedimentation. They suggested that drift sedimentation could be related to the initiation of the Antarctic Circumpolar Current (ACC) after the opening of Drake Passage around the Oligocene/Miocene boundary or related to major ice expansion during the Oligocene or Miocene. A hole drilled on the continental rise to intersect the base of the thick drift section could date the onset of drift formation and potentially record changes in continental rise sedimentation controlled by currents and continental sediment supply. The drift sediments should also contain a record of climate fluctuations, reflected in the interplay of continentally derived siliciclastic sediments fed by the Lambert Glacier drainage system and authigenic biogenic sedimentation.

F2. Model of trough mouth fan deposition, p. 30.

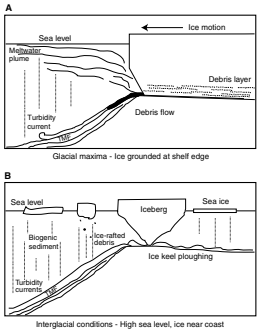

Late Neogene Fluctuations

A major change in Prydz Bay shelf progradation took place in the late Miocene to mid-Pliocene when a fast-flowing ice stream developed and excavated a channel across the shelf on the western side of Prydz Bay (O'Brien and Harris, 1996). Basal debris carried to the shelf edge was then deposited in a trough mouth fan on the upper slope (Fig. F2). This trough mouth fan may contain a reasonably complete record of glacial history because it received siliciclastic sediment when the shelf eroded

during major ice advances and hemipelagic material during interglacials and smaller glaciations (Vorren and Laberg, 1997). An Antarctic history of major ice advances is only just developing (e.g., ODP Leg 178; Barker et al., 1999; Cape Roberts Science Team, 1998, 1999, in press) and, at present, relies on outcrop studies that have poor time control (Denton et al., 1991) and seismic stratigraphic studies in which erosion surfaces are identified but the associated sediments have been sparsely sampled (e.g., Alonso et al., 1992). Identification of LGM grounding lines well in from the shelf edge in the Ross Sea (Licht et al., 1996) and Prydz Bay (Domack et al., 1998) reveals that glacial episodes can vary markedly in intensity. A section drilled through the Prydz Channel Fan will record the episodes that did produce a major advance and so provide insight into the mechanisms of ice sheet growth through multiple glacial cycles.

REGIONAL SETTING OF PRYDZ BAY

Bathymetry

Prydz Bay is an embayment along the Antarctic margin between 66°E and 79°E. It is bounded on the southwestern side by the Amery Ice Shelf, on the southeast by the Ingrid Christensen Coast, and by Mac. Robertson Land to the west, ending in Cape Darnley (Fig. F3). The eastern side of the bay has water depths from 200 to 300 m near the shelf edge forming Four Ladies Bank (Fig. F3). The bank surface slopes gently inshore and to the west. Along the Ingrid Christensen Coast, water depths reach 1000 m in the Svenner Channel. In front of the Amery Ice Shelf, the Amery Depression is mostly 600–700 m deep but reaches 1400 m in several closed depressions in the southwestern corner of the bay (the Lambert and Nanok Deeps) (Fig. F3). The western side of the bay is crossed by Prydz Channel, which runs from the Amery Depression to the shelf edge at 600 m below sea level. Prydz Channel separates Four Ladies Bank from Fram Bank, the shallow area around Cape Darnley (Fig. F3).

The steep continental slope on the eastern half of Prydz Bay is cut by submarine canyon tributaries and is overlain by slump deposits (O'Brien and Leitchenkov, 1997). On the western side of Prydz Bay, contours bulge seaward in the Prydz Channel Fan (Fig. F3), which slopes smoothly from the shelf edge to ~2700 m water depth. The head of Wilkins Canyon (Vanney and Johnson, 1985) is situated just west of Prydz Channel Fan and north of Fram Bank (Fig. F3). Wilkins Canyon runs north from the shelf edge before swinging northeast at ~65°S. To the west of Wilkins Canyon is a ridge of drift sediment separating it from Wild Canyon, which has its head on the continental slope off Mac. Robertson Land (Kuvaas and Leitchenkov, 1992).

Circulation in Prydz Bay

Surface circulation in Prydz Bay is characterized by a closed cyclonic gyre adjacent to the Amery Ice Shelf (Fig. F4) (Smith et al., 1984; Wong, 1994). There is inflow of cold water from the east near the West Ice Shelf and outflow near Cape Darnley. In contrast to the Ross and Weddell Sea basins, Prydz Bay holds a relatively small volume of highly saline deep water. It has been suggested that this is related to the geography and bathymetry of Prydz Bay (Smith et al., 1984). Because of

F3. Bathymetric features of and ODP sites in Prydz Bay, p. 31.

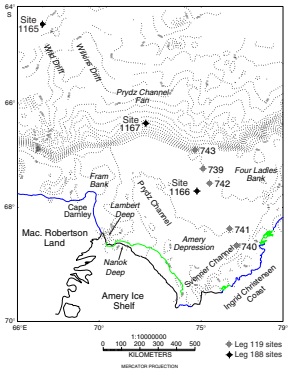

F4. Generalized map of circulation in the Prydz Bay region, p. 32.

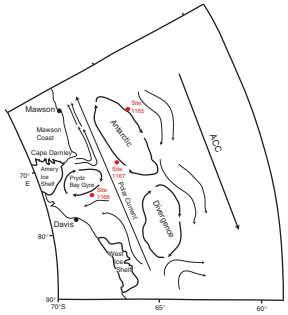

its closed circulation and lack of significant bottom-water production, water masses in Prydz Bay play a limited role in current activity beyond the shelf.

Circulation on the Continental Rise

Kuvaas and Leitchenkov (1992) interpret the deposits on the continental rise offshore from Prydz Bay to be the result of contour-current activity. These currents can be attributed to the activity of large Antarctic deep-water masses. Site 1165 is located within or near a large cyclonic gyre, known as the Antarctic Divergence (AD), between 60°E and 100°E (Fig. F4). Here, the eastward-moving ACC, driven by the prevailing westerlies, meets the westward moving Polar Current (PC). A study of deep-water circulation showed eastward flow north of 63°S and a band of westward-flowing water between the AD and the continental rise (Smith et al., 1984). Because of the proximity to the AD, sedimentation in this region may, at various times, have been subject to transportation via the ACC or PC, or it may have circulated around the region in accordance with the gyre. The position of the AD may be a key control on the nature of sedimentation at this site.

Glaciology

The major glacial drainage system in the region is the Lambert Glacier–Amery Ice Shelf system. The catchment is ~1.09 million km^2, representing ~20% of the East Antarctic Ice Sheet (Fig. F1) (Allison, 1979). The three largest glaciers are the Lambert, Fisher, and Mellor Glaciers that amalgamate in the southern Prince Charles Mountains to form the main Lambert-Amery ice stream (Fig. F1). They are joined by other glaciers of which the Charybdis Glacier, flowing from the western side of the Prince Charles Mountains (Fig. F1), is the largest. Most glaciers flowing into the Lambert-Amery system originate more than 200 km from the present coast, although a few small glaciers join the Amery Ice Shelf from the western side nearer the coast.

The ice-shelf grounding zone was thought to be a sinuous line running approximately east–west; however, more recent Global Positioning System and satellite image analysis has shown it to be in the southern Prince Charles Mountains, ~500 km upstream from the present seaward edge of the Amery Ice Shelf (Fig. F1). The ice reaches thicknesses of 2500 m in the Southern Prince Charles Mountains. This thins to ~400 m at the seaward edge of the Amery Ice Shelf, of which ~40% is snow that accumulates on the ice shelf and seawater ice that freezes onto the base (Budd et al., 1982).

Maximum ice velocities of 231–347 m/yr have been measured in the Prince Charles Mountains, whereas velocities up to 1200 m/yr have been measured for the centerline of the Amery Ice Shelf (Budd et al., 1982). The seaward edge of the Amery Ice Shelf is presently moving northward, but this is the result of spreading under its own weight rather than advance caused by an increase in mass balance (Budd, 1966). This spreading produces a major iceberg calving event every ~50 years, the last in 1963 (Budd, 1966).

The other source of glacial ice flowing into Prydz Bay is the Ingrid Christensen Coast, where ice cliffs and numerous relatively small glaciers enter the bay. The largest of these are the Sorsedal Glacier that flows south of the Vestfold Hills and the glaciers that contribute to the Publication Ice Shelf. The Svenner Channel consists of a series of swales

seaward of these larger glaciers, suggesting that the swales formed at the glaciers' confluence with the Lambert Glacier during periods when grounded ice filled the bay (O'Brien and Harris, 1996). The western side of Prydz Bay has only a few small glaciers that flow into the Amery Ice Shelf. The coast between the ice shelf and Cape Darnley provides only a small amount of ice because the ice divide is close to the coast.

GEOLOGY

Structure

Prydz Bay is an embayment in the East Antarctic margin caused by a major crustal structure, called the Lambert Graben, that extends 700 km inland (Fig. F5) (Federov et al., 1982; Stagg, 1985; Cooper et al., 1991a). Mapping of marine seismic data indicates that the outer part of the bay is underlain by a basin (named the Prydz Bay Basin by Stagg [1985]) that is separate from the Lambert Graben (Fig. F6). Gravity, magnetic, and seismic refraction data indicate maximum sediment thicknesses between 5 and 12 km (Cooper et al., 1991a). The Prydz Bay Basin is separated from the sediment underlying the outer shelf, slope, and rise by a northeast-plunging basement ridge that extends from the southwestern corner of Prydz Bay (Fig. F6). The ridge and basin sediments are extensively faulted with most faults in the southwest being normal down-to-basin faults. The northern end of the ridge is cut by east-west normal faults with large down-to-north displacement that may have formed as part of continental rifting process.

F5. Pre-Mesozoic geology of the Lambert Glacier drainage basin, p. 33.

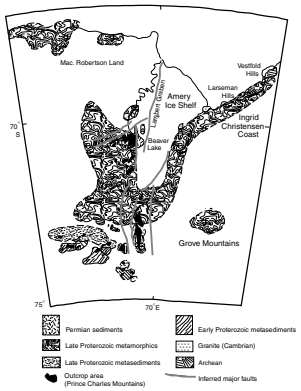

Prince Charles Mountains

Basement

The basement through which the Lambert Glacier and its tributaries flow is extensively exposed in the Prince Charles Mountains. Tingey (1991) distinguishes between the high-grade metamorphic rocks of the northern Prince Charles Mountains and the lower grade rocks of the southern Prince Charles Mountains. The northern Prince Charles Mountains consist largely of layered and massive granulite to upper amphibolite facies intruded by charnokite plutons, granite and pegmatite veins, and alkaline igneous dykes. Metapelites, marbles, skarns, metabasalts, metandesites, and metagabbros are all present (Tingey, 1991). The southern Prince Charles Mountains have Archean granitic orthogneiss basement overlain by Archean quartzites that are intruded by pegmatites and tholeiitic dykes. These Archean rocks are overlain by Proterozoic greenschist facies metasediments, including conglomerates, sandstone, schists, and phyllites that are intruded by Cambrian granite. Basement rocks in the Beaver Lake area are intruded by basic dykes, including some lamproites (Tingey, 1982).

F6. Structure contour map of the top of basement in Prydz Bay, p. 35.

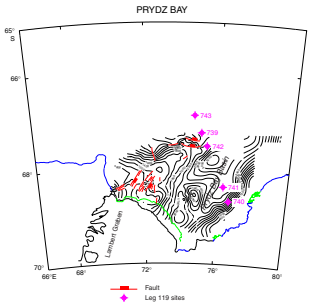

Phanerozoic Sediments

Geophysical data indicate that the Lambert Graben and Prydz Bay Basin contain several kilometers of sediment (Federov et al., 1982). The only outcrops are found at Beaver Lake in the northern Prince Charles Mountains, where a 270-m-thick section of coal-bearing, nonmarine sediment is exposed (Fig. F5) (McLoughlan and Drinnan, 1997). The

Amery Group is late Permian to Triassic in age (McLoughlan and Drinnan, 1997) and occupies a small fault angle depression on the western side of the Lambert Graben. These sediments are also thought to occur within the Lambert Graben.

Cenozoic sediments are present in the Prince Charles Mountains. In the northern Prince Charles Mountains at Beaver Lake, some 800 m of diamictons and minor mudstone and sandstone is exposed in Pagodroma Gorge. Hambrey and McKelvey (2000) interpret these deposits, the Pagodroma Group, as glaciomarine fjord infillings that include in situ mollusks and reworked diatoms that suggest middle Miocene, late Pliocene, and early Pleistocene ages (<3.5 Ma) (McKelvey and Stephenson, 1990; Quilty, 1993; Hambrey and McKelvey, 2000). Diamictites are also known from Fisher Massif and other parts of the Prince Charles Mountains at higher elevations than the Pagodroma Group. They are possibly of Miocene age (Hambrey and McKelvey, 2000).

Prydz Bay

Basement

Coastal outcrops along the eastern side of Prydz Bay comprise high-grade Archean and Proterozoic metamorphic rocks. In the Larseman Hills, 60% of the basement consists of medium- to coarse-grained garnet-bearing gneiss and 10% a distinctive blue gneiss rich in cordierite (Tingey, 1991). Smaller outcrops of Proterozoic gneisses and Cambrian granites are scattered along the eastern coast south of the largest area of outcrop in the Vestfold Hills. The basement of the Vestfold Hills is mostly Archean gneisses, including metagabbros and pyroxenites cut by several generations of Proterozoic mafic dykes (Tingey, 1991).

Pre-Cenozoic Sediments

Pre-Cenozoic sediments are known from ODP Sites 740 and 741 (Fig. F7). Two sequences are present: a lower red bed unit and an upper coal-bearing sequence of Aptian age (Turner, 1991; Turner and Padley, 1991).

The red bed sequence consists of sandstone interbedded with claystone and siltstone that may reach a thickness of 2–3 km in the center of the Prydz Bay Basin. The sediments are brown red to green gray in color. Sandstone units are as thick as 3 m and are medium to coarse grained, fining up to siltstone and claystone. Turner (1991) describes the sediments as quartzose with 17% to 66% clay matrix. The matrix is a mixture of chlorite, sericite, biotite, and muscovite. X-ray diffraction (XRD) indicates the presence of illite-smectite and kaolinite in the clay fraction. The red-colored beds contain abundant iron oxide in the matrix; green units are richer in chlorite. Framework grains are predominantly quartz with 6% rock fragments mostly composed of rounded granite gneiss grains made up of quartz, muscovite, chlorite, and feldspar. Feldspars are mostly orthoclase and microcline with very little plagioclase. Turner (1991) interprets the sediments as deposits of floodplains in an actively subsiding basin where rapid uplift, erosion, and deposition preserved their immature composition.

The upper sequence of pre-Cenozoic sediments in the Prydz Bay Basin is composed of mid-Aptian sandstone, siltstone, claystone, and minor conglomerate and coal (Turner and Padley, 1991). Sandstone units are 2–3 m thick and white to gray colored with cross-bedding and thin conglomerates at their base and abundant plant fragments scattered

F7. Top of the Lower Cretaceous structure contour map, p. 36.

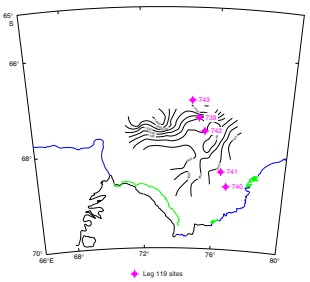

throughout. Sand grains are predominantly quartz and feldspar with garnet, biotite, and illmenite accessory minerals. Siltstones and claystones are rich in plant fragments with some ripple cross-laminations, and rootlets beds. They form coarsening upward sequences suggesting deposition in crevasse splay deposits in swampy, vegetated floodplains. Sandstone units were probably deposited in low-sinuosity fluvial channels. There is no evidence for marine deposition. The presence of coal and abundant plant debris suggests a humid climate (Turner and Padley, 1991).

Cenozoic Outcrops

Cenozoic sediments are exposed in several small areas along the east coast of Prydz Bay (Quilty, 1993). The Larseman Hills feature a thin, shallow marine sand containing shell fragments, Pliocene foraminifers, and diatoms that suggest an age of 2 to 3 Ma (Quilty, 1993). Of greater extent and significance are the Pliocene sediments of Marine Plain in the Vestfold Hills (Pickard, 1986; Quilty, 1993). They occupy an area of ~10 km² and reach thicknesses of 8–9 m. The sediment is diatomite, siltstone, and fine sandstone with sponge spicules, bivalves, and a diverse fauna of benthic organisms preserved in places (Quilty, 1993). The most spectacular fossils in the area are Cetacean skeletons, including dolphins and a right whale. Diatom assemblages suggest deposition shallower than 75 m below sea level between 4.2 and 3.5 Ma (Quilty, 1993). The faunas and preliminary isotope measurements led Quilty (1993) to infer warmer conditions during deposition than currently prevail. Water temperatures may have been as high as 5°C (Quilty, 1993).

Mac. Robertson Shelf

The area immediately to the south of Site 1165 is the Mac. Robertson Land Shelf, which may also have contributed to sedimentation on the continental rise. The Mac. Robertson Shelf is a narrow, rugged shelf west of Prydz Bay that is currently being eroded by iceberg scour and geostrophic currents (Harris and O'Brien, 1996). During the Pleistocene, coastal glaciers excavated U-shaped valleys to the shelf edge (Harris et al., 1996). The inner shelf is underlain by Precambrian metamorphics and half grabens containing Mesozoic sediments (Truswell et al., 1999). The outer shelf is underlain by offlapping sediments ranging from Cretaceous to Paleogene as indicated by reworked microfossils (Truswell et al., 1999; Quilty et al., 2000). Quilty et al. (2000) described Eocene and Oligocene foraminifers along with glauconite within surficial sediments on the shelf.

SEDIMENTATION IN PRYDZ BAY

Cenozoic

The Cenozoic sediments of Prydz Bay are extensively described in results from ODP Leg 119 (Barron, Larson, et al., 1989, 1991). Hambrey et al. (1991) recognized three major sequences composed chiefly of diamictites (Fig. F8). The upper sequence (PS.1 of Cooper et al., 1991a) is up to 250 m thick and flat lying (thickest under Four Ladies Bank) but thin to absent beneath Prydz Channel, Svenner Channel, and the Amery Depression. The second sequence lies unconformably beneath the upper

F8. Sketch of seismic sequences drilled during Leg 119, p. 37.

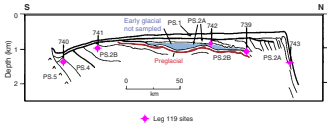

one at Sites 739 and 742 and consists of steeply prograding foresets of massive and stratified diamictite with some evidence of slumping (Fig. **F8**) (PS.2A of Cooper at al., 1991a). The lowermost sequence is a gently inclined massive clast-poor diamictite and bedded diamictite and poorly sorted mudstone. This sequence is richer in kaolinite than the overlying units. The lowermost sequence was dated as middle Eocene to early Oligocene; the upper sequence at Sites 739 and 742 was dated as late Miocene, Pliocene, and Pleistocene. Holocene siliceous muddy ooze overlies the diamictite in places (Domack et al., 1991).

Hambrey et al. (1991) interpret the massive diamictites as mostly water-lain till formed by rainout from the base of glacial ice close to the grounding zone. They interpret some intervals with deformed bedding, particularly in the dipping foreset units, as debris flows formed from glacial sedimentation with minor amounts of remobilized turbidites and ice-rafted sediment. Hambrey et al. (1991) describe some massive units with preferred orientation of clasts as possible subglacial till units, an interpretation supported by evidence of overcompaction of some intervals in the upper, flat-lying sequence (Solheim et al., 1991).

Hambrey et al. (1991) interpret the succession along the Leg 119 transect as indicating a history of earliest glaciation of the shelf in the Eocene to early Oligocene, reworking preglacial Eocene sediments, and depositing the lower, gently dipping sediments on the shelf. The ice then moved onto the shelf as a floating tongue and prograded the shelf edge in the early Oligocene. Hambrey et al. (1991) speculate that the largest pre-Quaternary expansion occurred during the late Oligocene to early Miocene based on a major erosion surface between early Oligocene and late Miocene rocks.

Seismic data through the Leg 119 drill sites indicate that the flat-lying upper sequences pass seaward into foreset beds that prograde the continental shelf edge (Fig. **F8**) (Cooper et al., 1991a, 1991b). Farther west where Prydz Channel crosses the shelf, the topsets are thin to absent and deposition has been concentrated on the upper slope in a trough mouth fan called the Prydz Channel Fan (Fig. **F9**). Landward of Four Ladies Bank, the topsets pinch out and the Amery Depression is covered with a thin layer of till and glaciomarine clayey silts and sands and siliceous muddy ooze overlying Cretaceous and older sediments. Leitchenkov et al. (1994) suggested that the shelf prograded more or less evenly across the bay until the late Miocene or Pliocene. A mappable erosion surface (PP12, Surface A of Mizukoshi et al., 1986) marks the development of Prydz Channel and the start of Prydz Channel Fan sedimentation at this time. The fan has been the major depocenter since then although Four Ladies Bank has continued to receive topsets of till (Fig. **F9**).

The Prydz Bay continental slope and rise are underlain by thick (>6000 m) drift sediments, some in elongated ridges aligned along the margins of deep channels, others having no clear correlation with channels. All of the drifts elongate approximately orthogonal to the continental margin (Kuvaas and Leitchenkov, 1992). The seismic geometry of these drifts suggests that they have been deposited as a result of the interaction of downslope mass flow and strong bottom (contour) currents. By analogy with other drift deposits on the Antarctic margin (Rebesco et al., 1997; Shipboard Scientific Party, 1999), the drifts are composed of alternating clastic- and biogenic-rich intervals that reflect alternations of glacial and interglacial conditions. Such records can be compared to proximal records from the continental shelf and upper

F9. Isopach map of postsurface PP12 sediments, p. 38.

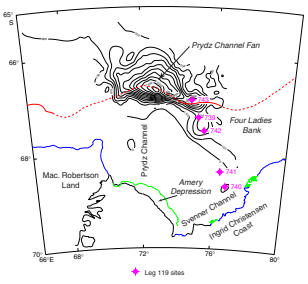

slope to understand the relationship between oceanographic conditions and the advance and retreat of the ice sheet.

The most conspicuous sediment drifts are developed in the western part of the Cooperation Sea between Wilkins and Wild Canyons and are referred to as the Wilkins and Wild Drifts (Fig. F3). Kuvaas and Leitchenkov (1992) recognized two regional seismic unconformities (P1 and P2). Additional data and reinterpretation have allowed the mapping of a third surface younger than P1 and P2. Surface P1 within these sediments marks the transition from a lower, homogeneous part of section with mostly irregular reflectors to an upper, heterogenous one in which a variety of well-stratified seismic facies are present. More distal data suggests that P1 may be as old as Cretaceous. Surface P2 marks a change to submarine canyons and to related channel and levee deposits and chaotic seismic facies. Kuvaas and Leitchenkov (1992) interpret this transition as resulting from the onset of continental glaciation in the Eocene or the arrival of grounded ice sheets at the shelf edge in the early Oligocene, as indicated by ODP Sites 739 and 742 (Barron et al., 1991). This sedimentation change produced thick, prograding foresets above the P2 unconformity beneath the Prydz Bay outer shelf (Kuvaas and Leitchenkov, 1992).

Surface P3, above P2, represents the base of deposits containing abundant, well-stratified sediment drift facies, including sediment waves. Sediment wave geometry implies that strong, westerly flowing bottom currents played a significant role in drift formation. The changes at this level could have been related to initiation of the ACC after the opening of Drake Passage around the Oligocene/Miocene boundary or may relate to a major ice expansion during the Oligocene or Miocene (G. Leitchenkov, pers. comm., 1998).

Quaternary to Modern Sediments

Areas of Prydz Bay shallower than 690 m are extensively ploughed by iceberg keels (O'Brien and Leitchenkov, 1997) and so are covered with a layer of disturbed sediment. Surface sediments and their diatom floras are described in Harris et al. (1998). Areas deeper than 690 m reveal undisturbed Quaternary sections. The Amery Depression inshore from grounding zone wedges in Prydz Channel is floored by fluted subglacial till and draped in places by clayey diatom ooze deposited since ice retreat over the last 12 k.y. (Domack et al., 1998; O'Brien et al., 1999). Within the Amery Depression, the tills are dark gray pebbly sandy clays with high magnetic susceptibility. In the southwestern corner of the Bay, in the Lambert Deep, tills are brown red with low susceptibility derived from pre-Cretaceous red bed sediments in the Lambert Graben (Domack et al., 1998). Prydz Channel, seaward of the grounding zone wedges, is floored by smooth seafloor and iceberg scours draped by gray clays and diatom ooze. These draped iceberg scours are likey relict features from LGM low sea levels.

PRINCIPAL RESULTS

Site 1166: Continental Shelf (Prydz Bay)

Site 1166 is situated on the Prydz Bay continental shelf on the southwestern flank of Four Ladies Bank, ~40 km southwest of ODP Site 742 (Leg 119) (Fig. F10). Prydz Bay is at the downstream end of a drainage

F10. Maps of Leg 188 drill sites and East Antarctic coastline, p. 39.

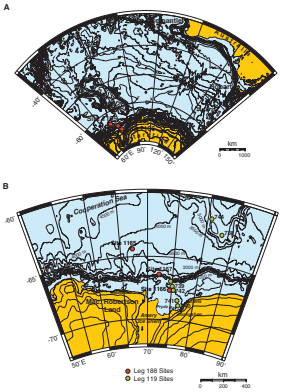

system that originates in the Gamburtsev Mountains of central East Antarctica. The early development and growth of the Cenozoic Antarctic Ice Sheet is believed to have started in middle Eocene to early Oligocene time, but to date, drilling on the continent and the continental margin has not sampled a stratigraphic section that clearly spans and includes the transition period from preglacial to glacial conditions. Site 1166 was chosen to recover core from the Cenozoic sediments below the horizon reached at Site 742. This was intended to provide an age for the arrival of glaciers in Prydz Bay and a record of changes in paleoenvironments and biota with the onset of glaciation.

When the *JOIDES Resolution* arrived in Prydz Bay, the drill site had to be moved to an alternate site because pack ice covered much of western Prydz Bay where the primary site was located. An additional 3-nmi displacement of the site was required because a tabular iceberg was floating directly over the alternate site. The target sedimentary section (Fig. **F11**) was thinner and likely a little younger near the base of the section at the final alternate site (i.e., Site 1166) than at the primary site. The drilling at Site 1166 was conducted safely and achieved the desired objective under the sometimes cold and stormy operating conditions.

Drilling at Site 1166 had to be halted temporarily about midway through the drilling because of a large storm with wind gusts exceeding 40 kt and swells >2 m, the maximum limit for shallow-water drilling. During the storm, an iceberg approached within 0.6 nmi and the drill pipe had to be pulled out of the seafloor without a reentry cone in place. The ship was moved away from the site. Following the storm, the ship returned to the site and successfully reentered the hole to continue uninterrupted drilling to a total depth of 381.3 mbsf (Table **T1**). Recovery at the site was 18.6%; low recovery was due partly to drilling through the upper section (135 mbsf) of diamictites, similar to those sampled at Site 742, and because of sandy fine-grain sediments in the lower part of the hole. Three full logging runs were obtained with excellent data from ~50 mbsf to the bottom of the hole.

The sedimentary section at Site 1166 comprises a diverse suite of strata that from the top down include glacial, early glacial, and preglacial rocks that consist of poorly sorted, sandy, and fine-grained sediments. The ages range from Holocene at the seafloor to Late Cretaceous at the bottom of the hole, with many disconformities throughout.

The sediments are divided into five lithostratigraphic units (Fig. **F12**). Lithostratigraphic Unit I is of late Pliocene to Holocene age and comprises four subunits. The uppermost subunit (Subunit IA; 0.0–2.74 mbsf) is a biogenic-rich clay interval with pebble-sized clasts. This unit is interpreted as an ice-keel turbate, based in part on iceberg furrows that occur in echo-sounder records in this area (O'Brien and Leitchenkov, 1997).

Below Subunit IA are two intervals of diamicton and one of poorly sorted clayey sandy silt. Subunits IB (2.79–106.36 mbsf) and ID (123.0–135.41 mbsf) are separated by a thin interval (Subunit IC; 113.30–117.22 mbsf) of biogenic-rich clayey silt. Subunit IB is predominantly clayey silt with rock pebbles and clasts that include common fibrous black organic matter. Minor (<2 cm thick) sand and granule beds are present. Subunit IC is interbedded dark gray sandy silt with lonestones and greenish gray diatom-bearing clayey silt with dispersed granules. Biogenic-rich intervals are slightly bioturbated. Contacts with the dark silt are sharp. Subunit ID has interbeds of dark gray clast-poor and clast-rich diamicton. Clast lithologies vary and include gneiss, granite, and diorite rocks. The diamictons suggest subglacial deposition; the sandy

F11. Seismic reflection profile over Site 1166, p. 40.

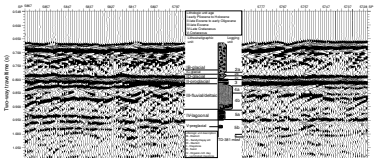

T1. Leg 188 site summary, p. 65.

F12. Composite stratigraphic section for Site 1166, p. 41.

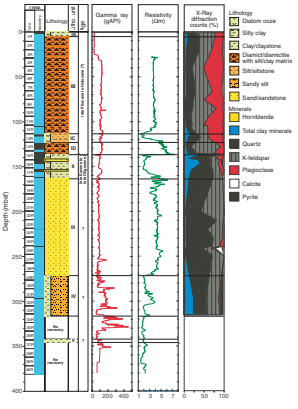

silt with IRD is a glaciomarine unit deposited during interglacial periods.

Unit I has lonestones throughout. For Subunits IB and ID, the diamictons suggest subglacial deposition or deposition of a proglacial morainal bank. Sandy silt intervals with shell fragments and microfossils (Subunit IC) suggest current reworking and glaciomarine sedimentation during times of significant glacial retreat. The lonestones signify deposition of IRD. In seismic reflection data, Unit I comprises the topset beds of the seaward-prograding sedimentary section of the outer continental shelf. The contact between lithostratigraphic Units I and II is an abrupt unconformity and was recovered (interval 188-1166A-15R, 8–11 cm [135.63 mbsf]). XRD data above and below the unconformity show shifts in relative abundances of mica, illite, kaolinite, hornblende, and plagioclase. The shifts suggest increased amounts of weathered terrigenous material within Unit I, just above the unconformity.

Unit II (135.63–156.62 mbsf) is an upper Eocene to lower Oligocene diatom-bearing claystone with thin interbedded sands and lonestones. Carbonate contents range from 0.4 to 3.3 wt%. Sands are poorly sorted and bioturbation is moderate. Rare fibrous black organic clasts are present within the sand beds. The bottom of Unit II has rhythmically interbedded centimeter-thick sand and dark claystone. XRD shows gibbsite and kaolinite in Unit II, suggesting erosion of chemically weathered material produced during soil formation. Unit II is a marine sequence that records ice rafting of pebbles during a marine transgression. At Site 742 (Leg 119), 40 km away, similar or younger-age sediments that were interpreted as proximal glacially influenced proglacial or subglacial deposits were sampled. The contact between lithostratigraphic Units II and III is abrupt and was also recovered (interval 188-1166A-17R, 77–78 cm).

Unit III (156.62–267.17 mbsf) consists of massive and deformed sands with a silty clay matrix. The unit contains late Eocene palynomorphs. Calcium carbonate content ranges from 0.4 to 8.4 wt%. The sands have a uniform fabric, are poorly sorted, and lack internal structure. Pebbles of quartzite and rare fibrous black organic fragments are widely dispersed throughout. Two calcite-cemented intervals are present in the sands. The lower part of Unit III is deformed and folded by soft-sediment deformation of sandy beds and includes black organic-rich material with pieces of wood. The coarse-grained sands record deposition on an alluvial plain or delta, and the deformed beds record some reworking of material from underlying organic-rich horizons. A similar-looking sequence of carbonaceous material was drilled in the bottom 2 m at Site 742 and was interpreted as fluvial or possibly lacustrine. At Site 742, however, a sequence comparable to the homogeneous coarse sands was not recovered. The coarse sands of Unit III may record a preglacial alluvial plain or a braided delta of a glacial outwash system. The contact between lithostratigraphic Units III and IV was not sampled.

Unit IV (276.44–314.91 mbsf) comprises black highly carbonaceous clay and fine sandy silt with organic-rich laminae and rare to moderate bioturbation. Palynomorphs suggest a Late Cretaceous (Turonian) age. The sandy silt contains abundant mica and some pyrite. The organic-rich laminae have organic carbon (OC) values as high as 9 wt% and contain common occurrences of authigenic sulfides. Calcium carbonate content ranges from 0.3 to 3.7 wt%. Unit IV records deposition in a restricted marine or lagoonal environment.

Unit V (342.80–342.96 mbsf) consists of a small sample of undated finely laminated gray claystone that was captured in the core catcher within a thick no-recovery zone at the bottom of the hole. From resistivity and velocity log data, the unit may have a relatively large clay content. The claystone is preglacial in origin. It is the same age as Unit IV.

Diatoms, radiolarians, foraminifers, and calcareous nannofossils were examined at Site 1166. Diatoms are present in limited intervals of the core and provide the primary biostratigraphic age control. Three distinct diatom assemblages were noted—Quaternary, Pliocene, and late Eocene–early Oligocene age. Extant Quaternary diatoms occur at 2.12–2.92 mbsf (age = <0.66 Ma). Quaternary to upper Pliocene diatoms occur in diamicts to at least 106.37 mbsf. Two layers of diatomaceous clay (~113.95–114.10 mbsf and ~114.50–115.15 mbsf) are present, containing the upper Pliocene diatom *Thalassiosira kolbei* (1.8–2.2 Ma) and the *Thalassiosira vulnifica* to *Thalassiosira striata–T. vulnifica* Zones (2.2–3.2 Ma), respectively. Radiolarians suggest an age of >2.4 Ma for the lower bed. The boundary between lithostratigraphic Units I and II is a major disconformity (~30 m.y.). Diatoms in Unit II between 135.73 and 153.48 mbsf are of early Oligocene–late Eocene age (~33–37 Ma). Diatoms were not recovered below Unit II, but several specimens of pollen, spores, dinoflagellates, and wood fragments were noted in lower intervals of the hole. Planktonic foraminifers are common above ~90 mbsf, and their ages generally agree with those for diatoms and radiolarians. Calcareous nannofossils are rare. Palynological samples give ages for Units II through V based on correlation with Australian palynozones (O'Brien et al., in press).

Paleomagnetic stratigraphy is difficult because of limited core recovery, but a clear pattern of magnetic polarity intervals is recorded where the recovery is relatively high. A correlation to the geomagnetic polarity time scale (GPTS) is in progress using key biostratigraphic datums (Fig. **F13**). Downhole variations in the concentration-dependent and magnetic mineralogy-dependent parameters show that the main lithostratigraphic units have alternating high and low magnetic mineral concentrations and distinct magnetic signatures. Iron sulfide minerals are present below ~140 mbsf.

Interstitial water profiles document downhole sediment diagenesis and diffusional exchange with bottom seawater. From 0 to 150 mbsf, the oxidation of organic matter reduces sulfate values from 28 to 8 mM and ammonium increases from 177 to 1277 mM. From 0 to 75 mbsf, alkalinity decreases from 4.5 to 1 mM, silica decreases from 800 to 200 mM, potassium decreases from 12 to 2 mM, and calcium increases from 10 to 22 mM. The profiles suggest diagenetic silicate reactions are occurring within the sulfate reduction zone. Between 150 and 300 mbsf, calcium and magnesium show minor changes in relative concentration (15 and 24 mM, respectively) suggesting diffusional processes are dominant.

OC contents of the sediments based on 14 samples (selected by dark color) vary according to lithostratigraphic unit. The diamictite (Subunit IB) has OC values of 0.4–1.4 wt%; the massive sand (Unit III) has OC values of 0.2–0.5 wt%, except for one bed near the base of the fluvial/deltaic sand section of Unit III that contains 9.2 wt% OC; and the carbonaceous claystone (Unit IV) has 1.5–5.2 wt% OC. Inorganic carbon was low (<0.1 wt%) throughout most of the recovered section. Gas analyses showed only background levels of methane (4–10 ppmv), and no other hydrocarbons were detected. Most samples are enriched in car-

F13. Plots showing biostratigraphic age control and magnetostratigraphic polarity intervals, p. 42.

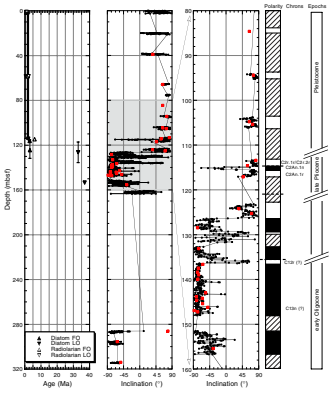

bon relative to nitrogen, which suggests the input of land-plant organic matter, especially for samples with >1 wt% OC. Rock-Eval pyrolysis analysis shows that the pyrolyzable fraction of the OC is low (hydrogen index values of 50 mg of hydrocarbon per gram of carbon or less), consistent with degraded plant material as the source of the carbon in the more carbonaceous (>2 wt%) samples. Samples with lower carbon contents (<1.4 wt%) may contain a recycled higher thermal maturity component. This recycled organic component is suggested by Rock-Eval T_{max} values that approach 490°C as OC decreases toward values of 0.5 wt%. The diamictites (Unit I) have a greater proportion of recycled organic matter than the carbonaceous units (base of Units III and IV), which contain mostly first-cycle organic matter.

The majority of the sedimentary section has porosities between 20% and 40%, with the exception of Unit II, where the average porosity is 50%. *P*-wave velocities change abruptly at most lithostratigraphic boundaries. The measured shear strengths show that the sediments, especially in Unit I, are overconsolidated, with an overconsolidation ratio of ~2 below 70 mbsf. The overconsolidation record implies at least one or two periods when sediments were either compacted by a 250- to 300-m-thick sediment column, now eroded away, or were loaded by 330- to 420-m-thick nonbuoyant ice during prior glaciations.

Wireline logging was carried out in Hole 1166A with excellent results (Fig. **F14**). Three runs were made using the triple combination (triple combo), sonic/geological high-sensitivity magnetic tool (GHMT), and Formation MicroScanner (FMS) tool from 33 mbsf to the bottom of the hole at 385 mbsf. Six logging units are recognized, and each stratigraphic unit has a distinctive signature and appearance, especially in the resistivity, sonic velocity, and FMS data. The deeper parts of the hole (logging Units 4b, 5a, 5b, and 6, equivalent to lithostratigraphic Units III [lower part], IV, and V) consist of preglacial to early glacial sediments that have large gamma-ray fluctuations indicative of heavy mineral K, Th, and U contents associated in part with the high OC values here. These units also have lower velocity, density, and resistivity than the thick overlying deltaic sands of lithostratigraphic Unit III. All log traces show abrupt shifts at the logging Units 3/4 and 2/3 boundaries (equivalent to lithostratigraphic Units II/III and I/II boundaries) and are recognized as unconformities. The diamictons with interbedded glaciomarine clays and silts of lithostratigraphic Unit I have generally high and variable magnetic susceptibilities that suggest high variability in magnetite concentrations. FMS images clearly show the variability in the lithostratigraphic units, the presence of lonestones, and the deformation of the organic-rich silt-sand horizons (lithostratigraphic Unit III) (Fig. **F15**). The resistivity and velocity logs, along with seismic reflection profiles, suggest the alluvial sands (Unit III) to glaciomarine diatom-bearing claystones (Unit II) transition represents a marine transgression.

Logging while drilling (LWD) was done in Hole 1166B to test the Power Pulse and compensated dual resistivity tools and record spectral gamma-ray and resistivity data in the uppermost 42 m of the sediment. This interval could not covered by wireline logging because of the pipe position. Resistivity values increase in linear segments from near zero at the seafloor to the 3.5-Ωm values measured by the wireline logs at the base of the pipe.

A primary objective of Leg 188 was achieved when a set of cores that record intervals in the history of Antarctic paleoenvironments for the Prydz Bay region extending back through the early stage of glaciation

F14. Downhole wireline logs of Site 1166, p. 43.

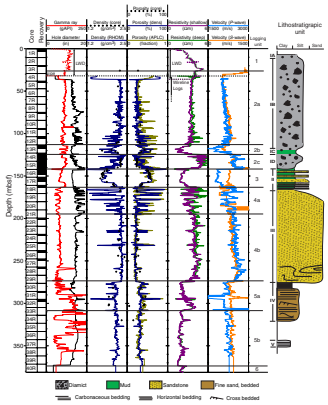

F15. Examples of FMS resistivity images, p. 45.

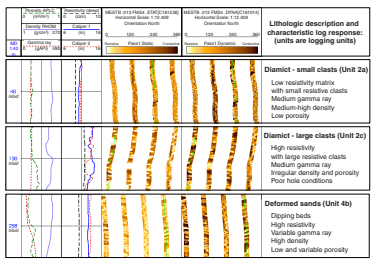

to preglacial times was recovered at Site 1166 (Fig. F16). Drilling during Leg 119 in Prydz Bay recovered a record of early proximal glaciation at Sites 739 and 742 but did not capture the transition to warmer climates as would be indicated by the presence of local vegetation. Correlation of Site 1166 to Site 742 (~40 km apart) by comparison of downhole logs and regional seismic stratigraphy shows that Units I and II at Site 1166 are equivalent to (or older than) similar units at Site 742. Below the level of Unit II, however, Site 1166 samples are stratigraphically lower and record a more temperate alluvial facies than seen at Site 742. The lower part of Unit III (i.e., the deformed organic-rich sands and silts) may have been sampled in the lowermost 2 m of core at Site 742, but confirmation of this awaits further comparison of the two drill sites. If the organic units are the same, then a thick section of sands (Unit III) is missing at Site 742. The deepest unit at Site 1166 (Unit V) lies below a regional seismic unconformity that can be traced to Site 741, ~110 km away, where gray claystones similar to those of Unit V were also sampled. The age of the claystone at Site 741 is Early Cretaceous, which is preglacial.

The paleoenvironmental record inferred from the cores at Site 1166 shows a systematic uphole change from preglacial warm to full-glacial cold climates, such as that envisioned for the Prydz Bay region in Figure F16. The rich carbonaceous strata (Cretaceous Unit IV), which overlie Unit V, record a time of more temperate climatic conditions when vegetation existed on Antarctica. The sands (late Eocene Unit III) of the alluvial plain environment may represent the transition into the progressively colder climates that are recorded in the proglacial (late Eocene to early Oligocene Unit II), glacial marine (Unit II and late Pliocene and younger Unit I), and subglacial (Unit I) sediments.

Site 1167: Continental Slope (Trough Mouth Fan)

Site 1167 is located in the middle of the Prydz Channel Trough Mouth Fan (Figs. F10, F17). Construction of the fan started in late Miocene to mid-Pliocene time when the Lambert Glacier formed a fast-flowing ice stream on the western side of Prydz Bay. The fan has grown most during episodes when the Lambert Glacier grounded at the shelf edge, delivering basal debris to the fan apex. This material was then redistributed by sediment gravity flows and meltwater plumes. Models of trough mouth fan sedimentation suggest that thick siliciclastic units should correspond to peaks in Antarctic ice volume, whereas periods of reduced ice volume should be represented by hemipelagic sediments. Thus, the alternation of facies should reflect the number of times the East Antarctic Ice Sheet has expanded to the shelf edge in latest Neogene time.

Hole 1167A was cored with the advanced hydraulic piston corer (APC) system to refusal at 39.7 mbsf. Coring then proceeded with the extended core barrel (XCB) system to a total depth of 447.5 mbsf (Table T1). Planned drilling time at the site was shortened by 42 hr because of icebergs and a ship schedule change, and the target depth of 620 mbsf (base of the Prydz Trough Mouth Fan) was not achieved. Four icebergs approached to within 0.1 nmi of the drill site, causing a total of 27 hr delay.

The sedimentary section at Site 1167 comprises a 447.5-m-thick sequence of clayey silty sands with dispersed rock clasts with minor beds of coarse sands, clays, and sandy clays. Two lithostratigraphic units are identified (Fig. F18).

F16. Diagrams of the Prydz Bay region from preglacial through full glaciation, p. 46.

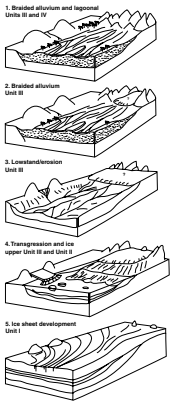

F17. Seismic reflection profile over Site 1167, p. 47.

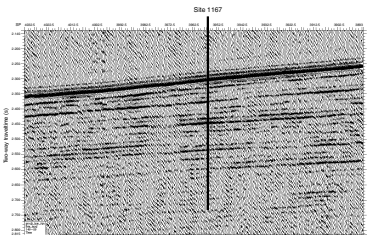

F18. Site 1167 lithostratigraphic units, facies, and interpretation, p. 48.

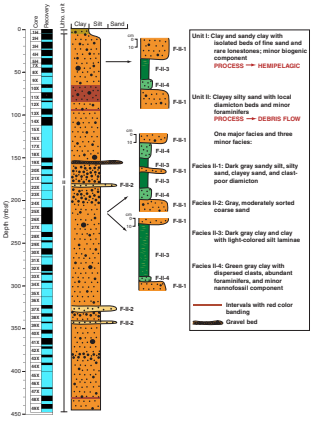

Unit I (0–5.17 mbsf) is composed of olive and reddish brown clay and sandy clay with minor admixtures of biogenic components (e.g., as much as 2% diatoms and 1% sponge spicules). There are isolated beds of fine sand and rare lonestones. Diffuse reddish brown color bands are present in several thin intervals. The transition to Unit II is gradational. Unit I records a period of hemipelagic deposition when fine particles, biogenic material, and IRD settled out of the water column.

Unit II (5.17–447.5 mbsf) makes up the majority of the section at Site 1167 and is composed of one major facies (II-1) and three minor facies. Facies II-1 is composed of interbedded, poorly sorted dark gray sandy silt, silty sand, clayey sand, and clast-poor diamicton. Numerous color alternations of dark gray and dark reddish gray with sharp contacts occur between 64 and 98 mbsf. Some decimeter- to meter-scale successions of clast-poor diamicton and gravel beds are noted. Lonestones are common, with variable lithologies including granite, granite gneiss, garnet-bearing gneiss, metaquartzite, and sandstone. Dolerite, schist, conglomerate, and rare carbonized wood are also present. Sandstone and granite components vary systematically in the hole, with sandstone lonestones common below 200 mbsf and granite lonestones common above 200 mbsf. Facies II-2 is composed of gray, moderately sorted coarse sand. Grains are subrounded and predominately quartz, K-feldspar, and mafic minerals. The first occurrence of Facies II-2 downcore is at 179 mbsf. Facies II-3 is composed of dark gray clay with silt laminations, rare sand grains, and no lonestones. Sharp contacts mark the top and base of this facies. Some silt laminae converge and indicate crossbedding. Facies II-4 is composed of green gray clay with dispersed clasts, abundant foraminifers, and few nannofossils. The upper contact is sharp, and the lower contact is gradational to sharp.

Unit II (Facies II-1 and II-2) records deposition by mass transport, probably massive debris flows, as evidenced by poor sorting, abundant floating clasts, little visible grading, and a lack of biogenic components. The debris flows most likely represent deposition during glacial periods when ice extended to the shelf break and could deliver large volumes of sediment to the upper continental slope. Individual flows cannot be identified visually. The thin intervals of fine-grained sediment (Facies II-3 and II-4) are similar in appearance and composition to muddy contourites observed at Site 1165, and hence, may denote times when contour currents were active on the fan. The silt laminae and bioturbation in Facies II-3 are not consistent with turbidite deposition. Facies II-4 may record short intervals, possibly interglacials, when pelagic deposition dominated.

Sixteen lithologic varieties of lonestones were cataloged, and they generally vary randomly in size, with only a small size increase downhole to 200 mbsf. Below ~160 mbsf, the number of lonestones per meter remains fairly consistent, except for three intervals (160–210, 300–320, and 410–420 mbsf) where there are downward increases. Systematic variations in concentration of sandstone and granite clasts (noted above) suggest that two different source areas may have delivered material to Site 1167 at different times (Fig. F19).

XRD analyses show that the total clay mineral content is relatively constant throughout the hole. XRD analyses of clay types give mixed results for Units I and II, with smectite more common in Unit I and at depths below 382 mbsf than elsewhere and illite found in all samples. Further detailed analyses are likely to clarify whether changes in illite-smectite ratios relate to times of glacial advances.

F19. Distribution and frequency of sandstone vs. granite/igneous lonestones, p. 49.

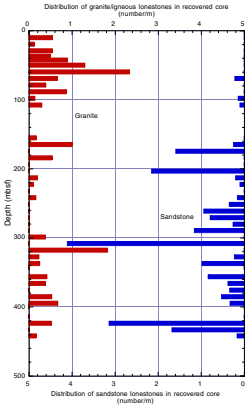

Chronostratigraphy at Site 1167 is poorly controlled because of the unexpected paucity of siliceous microfossils; however, dates in Unit I are younger than 0.66 Ma, and a sample from ~215 mbsf seems to be of early or middle Pleistocene age. Foraminifers are present consistently throughout the section and include pelagic foraminifer shelf faunas in diamictons and in situ midbathyal faunas in a few samples. Changes in foraminifer faunas closely match changes detected in various lithological parameters. Age control at this time is not adequate to determine average sedimentation rates.

Magnetostratigraphic analyses identified the Matuyama/Brunhes boundary between 30 and 34 mbsf (Fig. **F20**). The magnetic polarity below 34 mbsf remains mainly reversed and possibly includes the Jaramillo and Olduvai Subchrons. The concentration-dependent magnetic parameters (susceptibility and anhysteretic and isothermal remanent magnetization) indicate that magnetite concentrations have large-scale cyclic (tens to hundreds of meters) variations, which are not commonly seen (Fig. **F20**). The values increase abruptly uphole at ~208 mbsf, between 113 and 151.2 mbsf, and between 55 and 78.5 mbsf followed by a nearly linear uphole decrease. Superimposed on the large-scale cycles are small-scale variations. The anhysteretic over isothermal remanent magnetization ratio indicates that the magnetic grain size changes uphole from finer to coarser above 217 mbsf. The origin of the large-scale cycles is not yet understood, but it is likely related to systematic changes in sediment provenance caused by changes in the volume of ice from different sources and the location of areas of maximum erosion during glacial periods.

Interstitial water profiles document downhole sediment diagenesis, mixing of chemically distinct subsurface interstitial waters, and diffusional exchange with modern bottom seawater. From 0 to 20 mbsf, chlorinity and sulfate increase by ~3% over seafloor values, suggesting that high-salinity LGM seawater is preserved (Fig. **F21**). Sulfate decreases downhole from the seafloor (30 mM) to 433 mbsf (24 mM) in a stepped profile, raising the possibility that a number of "fossil" sulfate reduction zones may also be preserved (Fig. **F21**). Dissolved manganese increases downhole from 15 to 20 mM between the seafloor and ~25 mbsf. Alkalinity decreases downhole from 3 to 1.3 mM between the seafloor and 40 mbsf before steadily increasing to 2 mM at 433 mbsf. From 0 to ~60 mbsf, dissolved downhole profiles of calcium (10–25 mM), magnesium (56–42 mM), potassium (12–2 mM), and lithium (30–5 mM) all suggest diagenetic silicate-clay reactions are occurring. Below 5 mbsf, dissolved silica concentrations are enriched slightly over modern bottom waters (~300 vs. ~220 mM), reflecting the absence of biogenic opal within the sediments. Calcium carbonate is a minor component in the matrix sediments throughout the hole and is slightly more abundant in lithostratigraphic Unit II than in Unit I.

The concentration of hydrocarbon gases was at background levels (4–10 ppmv) for methane, and ethane was present above detection limits only in a few cores deeper than 350 mbsf. The OC content averages ~0.4 wt% with no apparent trend with depth. Organic matter characterization by Rock-Eval pyrolysis indicates that all samples contain predominantly recycled and degraded thermally mature organic matter.

Sediment water content and void ratio decrease sharply with depth in lithostratigraphic Unit I, reflecting normal compaction. Within Unit II, these properties were relatively uniform, except for a downhole decrease at 210 mbsf, where grain density and magnetic susceptibility values also decrease abruptly. *P*-wave velocities increase at this depth.

F20. Plots showing magnetostratigraphy, magnetic susceptibility, and ARM/IRM, p. 50.

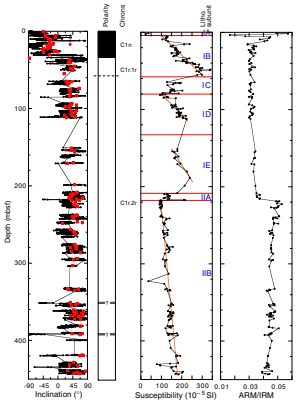

F21. Plots of chloride and sulfate interstitial water values, p. 52.

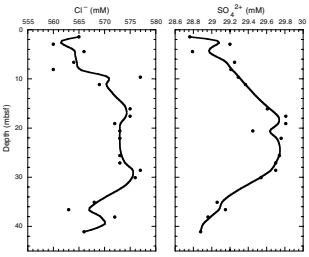

Undrained shear strength values increase uniformly throughout the hole at a lower than typical rate, possibly because of the clay mineralogy combined with the high proportions of silt and sand within the sediment. There is no evidence of sediment overcompaction.

Wireline logging operations in Hole 1167A were attempted with the triple combo tool string. The tool string was lowered to 151 mbsf, where an obstruction halted further progress. A conglomerate interval was noted in the cores at this depth. Log data were collected from this depth to the base of pipe at 86.9 mbsf, covering an interval of 66 m. Time constraints, poor hole conditions, and problems encountered with the lockable flapper valve resulted in a decision to switch to LWD in a new hole. Excellent spectral gamma-ray and resistivity data were recorded to 261.8 mbsf before time ran out. Resistivity data show several clay and gravel-rich beds, with high gamma-ray values for a red bed interval at 60–90 mbsf, and low values between 90 and 120 mbsf and 215 and 255 mbsf. The change to low values may be due to a reduced concentration of granitic clasts or a change from a clay-rich to a sandier matrix.

Site 1167 is the first drill site where the sedimentary fans that are common on the upper continental slope around Antarctica, seaward of glacially carved sections of the continental shelf, were directly sampled. The site reveals previously unknown large-scale (20- to >200-m-thick) cycles in magnetic susceptibility and other properties that are not yet fully explained but are likely due to systematic changes in the Lambert Glacier ice-drainage basin during Pleistocene and late Pliocene(?) time. Within the large cycles are likely many separate debris flows and interbedded hemipelagic muds that indicate times of individual advances and retreats of the ice front to, or near, the continental shelf edge. The debris flows are well represented in the cores, but the mud intervals are sparse and may either have not been recovered or have been removed by younger flows. Because there are few age control points, it is not yet possible to determine sedimentation rates at Site 1167. If the rates are high, as we suspect from the few available age dates, then almost all sediment during the latest Neogene glacial intervals sampled at Site 1167 were deposited as debris flows on the trough mouth fan and are not reaching Wild Drift (Site 1165), where sediment rates are low. Alternatively, some of the fine component of the latest Neogene glacial sediment is being carried away by deep ocean currents.

Site 1165: Continental Rise (Wild Drift)

Site 1165 is situated on the continental rise offshore from Prydz Bay over mixed pelagic and hemipelagic sediments of the central Wild Drift (Figs. **F10, F22A, F22B**). The drift is an elongate sediment body formed by the interaction of sediment supplied from the shelf and westward-flowing currents on the continental rise. The site is in 3537 m of water and was selected to provide a record of sedimentation that extends back to the onset of contour current–influenced deposition on the rise. The main objective was to obtain a proximal continental-rise record of Antarctic glacial and interglacial periods for comparison with other sites around Antarctica and with those of Northern Hemisphere ice sheets.

Prior to drilling, a single seismic-reflection profile was recorded across the location of Site 1165, using the ship's water-gun, to verify the location of the site. Three holes were drilled at the site (Table **T1**). Hole 1165A consisted of a mudline core that was dedicated to high-resolution interstitial water sampling. Hole 1165B was cored with the APC to

F22. Seismic reflection profile across Site 1165, p. 53.

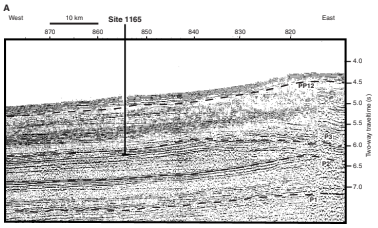

147.9 mbsf (86.4% recovery) and deepened with the XCB to 682.2 mbsf (57.3% recovery). Hole 1165C was washed down to a depth of 54 mbsf, where a single core was taken at an interval that had been missed in Hole 1165B. Continuous RCB coring began at 673 mbsf and continued to a total depth of 999.1 mbsf, with 80% recovery. Coring operations were interrupted by five icebergs that came to within 200 m of the drill site and caused a total loss of 98 hr. Hole 1165C was successfully logged with the triple combo tool string from 176 to 991 mbsf and with the sonic tool from 176 to 580 mbsf.

Drilling at Site 1165 yielded a relatively continuous 999-m-thick sedimentary section of early Miocene- to Pleistocene-age terrigenous and hemipelagic deposits (Fig. F23) with only few minor (<2 m.y.) disconformities. Dispersed clasts (IRD) are present down to the bottom of the hole, but lonestones are infrequent below 500 mbsf (lower Miocene). Both dispersed clasts and lonestones are relatively abundant above 300 mbsf (middle Miocene and younger).

The sedimentary section is divided into three lithostratigraphic units that are characterized by cyclic variations between biogenic-bearing (lighter) and terrigenous-dominated (darker) intervals. The cyclic variations in lithology are also recorded as visual color alternations and cycles in spectrophotometer lightness factor, bulk density, magnetic susceptibility, and other laboratory and downhole log parameters to varying degrees. In general, cores get darker downhole as biogenic intervals become thinner relative to the thickness of terrigenous-bearing intervals. For the same reason, light-dark cyclicity is more prominent above ~400 mbsf. Darker units generally have higher bulk density, magnetic susceptibility, and OC values. The sediment consists mostly of quartz, calcite, plagioclase, K-feldspar, and a mixture of clay minerals, as well as minor hornblende and pyrite. Silt-sized components are mainly quartz, but plagioclase, biotite, amphibole, and other heavy minerals are common.

Unit I (0–63.8 mbsf) consists of structureless brown clay and diatom-bearing clay. There are beds with minor diatom-bearing greenish gray clay that have dispersed sand grains, granules, and lonestones. There is minor laminated silt and minor brown foraminifer-bearing clay. Foraminifers comprise 5%–15% of the sediment above 13 mbsf. One interval within Unit I (20–30 mbsf) is characterized by alternations between two facies like those of Unit II (i.e., Facies II-1 and II-2).

Unit II (63.8–307.8 mbsf) is characterized by alternations of two main facies that differ in color and composition. Facies II-1 consists of structureless, homogeneous greenish gray diatom clay, and Facies II-2 is mostly dark gray diatom-bearing clay with some intervals of scattered silt laminae. Many lower boundaries of Facies II-2 are sharp, and upper boundaries are transitional with bioturbation that increases upward into Facies II-1. Higher amounts of siliceous microfossils and IRD (floating sand grains and pebbles) are found in Facies II-1 than II-2. Facies II-1 is characterized by lower grain density because of the higher diatom content. A third facies (II-3) occurs rarely and consists of several 15- to 40-cm-thick nannofossil chalk beds that have a sharp base and pass gradually up into Facies II-1. Within Unit II, three subunits are identified based on the different proportions of Facies II-1 and II-2. Subunit boundaries are at 160 and 252 mbsf and partially denote amounts of IRD, with greater amounts of IRD in Subunits IIA and IIC than in Subunit IIB.

Unit III (307.8–999.1 mbsf) comprises a section of thinly bedded planar-laminated claystone that is divided, like Unit II, into two main fa-

F23. Composite stratigraphic section for Site 1165, p. 55.

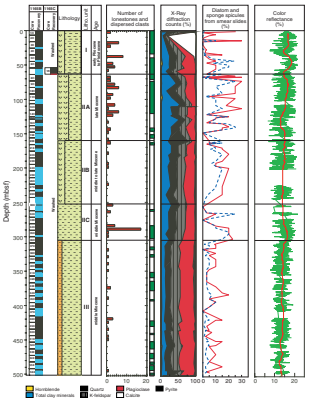

cies that differ in color, composition, and bedding characteristics. Facies III-1 consists of greenish gray bioturbated structureless clay and claystone and diatom-bearing clay and claystone with dispersed coarse sand grains and rare granule to pebble-sized lonestones. Facies III-2 is composed of dark gray thinly bedded planar-laminated clay and claystone with abundant silt laminae. Lonestone (dolerite, diorite gneiss, and mudstone) abundance in Unit III is low and decreases downhole.

In Facies III-1, the thickness of the greenish gray intervals is generally <1 m and some intervals have higher concentrations of silt- and sand-sized material. The upper contacts are commonly sharp, laminae are rare, and bioturbation increases upcore. Angular mud clasts and benthic foraminifers are present in this facies below 800 mbsf. Siliceous microfossil content is low.

Facies III-2 becomes increasingly fissile with depth and changes to very dark gray or black below 894 mbsf. Bioturbation is rare in Facies III-2, and light-color silt laminae are a conspicuous feature (average = 150–200 laminae/m). Many cross-laminated silt ripples are present, and ripples are more common below 673 mbsf than above. Microfossils are rare and seem to disappear completely below ~600 mbsf. Below 842 mbsf, laminae with calcite cement are present and sections of the core become increasingly cemented with what are most likely authigenic carbonates. A change to darker-color claystones occurs at 894 mbsf, where fracture patterns also become curved.

In both Facies III-1 and III-2, individual 0.5-cm-sized horizontal *Zoophycos* burrows are evident along with clusters of unidentified millimeter-sized burrows.

An excellent record of siliceous microfossils is found at Site 1165 down to 600 mbsf, where biogenic opal disappears because of an opal-A/opal-CT diagenetic transition. Neogene high-latitude zonal schemes for both diatoms and radiolarians yielded identification of 21 diatom and 12 radiolarian biostratigraphic datums between 0 and 600 mbsf. Below 600 mbsf, age assignments are inferred from calcareous nannofossils, which are present in only a few discrete intervals with moderate to good preservation of low-diversity assemblages. Nannofossils yield Pleistocene to earliest Miocene ages. Benthic foraminifers are more common than planktonics, which are rare. The foraminifers indicate several intervals of redeposited material.

A magnetostratigraphy was determined for Site 1165 for the interval 0–94 mbsf and below 362 mbsf (Fig. **F24**). The magnetostratigraphic record and biostratigraphic ages, when combined, yield an age vs. depth model that shows relatively rapid deposition in early Miocene time (~120 m/m.y.), somewhat slower deposition in middle to late Miocene time (~50 m/m.y.), and even slower deposition since late Miocene time (~15 m/m.y.) (Fig. **F25**). From magnetostratigraphy, the bottom of Hole 1165C (999.1 mbsf) has an age of ~21.8 Ma. The uncertainty in ages is larger below 600 mbsf, where only few biostratigraphic ages exist to constrain the paleomagnetic reversal stratigraphy.

Measurements of rock magnetic properties in the interval 114–370 mbsf indicate that magnetic mineral concentrations (i.e., concentrations of magnetite) drop significantly, with nearly a complete loss of magnetic intensity. Shipboard analysis suggests that this unusual loss of magnetic signal is caused by diagenetic dissolution of magnetite in the presence of silica-rich pore-waters. A zone of low grain density is observed in cores from part of this zone ~140 mbsf and may also coincide with the disappearance of magnetite.

F24. Magnetostratigraphy for Site 1165, p. 58.

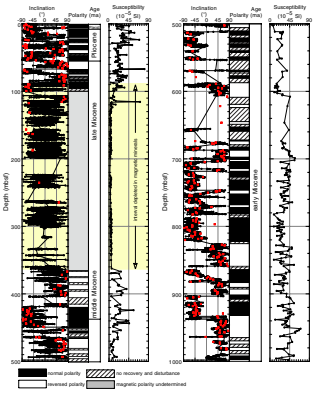

F25. Age-depth plot for Site 1165, p. 59.

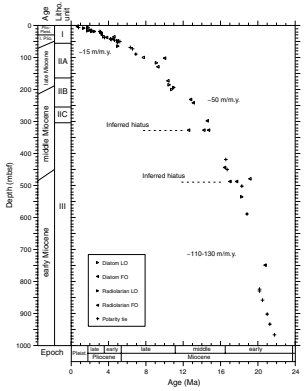

The interstitial water profiles document increasing downhole sediment diagenesis at Site 1165. Sulfate values decrease linearly from 30 to 2 mM in the interval from 0 to 150 mbsf, but increases occur in ammonium (20–384 µM), phosphate (3–10 µM), and alkalinity (3–8 mM) throughout the same interval because of destruction of organic matter. Ammonium increases (to 800 µM), phosphate decreases (to 0), and alkalinity decreases linearly (to 1 mM at 999 mbsf) throughout the interval from 150 to 400 mbsf. Concentrations of dissolved silica increase from 522 µM at the seafloor to a maximum of 1000 µM at 200 mbsf and reflect the dissolution of abundant siliceous microfossils. Silica values decrease from 400 to 999 mbsf. The theoretical opal-A/opal-CT transition is at ~600 mbsf, based on measured downhole temperatures. A strong seismic reflection is observed at this depth. Below 150 mbsf, calcium and magnesium values correlate inversely, which suggests diagenetic control and an unidentified Ca-rich lithology below the drilled section. A decrease in potassium values below 50 mbsf and an increase in fine-grained K-feldspar, identified by XRD measurements, suggests an authigenic origin for the K-feldspars.

Hydrocarbon gas contents of cores are low (<400 ppmv) within the sulfate reduction zone down to ~150 mbsf (Fig. **F26**). Below 150 mbsf, methane increases rapidly and reaches values of 20,000–40,000 ppmv between 270 and 700 mbsf, and 40,000–100,000 ppmv from 700 to 970 mbsf. These headspace gas measurements indicate only the residual gas in the pore water of cores after outgassing upon retrieval to the surface. The gas concentrations are equivalent to ~8–35 mM dissolved methane when adjusted for sample size variation, density, and porosity. Cores deeper than 700 mbsf may contain more gas because of increased lithification and retarded outgassing. Ethane is present in headspace gas samples deeper than 157 mbsf, and the C_1/C_2 value shows the expected decrease with depth for the observed geothermal gradient at this site (secant temperature gradient of 43.6°C/km). OC contents of Site 1165 sediments are low (0.1–0.8 wt%), except for high OC (1.8–2 and 1.3 wt%) beds at 122 and 828 mbsf (Fig. **F26**). Cores from within the gas hydrate stability zone (seafloor to 460 mbsf) were examined immediately upon recovery, but no hydrates were observed.

Acoustic velocities and shear-strength measurements increase as a result of normal compaction (in the upper 500 mbsf) and diagenesis (with a greater effect below 600 mbsf). Horizontal downhole *P*-wave velocities increase abruptly at 114 mbsf from ~1535 to 1575 m/s and then linearly from 114 to 603 mbsf. Other significant downhole *P*-wave velocity increases occur at 692 mbsf, at 800 mbsf (to 2660 m/s), and 960 mbsf (to 2840 m/s). These abrupt increases are observed as reflections on seismic data.

Hole 1165C was logged with a single pass of the triple combo tool from 176 to 994 mbsf and a single pass of the sonic tool from 176 to 580 mbsf. Total gamma-ray and bulk-density log traces covary, suggesting that lower-density diatom-bearing strata are present throughout the hole. The boundary between lithostratigraphic Units II and III at 305 mbsf is marked by a large fluctuation in total gamma-ray values, which suggests a shift in clay content at the boundary. The distinct silica- and calcite-cemented intervals observed in the cores are marked by inflections in most log traces.

Site 1165 provides paleontologic and sedimentologic evidence that numerous alternations or cycles between biogenic material and clay-sized terrigenous debris from Antarctica have occurred since earliest Miocene time (Fig. **F27**). The cyclicity observed in the lightness values for

F26. Organic gases and carbon in Holes 1165B and 1165C, p. 60.

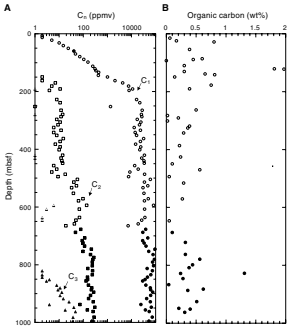

F27. Example of cyclicity observed at Site 1165, p. 61.

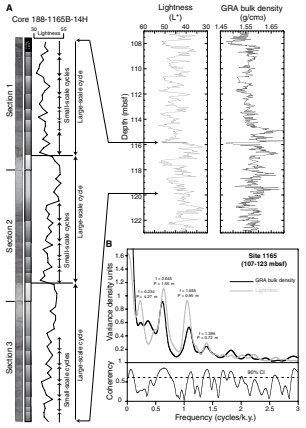

two intervals (83–100 mbsf and 107–123 mbsf; in lithostratigraphic Unit II) in the cores was analyzed for spectral content to evaluate the potential effect of Milankovitch periodicities on biogenic/terrigenous sedimentation cycles at this site (Fig. F27). For the shallower interval, significant spectral peaks are found at periods of 3.28, 1.45, 1.08, and 0.64 m thickness. A sedimentation rate of 3.5 cm/k.y. is reasonably well constrained for the interval and gives periods of 93.7, 41.5, 20.8, and 18.2 k.y., respectively. These periods are similar to the Milankovitch cycles of 100 k.y. (eccentricity), 41 k.y. (obliquity), 23 k.y., and 19 k.y. (precession), suggesting an orbitally forced origin for the light–dark cyclicity. For the deeper interval, significant spectral peaks are at 4.27, 1.55, 0.95, and 0.72 m, which have similar peak periodicity ratios to the upper interval, again suggesting an orbital origin for the deeper cycles. In the deeper interval, the sedimentation rate is less well constrained. But, by using the peak-to-peak ratios as a guide, an inferred sedimentation rate of 3.8 to 4.1 cm/k.y. would give the same periods as the shallow interval (i.e., 93.7, 41.5, 20.8, and 18.2 k.y.). The observed lightness changes correlate also to variations in bulk density and magnetic susceptibility, indicating that the lightness (color) data likely document orbitally driven changes in the Site 1165 depositional environment since at least early Miocene time. A similar approach has been used recently to detect orbital signals in upper Oligocene to lower Miocene sedimentary sequences drilled in the Ross Sea, Antarctica, by the Cape Roberts Project (Claps et al., in press). Milankovitch cyclicities have been reported for late Miocene-age and younger diatom-bearing hemipelagic and terrigenous sediments at ODP Site 1095 from a drift deposit, like the Wild Drift, adjacent to the Antarctic Peninsula (Shipboard Scientific Party, 1999).

In addition to the cyclic variations, significant uphole changes occurred at Site 1165 from early to late Miocene times (Units III and II), and include an eightfold decrease in average sedimentation rates from 12 to 1.5 cm/k.y., an increase in the total clay content, an increase in amount of sand-sized and lonestone IRD, and other changes (e.g., first appearance of glauconite) (Figs. F22, F25). The changes likely reflect shifts in the onshore Prydz Bay region (sediment source area) to paleoenvironments that produced less terrigenous sedimentation, a lower-energy current regime, and more floating ice at Site 1165 starting in middle Miocene time. The uphole shift to increased clay (~305 mbsf) and first appearance of glauconite (~220 mbsf) heralds (1) a mid-Miocene change to erosion of sedimentary basins on the shelf and (2) subsequent inferred overdeepening of the shelf to the large water depths of today. Such deep-cut erosion would be by grounded glaciers crossing the continental shelf and dispersing icebergs with entrained sediment. The times of lowest sediment supply, in the latest Neogene (i.e., above 60 mbsf), have upward-decreasing silica contents (i.e., fewer diatoms and sponge spicules) and varied (cyclic?) IRD concentrations, which may reflect increasing extent of sea ice cover and ice sheet fluctuations. During latest Neogene time, a widely recognized period of intense Antarctic (and Arctic) glacier fluctuations, thick debris flows blanketed the adjacent continental slope (Site 1167), but little sediment was deposited on Wild Drift (Site 1165).

SUMMARY

During Leg 188, three sites were drilled proximal to the East Antarctic Ice Sheet (Table T1). The transect across the Prydz Bay continental shelf, slope, and rise provides new evidence of long- and short-term variations in paleoenvironments (i.e., depositional, glacial, and inferred climate) extending from Holocene to Mesozoic times. The shelf site (Site 1166) documents the earliest stages of East Antarctic glaciation from inferred temperate climates (i.e., with vegetation) to transitional environments of proximal glaciers to full glacial and interglacial conditions with intermittently grounded glaciers on the shelf. Samples from Site 1167 on the slope are latest Neogene sediments that attest to rapid deposition and the variability of onshore erosion areas and glaciomarine depositional settings in front of grounded ice sheets during glacial–interglacial periods. On the continental rise, at Site 1165, the drilling record documents a long-term lower to upper Miocene transition from temperate to cold-climate glaciation, with superimposed short-term glacier fluctuations since early Miocene time.

These sites document changing paleoenvironments (Fig. F28), with long-period changes that may mark the transition from more temperate times of wet-based onshore glacier systems with fluvial outwash (i.e., before 13–14 Ma; middle Miocene) to cold times of dry-based systems with overdeepened shelf and subglacial deposition (late Miocene and younger). The notable variability in IRD concentrations since middle Miocene time suggests that the transition period switched repeatedly between the temperate and cold glacier systems. The short cyclic variations (at Milankovitch periodicities) recorded by the gray/green (dark/light) facies observed at Site 1165 may track the persistent seaward-landward movements of onshore ice sheets and their internal ice streams. The glacier systems provided more terrigeneous sediments (gray facies) during times of glacial advances and less terrigenous sediment during periods of glacial retreat (interglacials; green facies).

Leg 188, together with previous (e.g., ODP Legs 119 and 178) and future Antarctic continental margin drilling transects, can provide the hard-earned proximal geologic samples needed to link the histories of the Antarctic Ice Sheet and the distal ocean-current and climate systems.

F28. Conceptual diagrams showing changes in glacial erosion and sedimentation on the Antarctic continental margin, p. 63.

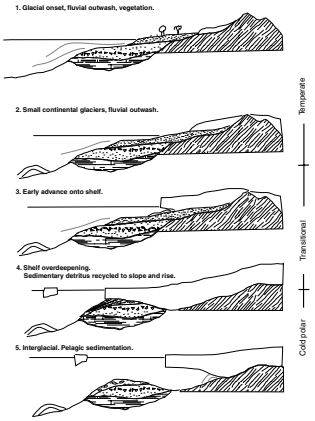

REFERENCES

Abreu, V.S., and Anderson, J.B., 1998. Glacial eustasy during the Cenozoic: sequence stratigraphic implications. *AAPG Bull.,* 82:1385–1400.

Allison, I.F., 1979. The mass budget of the Lambert Glacier drainage basin, Antarctica. *J. Glaciol.,* 22:223–235.

Alonso, B., Anderson, J.B., Diaz, J.I., and Bartek, L.R., 1992. Pliocene-Pleistocene seismic stratigraphy of the Ross Sea: evidence for multiple ice sheet grounding episodes. *In* Elliot, D.H. (Ed.), *Contributions to Antarctic Research III,* Antarct. Res. Ser., 57:93–103.

Barker, P.F., Barrett, P.J., Camerlenghi, A., Cooper, A.K., Davey, F.J., Domack, E., Escutia, C., Kristoffersen, Y., and O'Brien, P.E., 1998. Ice sheet history from Antarctic continental margin sediments: the ANTOSTRAT approach. *Terra Antart.,* 5:737–760.

Barker, P.F., Camerlenghi, A., Acton, G.D., et al., 1999. *Proc. ODP, Init. Repts.,* 178: College Station (Ocean Drilling Program).

Barrett, P., 1999. Antarctic climate history over the last 100 million years. *In* Barrett, P., and Orombelli, G. (Eds.), *Proceedings of the Workshop: Geological Records of Global and Planetary Changes. Siena, 1998*. Terra Antart. Rep., 3:53–72.

Barron, J., Larsen, B., et al., 1989. *Proc. ODP, Init. Repts.,* 119: College Station, TX (Ocean Drilling Program).

————, 1991. *Proc. ODP, Sci. Results,* 119: College Station, TX (Ocean Drilling Program).

Barron, J.A., Baldauf, J.G., Barrera, E., Caulet, J.-P., Huber, B.T., Keating, B.H., Lazarus, D., Sakai, H., Thierstein, H.R., and Wei, W., 1991. Biochronologic and magnetochronologic synthesis of Leg 119 sediments from the Kerguelen Plateau and Prydz Bay, Antarctica. *In* Barron, J., Larsen, B., et al., *Proc. ODP, Sci. Results,* 119: College Station, TX (Ocean Drilling Program), 813–848.

Boulton, G.S., 1990. Sedimentary and sea level changes during glacial cycles and their control on glacimarine facies architecture. *In* Dowdeswell, J.A., and Scourse, J.D. (Eds.), *Glacimarine Environments: Processes and Sediments*. Geol. Soc. Spec. Publ. London, 53:15–52.

Budd, W., 1966. The dynamics of the Amery Ice Shelf. *J. Glaciol.,* 6:335–358.

Budd, W., Cory, M.J., and Jacka, T.H., 1982. Results from the Amery Ice Shelf Project. *Ann. Glaciol.,* 3:36–41.

Cape Roberts Science Team, 1998. Initial report on CRP-1. *Terra Antart.,* 5.

————, 1999. Studies from the Cape Roberts Project, Ross Sea, Antarctica—Initial report on CRP-2/2A. *Terra Antart.,* 6(½).

————, in press. Initial report of the Cape Roberts Project CRP-3. *Terra Antart.,* 7(1/2).

Claps, M., Niessen, F., and Florindo, F., in press. High-frequency analysis of physical properties from CRP-2/2A and implication for sedimentation rate. *Terra Antart.*

Cooper, A., Stagg, H., and Geist, E., 1991a. Seismic stratigraphy and structure of Prydz Bay, Antarctica: implications from Leg 119 drilling. *In* Barron, J., Larsen, B., et al., *Proc. ODP, Sci. Results,* 119: College Station, TX (Ocean Drilling Program), 5–26.

Cooper, A.K., Barrett, P.J., Hinz, K., Traube, V., Leitchenkov, G., and Stagg, H.M.J., 1991b. Cenozoic prograding sequences of the Antarctic continental margin: a record of glacio-eustatic and tectonic events. *Mar. Geol.,* 102:175–213.

Denton, G.H., and Hughes, T.J. (Eds.), 1981. *The Last Great Ice Sheets:* New York (Wiley).

Denton, G.H., Prentice, M.L., and Burckle, L.H., 1991. Cainozoic history of the Antarctic ice sheet. *In* Tingey, R.J. (Ed.), *The Geology of Antarctica.* Oxford Monogr. Geol. Geophys., 17:365–433.

Domack, E., Jull, A.J.T., and Donahue, D.J., 1991. Holocene chronology for the unconsolidated sediments at Hole 740A: Prydz Bay, East Antarctica. *In* Barron, J.,

Larsen, B., et al., *Proc. ODP, Sci. Results,* 119: College Station, TX (Ocean Drilling Program), 747–750.

Domack, E., O'Brien, P.E., Harris, P.T., Taylor, F., Quilty, P.G., DeSantis, L., and Raker, B., 1998. Late Quaternary sedimentary facies in Prydz Bay, East Antarctica and their relationship to glacial advance onto the continental shelf. *Antarct. Sci.,* 10:227–235.

Fedorov, L.V., Grikurov, G.E., Kurinin, R.G., and Masolov, V.N., 1982. Crustal structure of the Lambert Glacier Area from geophysical data. *In* Craddock, C., Loveless, J.K., Vierima, T.L., and Crawford, K. (Eds.), *Antarctic Geoscience:* Madison (Univ. Wisconsin Press), 931–936.

Fielding, C.R., Woolfe, K.J., Howe, J.A., and Lavelle, M.A., 1998. Sequence stratigraphic analysis of CRP-1, Cape Roberts Project, McMurdo Sound, Antarctica. *Terra Antart.,* 5:353–361.

Flower, B.P., 1999. Cenozoic deep-sea temperatures and polar glaciation: the oxygen isotope record. *In* Barrett, P., and Orombelli, G. (Eds.), *Proceedings of the Workshop: Geological Records of Global and Planetary Changes*. Terra Antart. Rep., 3:27–42.

Forsberg, C.F., Solheim, A., Elverhøi, A., Jansen, E., Channell, J.E.T., and Andersen, E.S., 1999. The depositional environment of the western Svalbard margin during the late Pliocene and the Pleistocene; sedimentary facies changes at Site 986. *In* Raymo, M.E., Jansen, E., Blum, P., and Herbert, T.D. (Eds.), *Proc. ODP, Sci. Results,* 162: College Station, TX (Ocean Drilling Program), 233–246.

Goodwin, I., 1992. Holocene deglaciation, sea level change and the emergence of the Windmill Islands, Budd Coast, Antarctica. *Quat. Res.,* 40:70–80.

Hambrey, M.J., 1991. Structure and dynamics of the Lambert Glacier-Amery ice shelf system: implications for the origin of Prydz Bay sediments. *In* Barron, J.A., Larsen, B., et al., *Proc. ODP, Sci. Results,* 119: College Station, TX (Ocean Drilling Program), 61–75.

Hambrey, M.J., Ehrmann, W.U., and Larsen, B., 1991. Cenozoic glacial record of the Prydz Bay continental shelf, East Antarctica. *In* Barron, J., Larsen, B., et al., *Proc. ODP, Sci. Results,* 119: College Station, TX (Ocean Drilling Program), 77–132.

Hambrey, M.J., and McKelvey, B., 2000. Neogene fjordal sedimentation on the western margin of the Lambert Graben, East Antarctica. *Sedimentology,* 47:577–608.

Harris, P.T., and O'Brien, P.E., 1996. Geomorphology and sedimentology of the continental shelf adjacent to Mac Robertson Land, East Antarctica: a scalped shelf. *Geo-Mar. Lett.,* 16:287–296.

Harris, P.T., O'Brien, P.E., Sedwick, P., and Truswell, E.M., 1996. Late Quaternary history of sedimentation on the Mac.Robertson Shelf, East Antarctica: problems with ^{14}C-dating of marine sediment cores. *Pap. Proc. R. Soc. Tasmania,* 130:47–53.

Harris, P.T., Taylor, F., Pushina, Z., Leitchenkov, G., O'Brien, P.E., and Smirnov, V., 1998. Lithofacies distribution in relation to geomorphic provinces of Prydz Bay, East Antarctica. *Antarct. Sci.,* 10:227–235.

Huybrechts, P., 1993. Glaciological modelling of the Late Cenozoic East Antarctic ice sheet: stability or dynamism. *Geograf. Ann.,* 75A:221–238.

Kuvaas, B., and Leitchenkov, G., 1992. Glaciomarine turbidite and current-controlled deposits in Prydz Bay, Antarctica. *Mar. Geol.,* 108:365–381.

Leitchenkov, G., Stagg, H.M.J., Gandjukhin, V., Cooper, A.K., Tanahashi, M., and O'Brien, P., 1994. Cenozoic seismic stratigraphy of Prydz Bay (Antarctica). *In* Cooper, A.K., Barker, P.F., Webb, P.-N., and Brancolini, G. (Eds.), *The Antarctic Continental Margin: Geophysical and Geological Stratigraphic Records of Cenozoic Glaciation, Paleoenvironments and Sea-level Change*. Terra Antart., 1:395–398.

Licht, K.M., Jennings, A.E., Andrews, J.T., and Williams, K.M., 1996. Chronology of late Wisconsin ice retreat from the western Ross Sea. *Geology,* 24:223–226.

McKelvey, B.C., and Stephenson, N.C.N., 1990. A geological reconnaissance of the Radok Lake area, Amery Oasis, Prince Charles Mountains. *Antarct. Sci.,* 2:53–66.

McLoughlan, S., and Drinnan, A.N., 1997. The sedimentary and revised stratigraphy of the Permian-Triassic Flagstone Bench Formation, Northern Prince Charles Mountains, east Antarctica. *Geol. Mag.,*134:335–353.

Miall, A.D., 1986. Eustatic sea level changes interpreted from seismic stratigraphy: a critique of the methodology with particular reference to the North Sea Jurassic record. *AAPG Bull.,* 70:131–137.

Miller, K.G., Barrera, E., Olsson, R.K., Sugarman, P.J., and Savin, S.M., 1999. Does ice drive early Maastrichtian eustacy? *Geology,* 27:783–786.

Mizukoshi, I., Sunouchi, H., Saki, T., Sato, S., and Tanahashi, M., 1986. Preliminary report of geological geophysical surveys off Amery Ice Shelf, East Antarctica. *Mem. Nat. Inst. Polar Res. Spec. Iss. Jpn.,* 43:48–61.

O'Brien, P.E., De Santis, L., Harris, P.T., Domack, E., and Quilty, P.G., 1999. Ice shelf grounding zone features of western Prydz Bay, Antarctica: sedimentary processes from seismic and sidescan images. *Antarct. Sci.,* 11:78–91.

O'Brien, P.E., and Harris, P.T., 1996. Patterns of glacial erosion and deposition in Prydz Bay and the past behaviour of the Lambert Glacier. *Pap. Proc. R. Soc. Tasmania,*130:79–86.

O'Brien, P.E., and Leitchenkov, G., 1997. Deglaciation of Prydz Bay, East Antarctica, based on echo sounder and topographic features. *In* Barker, P.F., and Cooper, A.K. (Eds.), *Geology and Seismic Stratigraphy of the Antarctic Margin* (Pt. 2). Am. Geophys. Union Antarct. Res. Ser., 71:109–125.

O'Brien, P.E., Cooper, A.K., Richter, C., Macphail, M., Truswell, E.M., and Leg 188 Shipboard Scientific Party, in press. Results from ODP Leg 188—glacial onset and late Neogene fluctuations. *AGU 2000 Fall Meeting Abstract.*

Pickard, J. (Ed.), 1986. *Antarctic Oasis: Terrestrial Environments and History of the Vestfold Hills, East Antarctica:* Sydney (Academic Press).

Quilty, P.G., 1991. The geology of Marine Plain, Vestfold Hills, East Antarctica. *In* Thomson, M.R.A., Crane, J.A., and Thomson, J.W. (Eds.), *The Geological Evolution of Antarctica:* New York (Cambridge Univ. Press).

————, 1993. Coastal Neogene sections and their contribution to the ice sheet evolution debate. *In* Kennett, J.P., and Warnke, D.A. (Eds.), *The Antarctic Paleoenvironment: a Perspective on Global Change.* Am. Geophys. Union, Antarct. Res. Ser., 60:251–264.

Quilty, P.G., Truswell, E.M., O'Brien, P.E., and Taylor, F., 2000. Paleocene-Eocene biostratigraphy and palaeoenvironment of East Antarctica: new data from the Mac. Robertson Shelf and western parts of Prydz Bay. *AGSO Journal of Geology and Geophysics,* 17(5/6): 1333–1343.

Rebesco, M., Larter, R.D., Barker, P.F., Camerlenghi, A., and Vanneste, L.E., 1997. The history of sedimentation on the continental rise west of the Antarctic Peninsula. *In* Barker, P.F., and Cooper, A.K. (Eds.), *Geology and Seismic Stratigraphy of the Antarctic Margin* (Pt. 2). Antarctic Res. Ser., 71:29–50.

Scott, R.F., 1905. *The Voyage of the Discovery:* London (Charles Scribners and Sons).

Shipboard Scientific Party, 1999. Leg 178 summary: Antarctic glacial history and sea-level change. *In* Barker, P.F., Camerlenghi, A., Acton, G.D., et al., *Proc. ODP, Init. Repts.,* 178: College Station TX (Ocean Drilling Program), 1–58.

Smith, N.R., Zhaoqian, D.J., Kerry, K.R., and Wright, S., 1984. Water masses and circulation in the region of Prydz Bay, Antarctica. *Deep-Sea Res. Part A,* 31:1121–1147.

Solheim, A., Forsberg, C.F., and Pittenger, A., 1991. Stepwise consolidation of glacigenic sediments related to the glacial history of Prydz Bay, East Antarctica. *In* Barron, J., Larsen, B., et al., *Proc. ODP, Sci. Results,* 119: College Station, TX (Ocean Drilling Program), 169–184.

Stagg, H.M.J., 1985. The structure and origin of Prydz Bay and MacRobertson Shelf, East Antarctica. *Tectonophysics,* 114:315–340.

Tingey, R.J., 1982. The geologic evolution of the Prince Charles Mountains—an Antarctic Archean cratonic block. *In* Craddock, C. (Ed.), *Antarctic Geoscience:* Madison (Univ. Wisconsin Press), 455–464.

————, 1991. Commentary on schematic geological map of Antarctica, scale 1:10,000,000. *Bull.—Bur. Miner. Resour., Geol. Geophys. (Aust.),* Rep. 238.

Truswell, E.M., Dettmann, M.E., and O'Brien, P.E., 1999. Mesozoic palynofloras from the Mac Robertson Shelf, East Antarctica: geological and phytogeographic implications. *Antarct. Sci.,* 11:239–255.

Turner, B.R., 1991. Depositional environment and petrography of preglacial continental sediments from Hole 740A, Prydz Bay, Antarctica. *In* Barron, J., Larsen, B., et al., *Proc. ODP, Sci. Results,* 119: College Station, TX (Ocean Drilling Program), 45–56.

Turner, B.R., and Padley, D., 1991. Lower Cretaceous coal-bearing sediments from Prydz Bay, Antarctica. *In* Barron, J., Larsen, B., et al., *Proc. ODP, Sci. Results,* 119: College Station, TX (Ocean Drilling Program), 57–60.

Vanney, J.R., and Johnson, G.L., 1985. GEBCO bathymetric sheet 5.18 (circum-Antarctic). *In* Jacobs, S.S. (Ed.), *Oceanology of the Antarctic Continental Shelf*. Am. Geophys. Union, Antarct. Res. Ser., 43:1–3.

Vorren, T.O., and Laberg, J.S., 1997. Trough mouth fans—palaeoclimate and ice sheet monitors. *Quat. Sci. Rev.,* 16:865–881.

Warnke, D.A., Marzo, B., and Hodell, D.A., 1996. Major deglaciation of east Antarctica during the early late Pliocene? Not likely from a marine perspective. *In* Poore, R.Z. and Sloan, L.C. (Eds.), *Climates and Climate Variability of the Pliocene.* Mar. Micropaleontol., 27:237–251.

Webb, P.N., Harwood, D.M., McKelvey, B.C., Mercer, J.H., and Stott, L.D., 1984. Cenozoic marine sedimentation and ice-volume variation on the East Antarctic Craton. *Geology,* 12:287–291.

Wise, S.W., Jr., Breza, J.R., Harwood, D.M., Wei, W., and Zachos, J.C., 1992. Paleogene glacial history of Antarctica in light of Leg 120 drilling results. *In* Wise, S.W., Jr., Schlich, R., et al., *Proc. ODP, Sci. Results,* 120: College Station, TX (Ocean Drilling Program), 1001–1030.

Wong, A.P.S., 1994. Structure and dynamics of Prydz Bay, Antarctica, as inferred from a summer hydrographic data set [M.S. thesis]. Univ. Tasmania.

Figure F1. The Lambert Glacier drainage basin, East Antarctica, showing the location of the Gamburtsev Mountains. Ice surface elevations are in meters (modified from Hambrey, 1991). Gl. = Glacier.

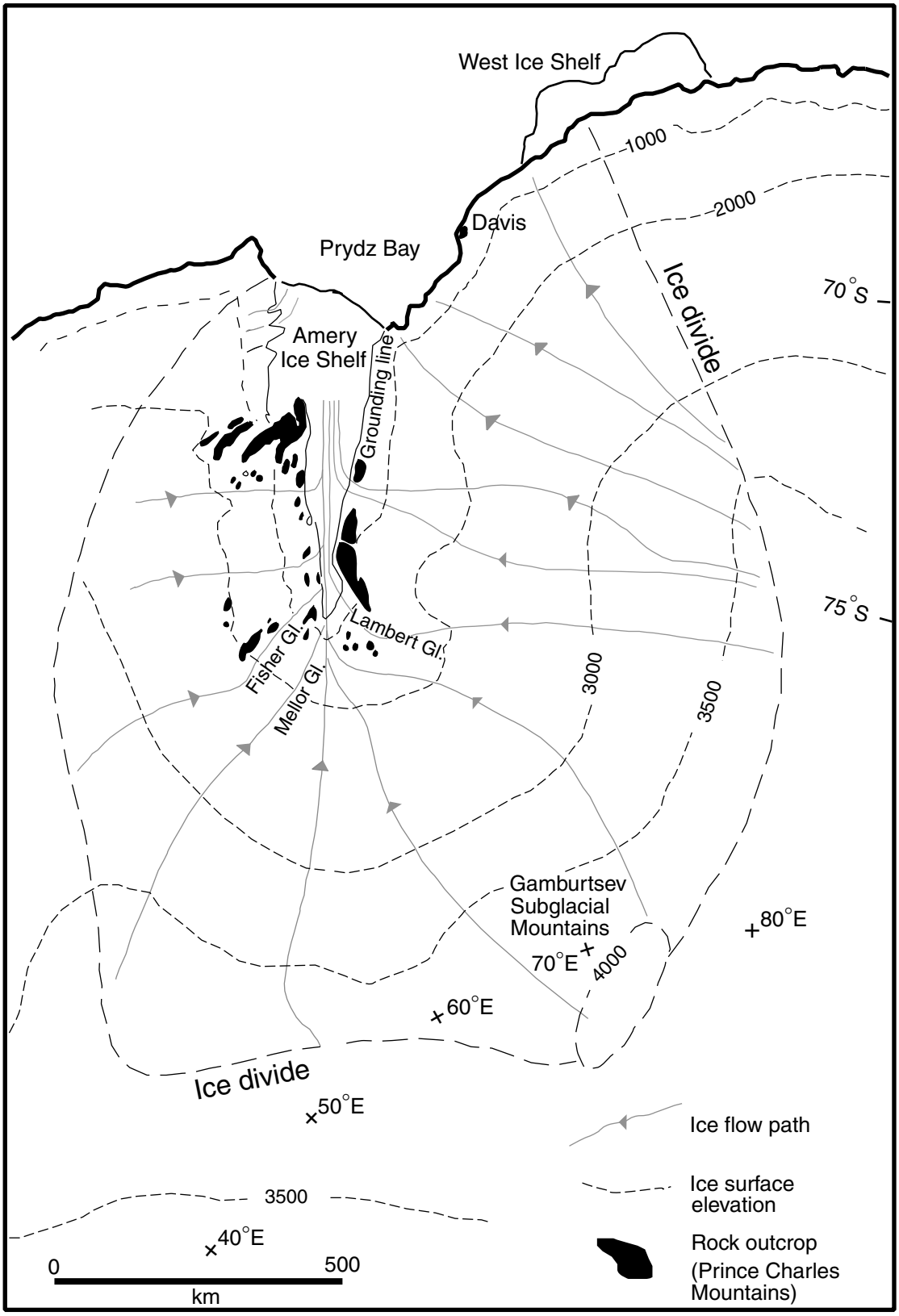

Figure F2. Model of trough mouth fan deposition. **A.** During periods of maximum ice advance, basal debris is delivered to the shelf edge by grounded ice and redistributed by sediment gravity flows and meltwater plumes. **B.** During interglacial conditions, the outer shelf is reworked by iceberg ploughing and biogenic input from the water column. TMF = trough mouth fan.

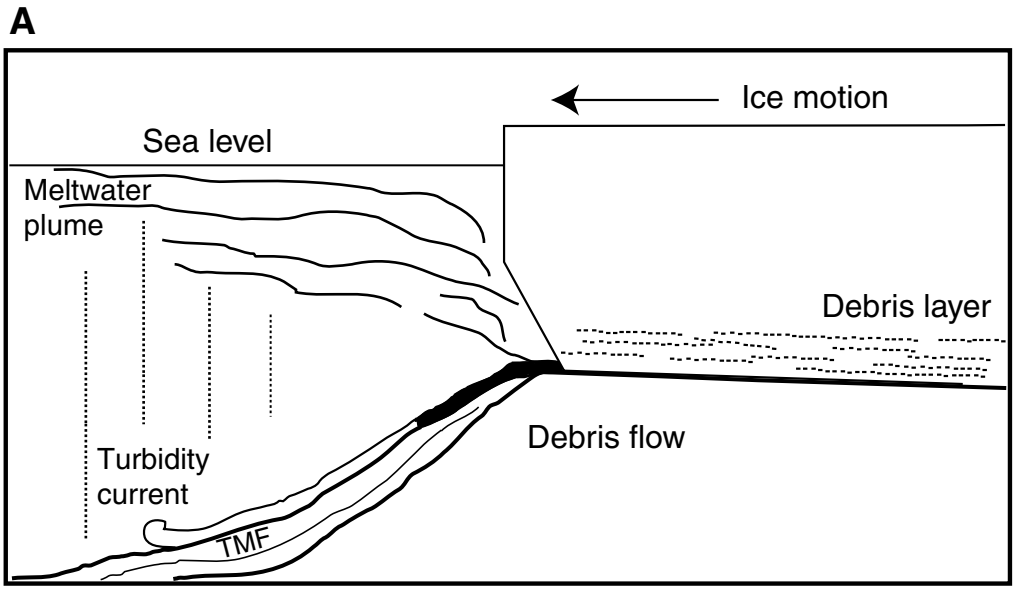

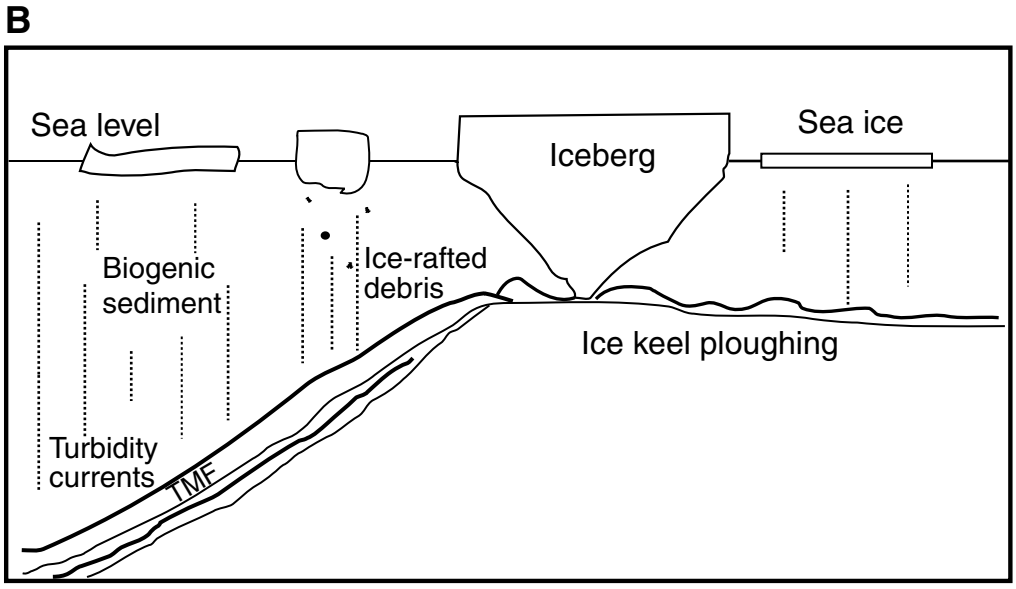

Figure F3. Bathymetric features of and ODP sites in Prydz Bay, Antarctica. Contours are in meters below sea level. The outer edge of the Amery Ice Shelf is shown for the years 1964 (black) and 1991 (shaded).

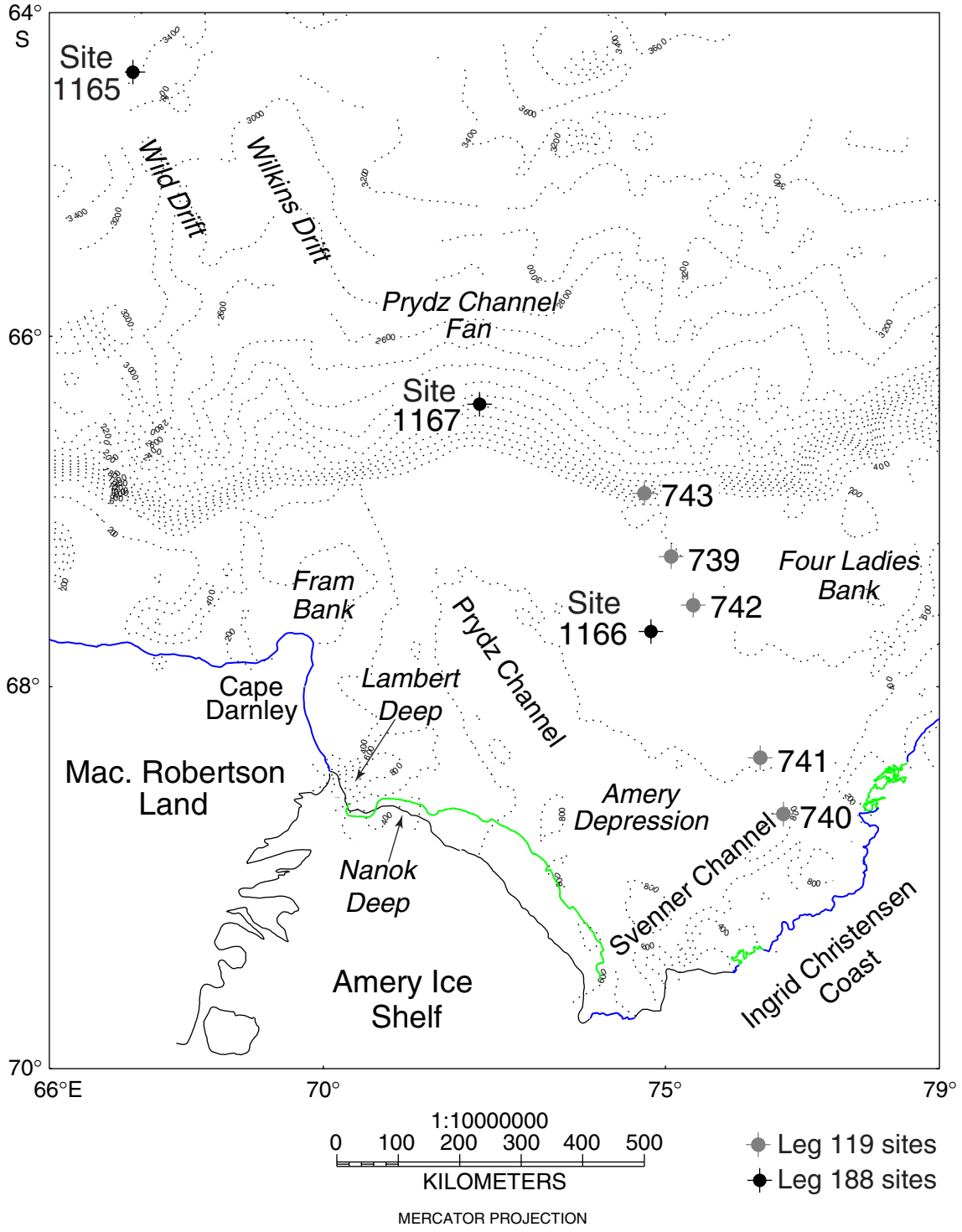

Figure F4. Generalized map of circulation in the Prydz Bay region (modified from Smith et al., 1984). The direction of flow is indicated by arrows. Site 1165 is located on the margin of the Antarctic Divergence, a series of cyclonic gyres at the boundary between the Antarctic Circumpolar Current (ACC) and the Polar Current. These major currents move in opposite directions and extend into Antarctic deep water.

Figure F5. Pre-Mesozoic geology of the Lambert Glacier drainage basin and Prydz Bay region after Tingey (1982) and Federov et al. (1982). Late Proterozoic metamorphic rocks in the northern Prince Charles Mountains, Mac. Robertson Land, and Ingrid Christensen Coast are mostly granulite facies. The southern Prince Charles Mountains metasediments are generally chlorite grade in some outcrops displaying primary sedimentary structures. Not shown are Mesozoic and Eocene basic igneous dykes in the Beaver Lake area. (**Figure shown on next page.**)

Figure F5 (continued). (Caption shown on previous page.)

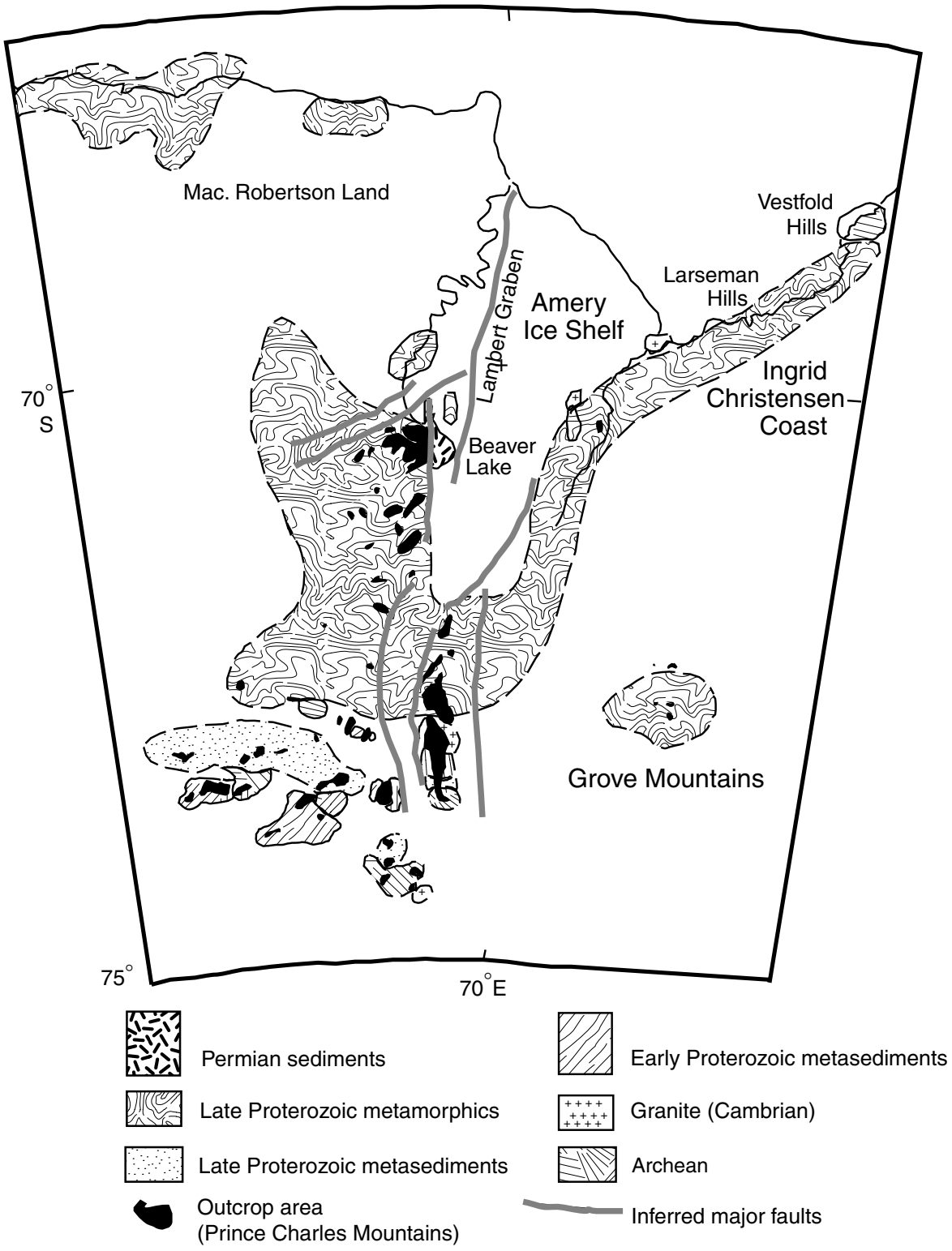

Figure F6. Structure contour map of the top of basement in Prydz Bay. Contours are in milliseconds two-way traveltime below sea level. A northeast-trending, faulted ridge separates the Prydz Bay Basin from the outer shelf.

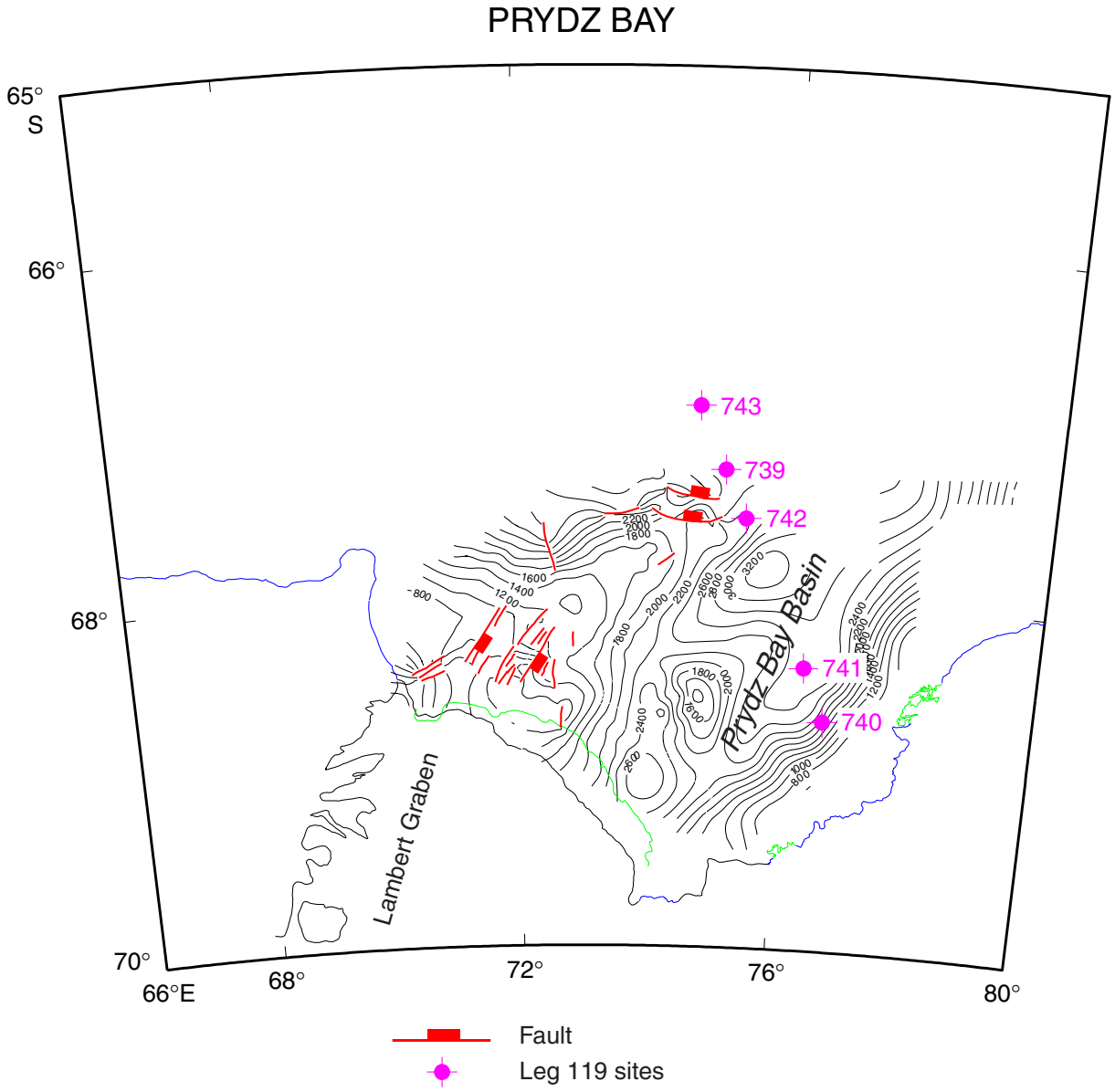

Figure F7. Top of the Lower Cretaceous structure contour map (surface PS.2B of Cooper et al., 1991a). Contours are in milliseconds two-way traveltime below sea level.

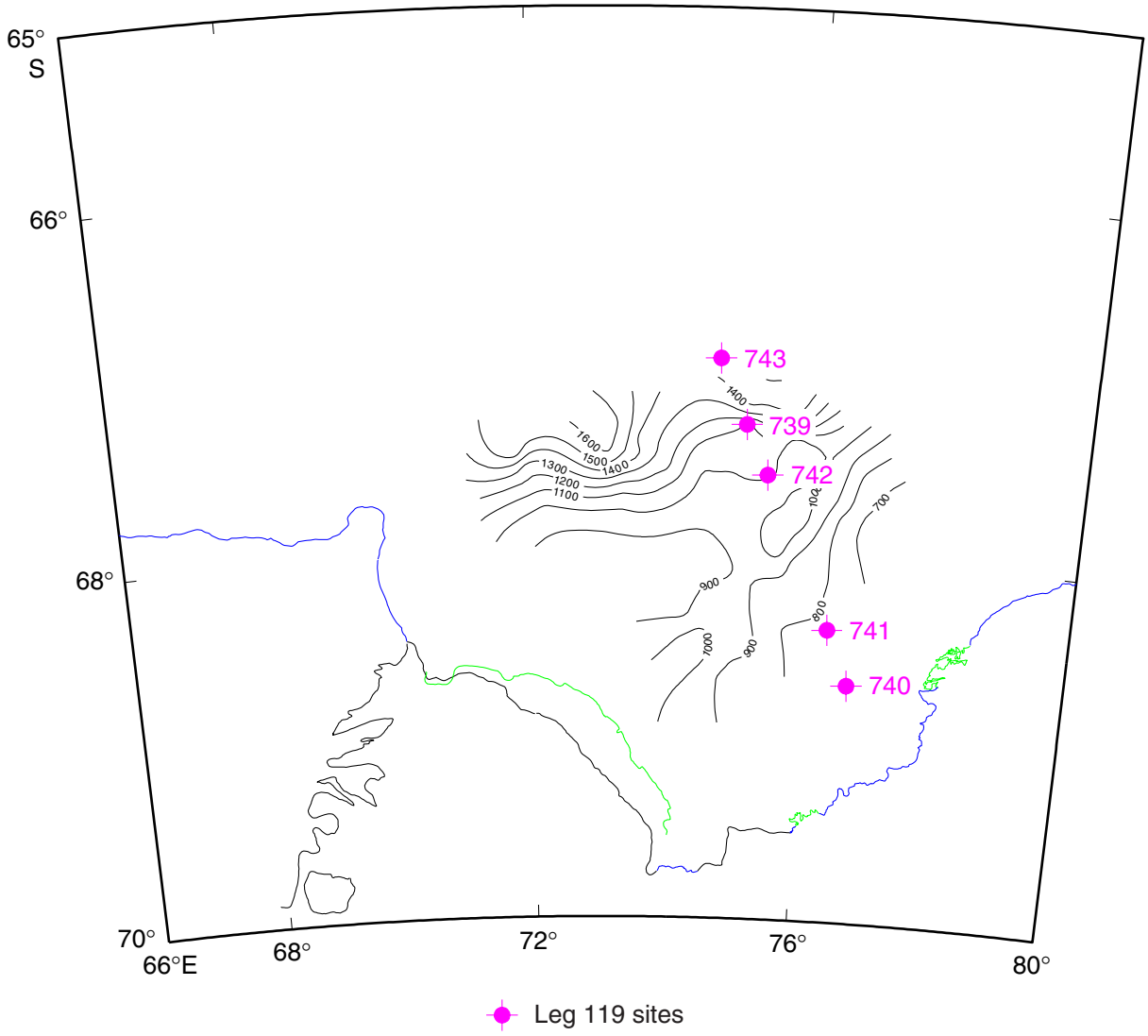

Figure F8. Sketch profile of seismic sequences drilled during Leg 119, based on line BMR 33-21. PS.1 is composed of Neogene topset and foreset beds, PS.2A is Paleogene glacial and preglacial sediment, PS.2B is Lower Cretaceous nonmarine sediment, PS.4 is undated nonmarine red beds, and PS.5 is basement.

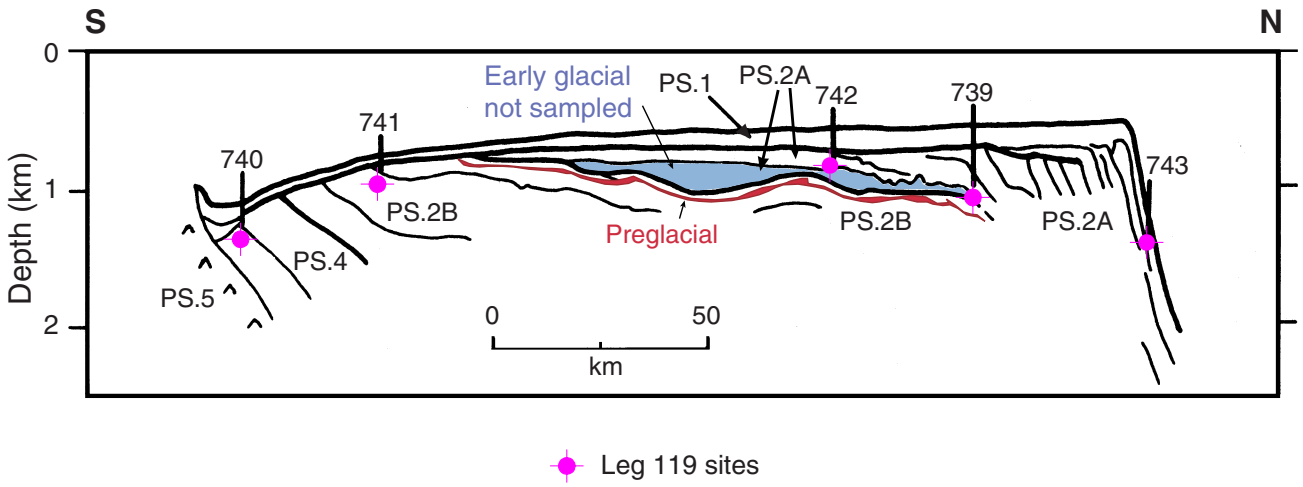

Figure F9. Isopach map of postsurface PP12 sediments. Contours are in milliseconds two-way traveltime; dashed line = the shelf edge. Deposition is concentrated in the Prydz Channel Fan with relatively thin subglacial sediment on Four Ladies Bank, several patches of diatom ooze in Svenner Channel, and a morainal bank on the western side of the bay. Elsewhere, post-PP12 sediments are present but are too thin to be resolved on seismic records.

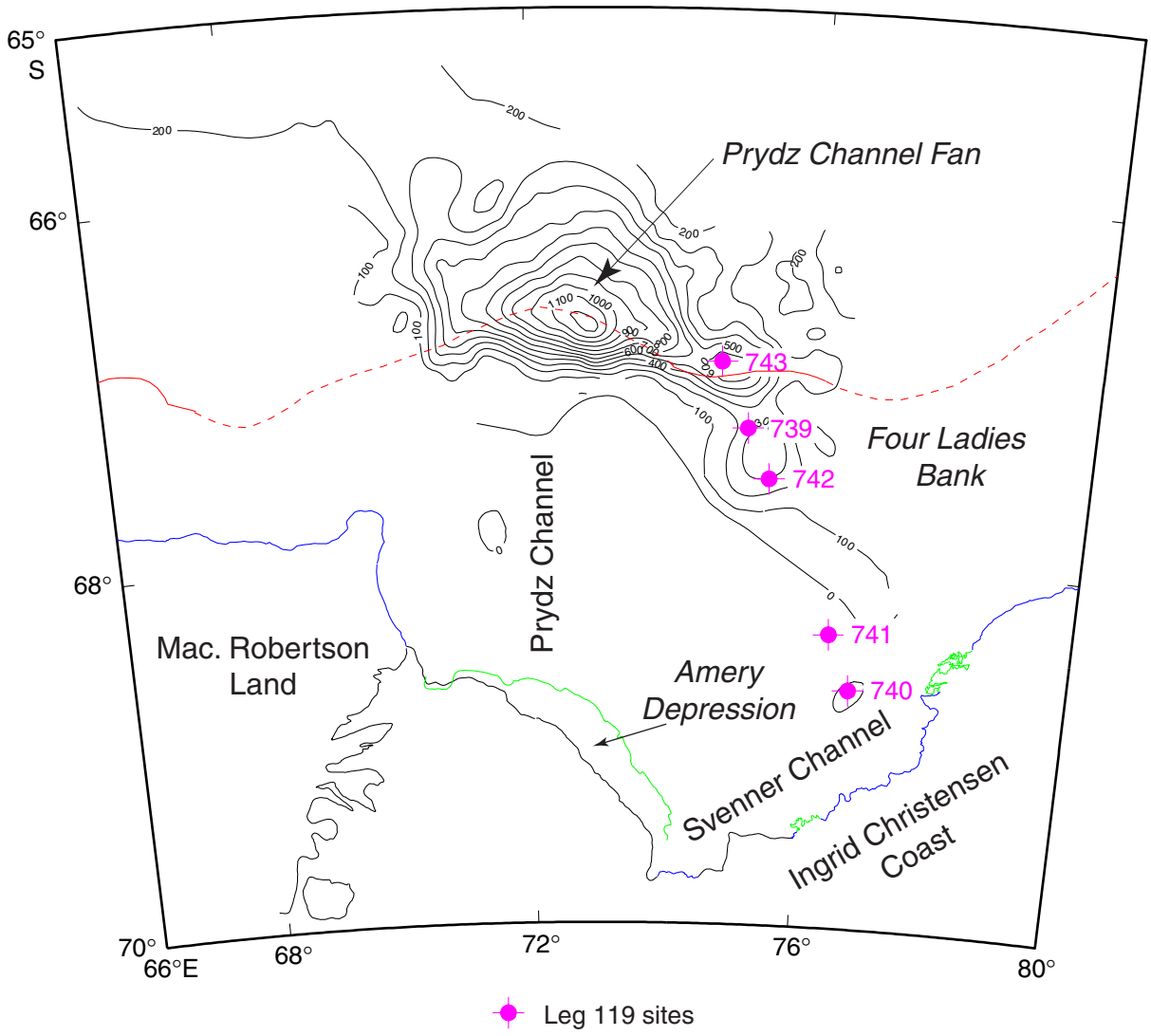

Figure F10. A. Overview map of the primary Leg 188 drill sites with respect to port of origin (Fremantle) and destination port (Hobart). **B.** Map of East Antarctic coastline between 50°E and 90°E, showing the location of Prydz Bay, Mac. Robertson Land, Antarctic stations, Leg 119 drill sites (light circles), and Leg 188 drill sites (dark circles).

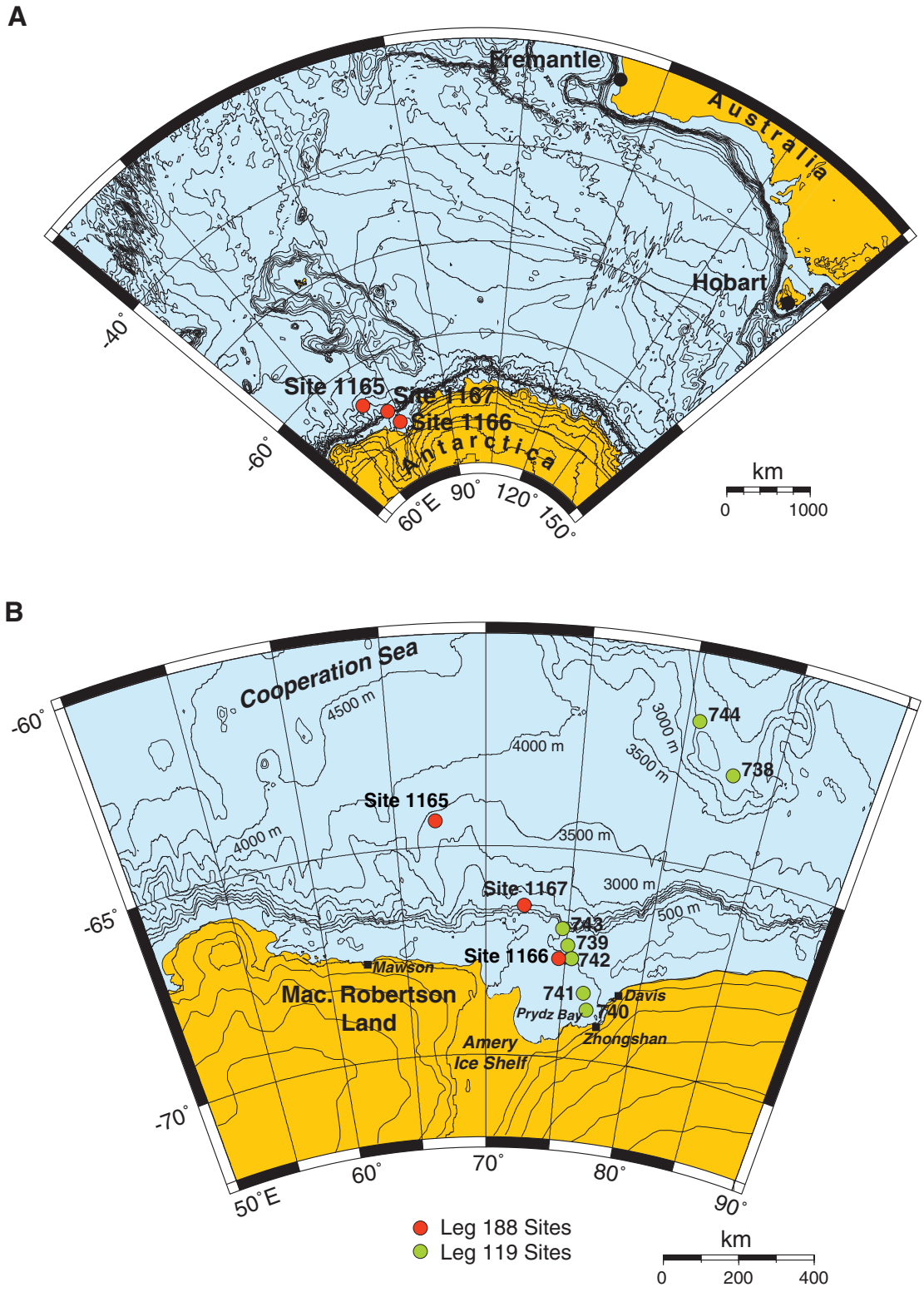

Figure F11. Seismic reflection profile BMR 33-23P3 over Site 1166 showing lithostratigraphic units, ages, rock types, paleoenvironmental interpretation, the schematic section, and downhole-logging units. See Figure **F14,** p. 43, for the key to lithostratigraphic diagrams. SP = shotpoints; TD = total depth.

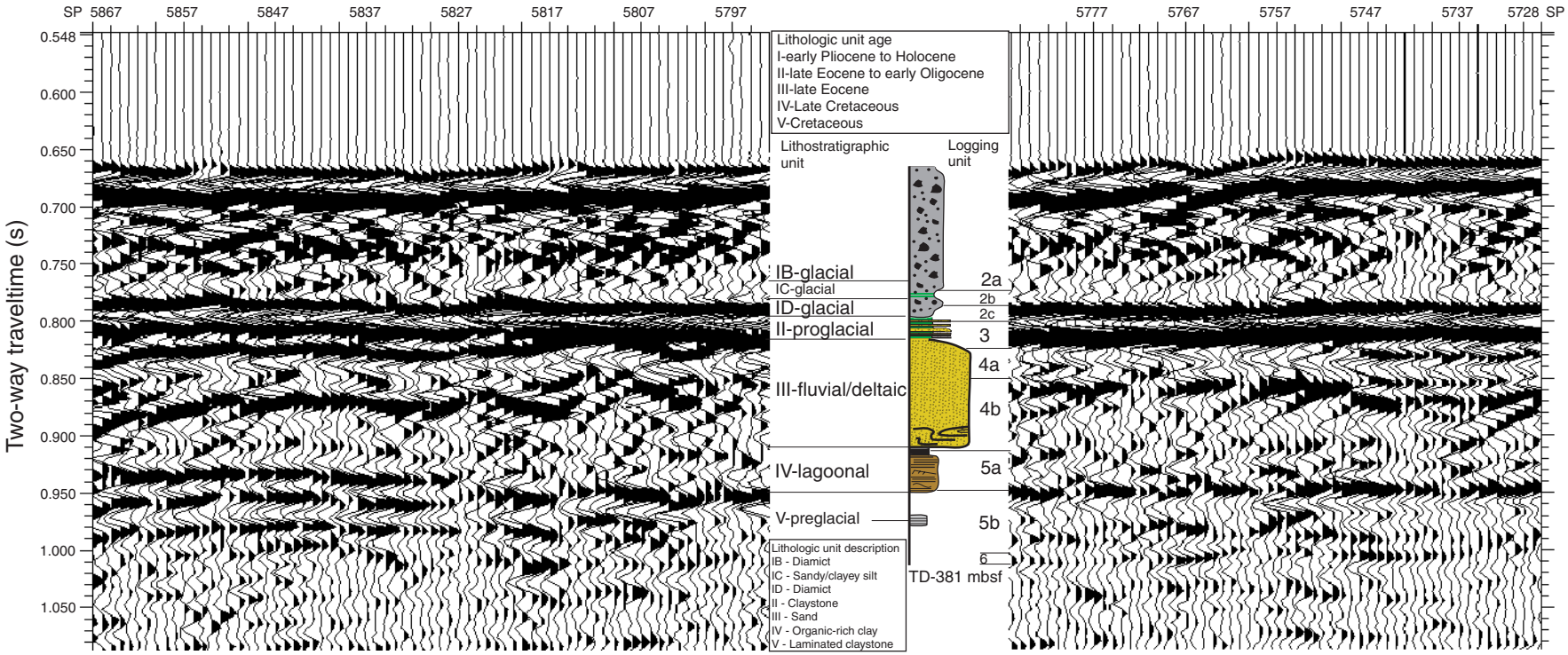

Figure F12. Composite stratigraphic section for Site 1166 showing core recovery, a simplified summary of lithology, lithostratigraphic unit boundaries, and age. Gamma-ray and resistivity curves are derived from downhole logs along with minerals identified by XRD, which shows the percentage of the most abundant minerals.

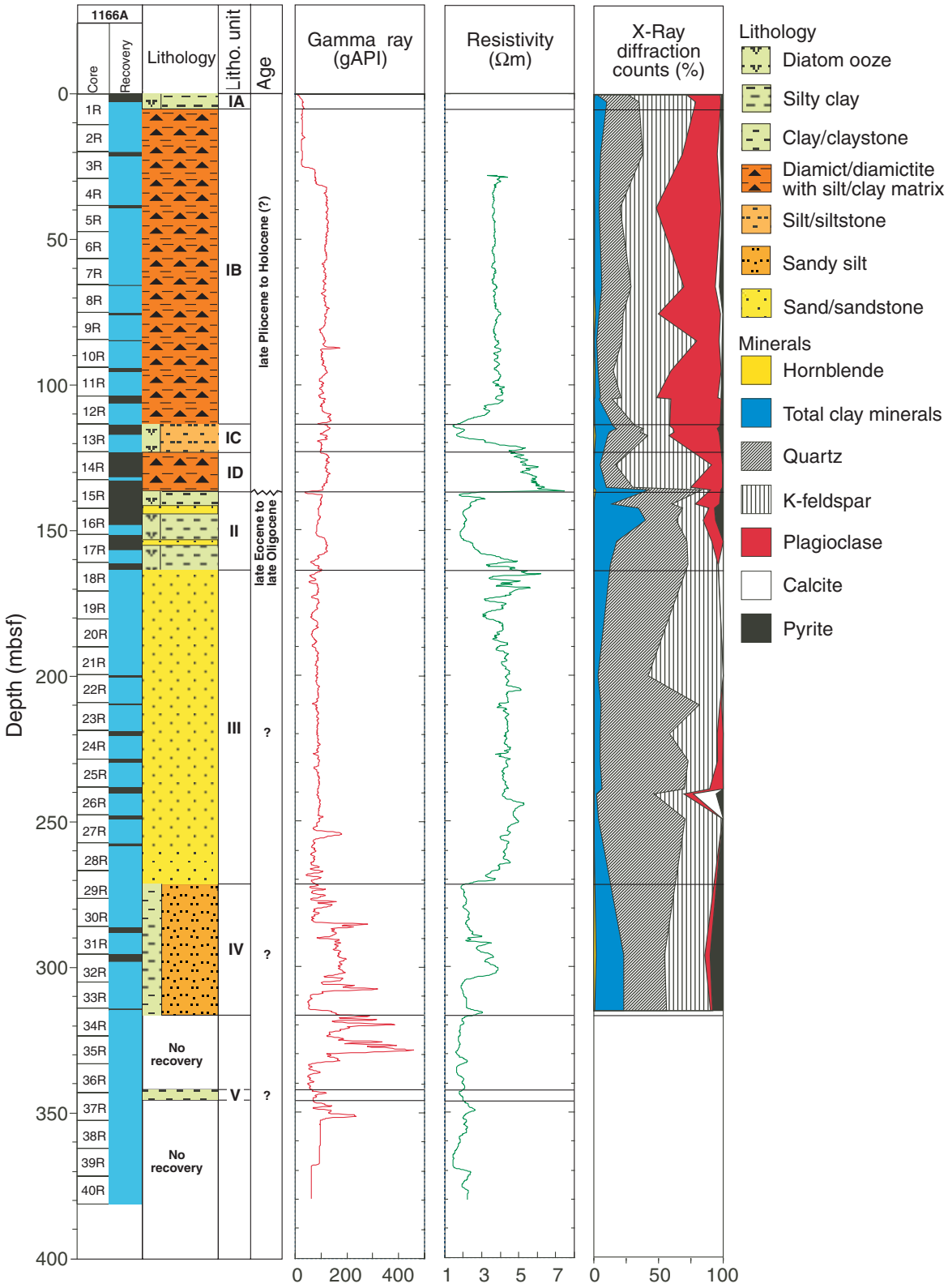

Figure F13. Plots showing biostratigraphic age control and magnetostratigraphic polarity intervals for Site 1166. FO = first occurrence and LO = last occurrence. The inclinations obtained from split cores are compared with inclinations from stepwise-demagnetized discrete samples (solid squares). Polarity is shown on the log to the right. Black represents normal and white represents reversed polarity intervals.

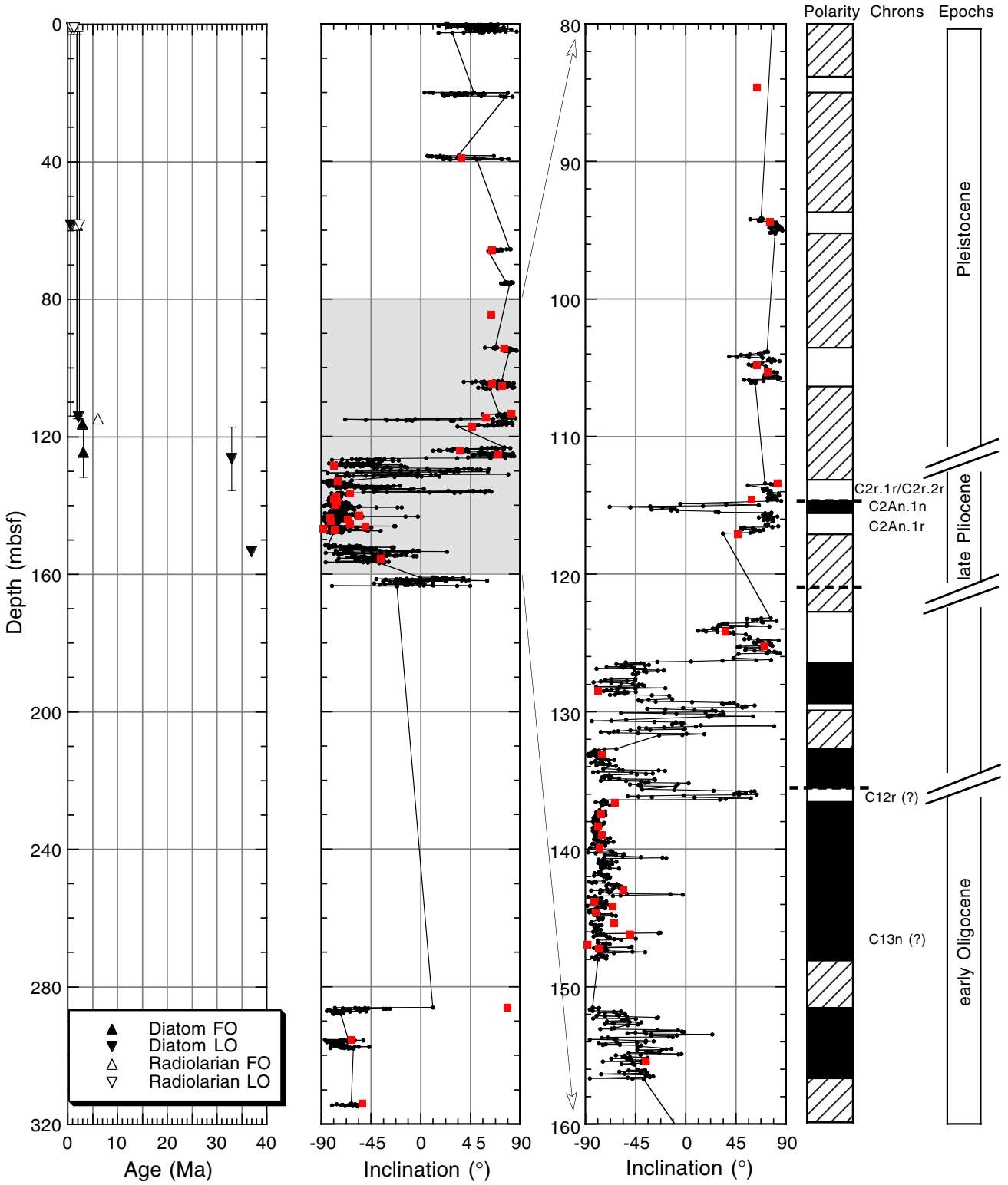

Figure F14. Downhole wireline logs from Site 1166 showing density, porosity, resistivity, and sonic velocity curves with the logging units marked. The core index property measurements of density and porosity and the lithostratigraphic units from core analysis are also shown. LWD = logging while drilling, RHOM = corrected bulk density in g/cm^3, and APLC = accelerator porosity sonde near-array limestone porosity corrected in m^3/m^3. (**Figure shown on next page.**)

Figure F14 (continued). (Caption shown on previous page.)

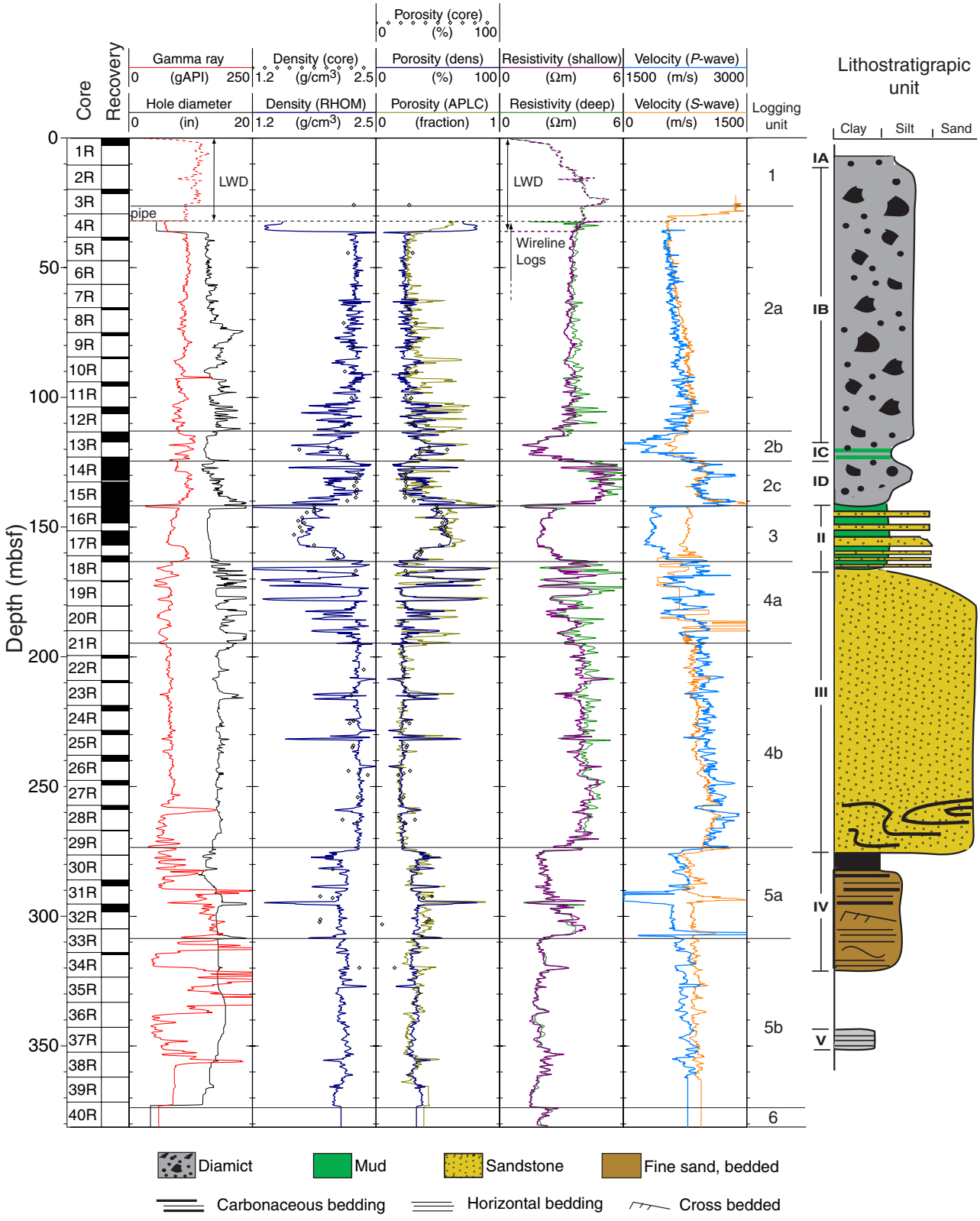

Figure F15. Representative examples of Formation MicroScanner (FMS) resistivity images from Hole 1166A, with lithologic descriptions, porosity, density, gamma-ray, and caliper and resistivity curves from downhole logging. APLC = accelerator porosity sonde near-array limestone porosity corrected (decimal fraction), and RHOM = corrected bulk density (g/m³).

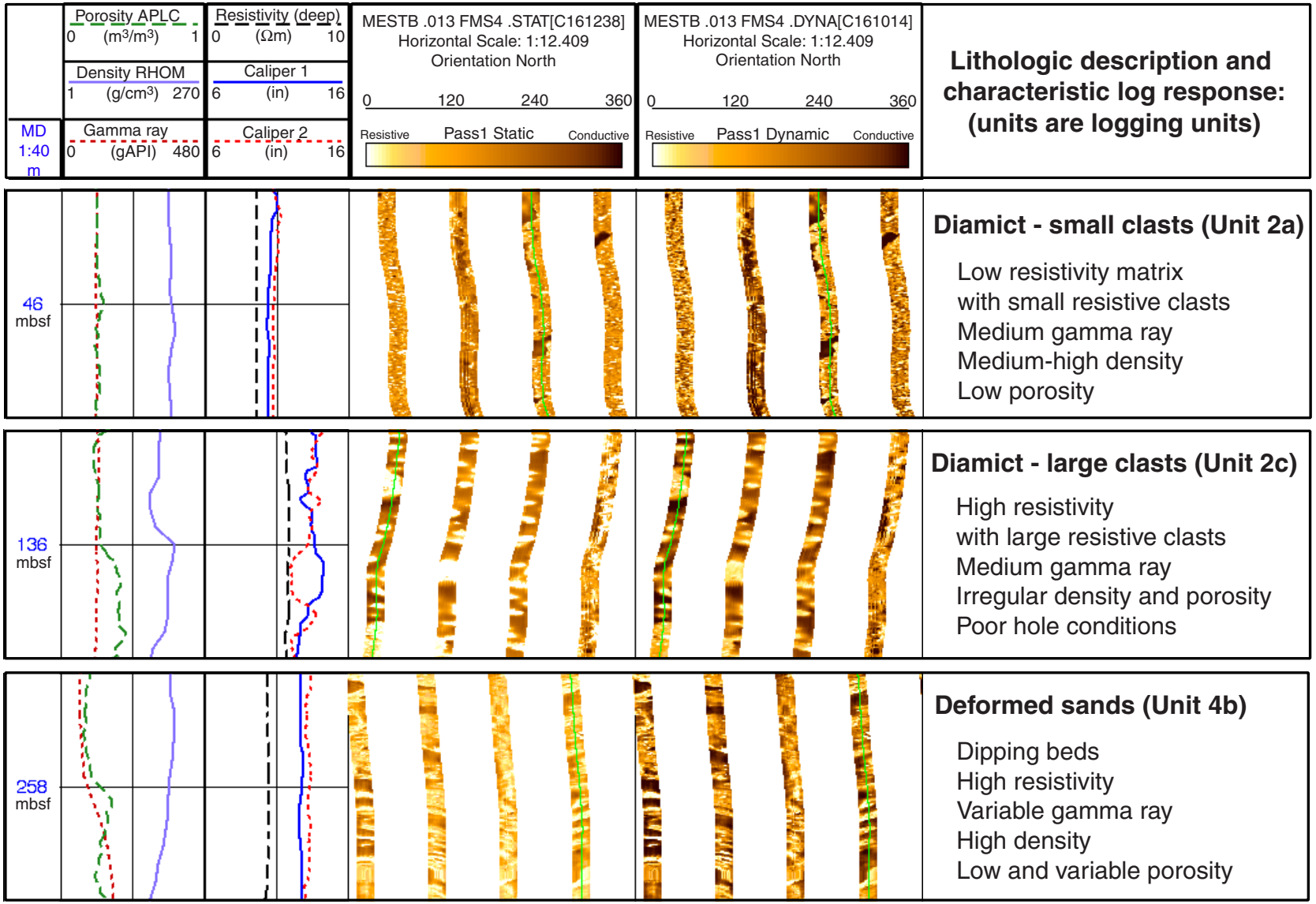

Figure F16. Conceptual diagrams for the setting of the Prydz Bay region from preglacial (scene 1) to the initiation of glaciation with marine transgressions (scenes 2, 3, and 4) to full glaciation with ice sheets on the overdeepened continental shelf (scene 5).

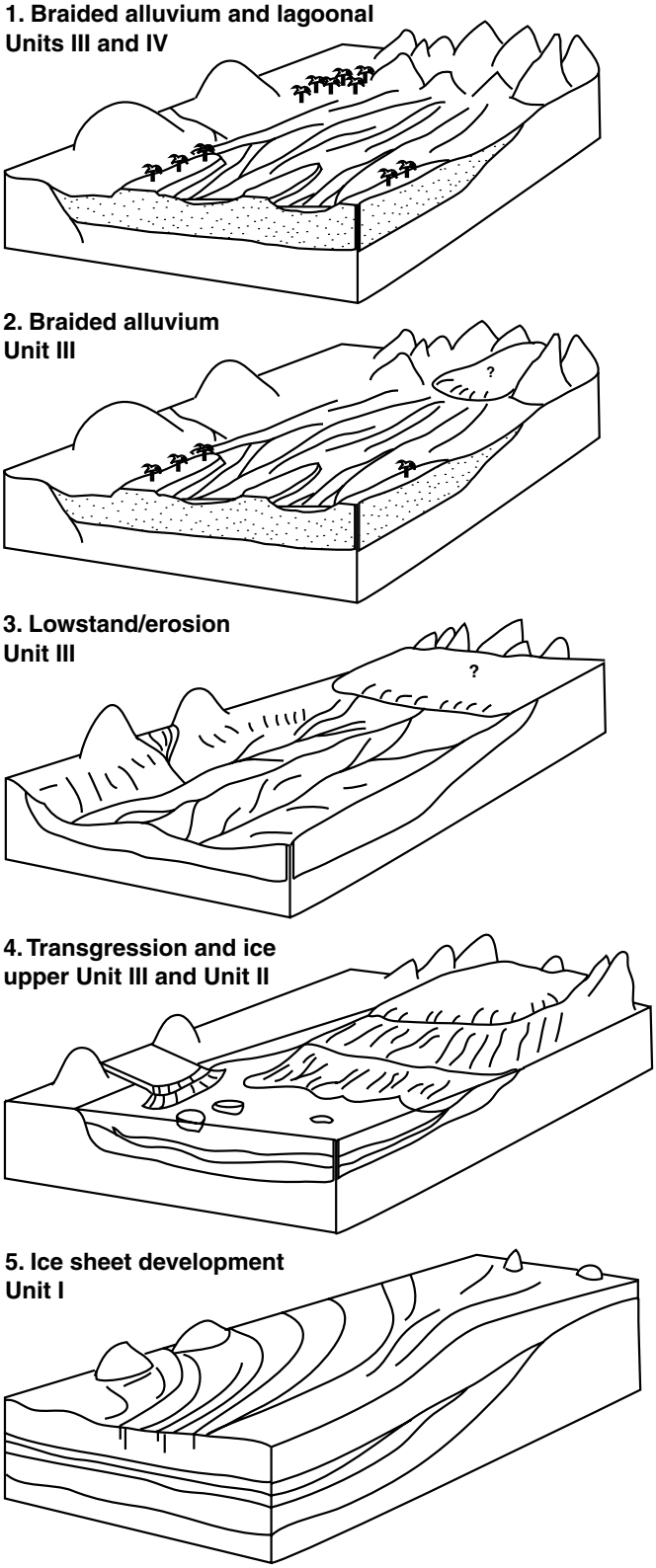

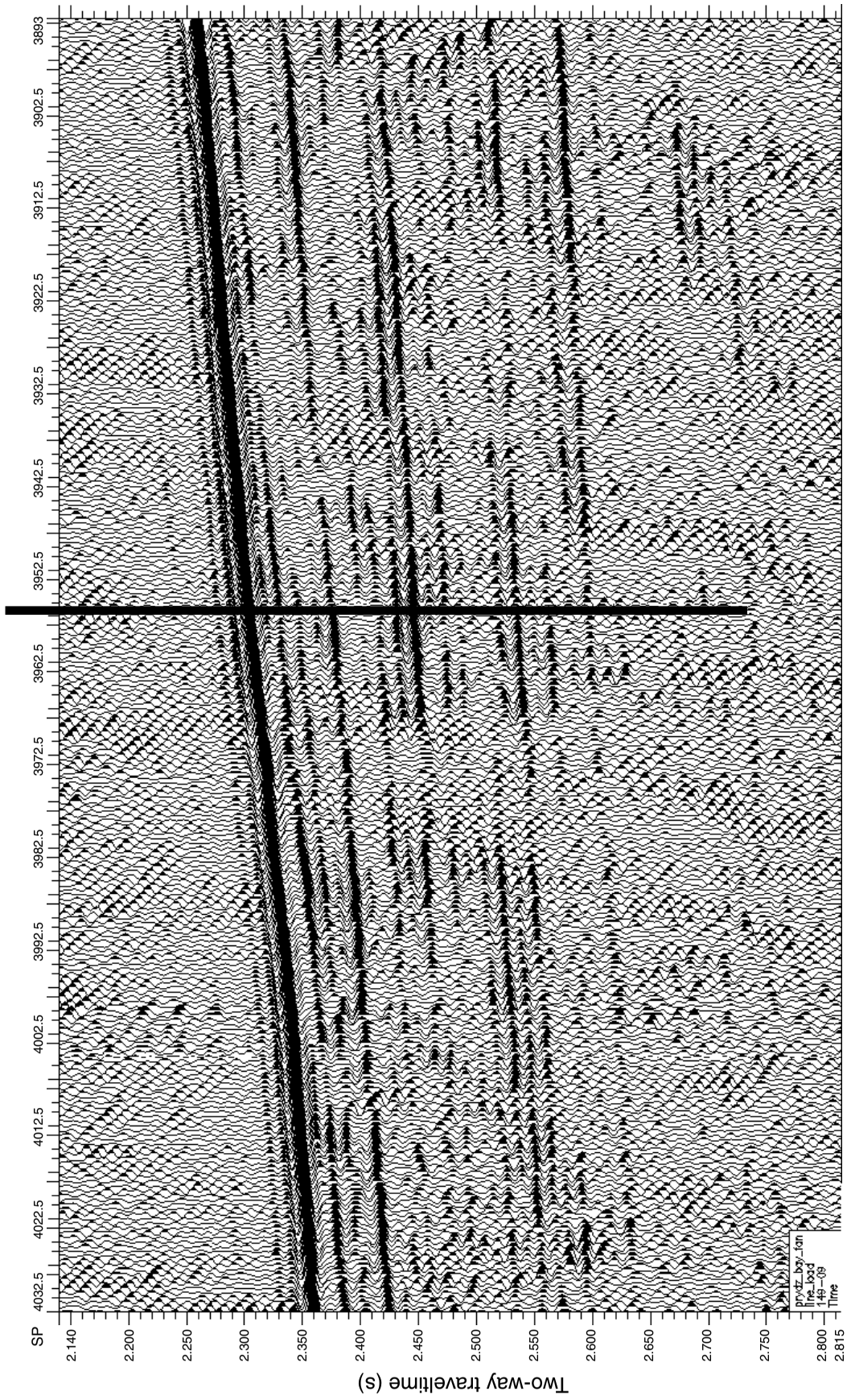

Figure F17. Seismic reflection profile AGSO 49/0901 over Site 1167. SP = shotpoint.

Figure F18. Site 1167 lithostratigraphic units, facies, and interpretation. In Recovery column, black = recovered and shaded areas = not recovered. See Figure F14, p. 43, for key to lithostratigraphic diagrams.

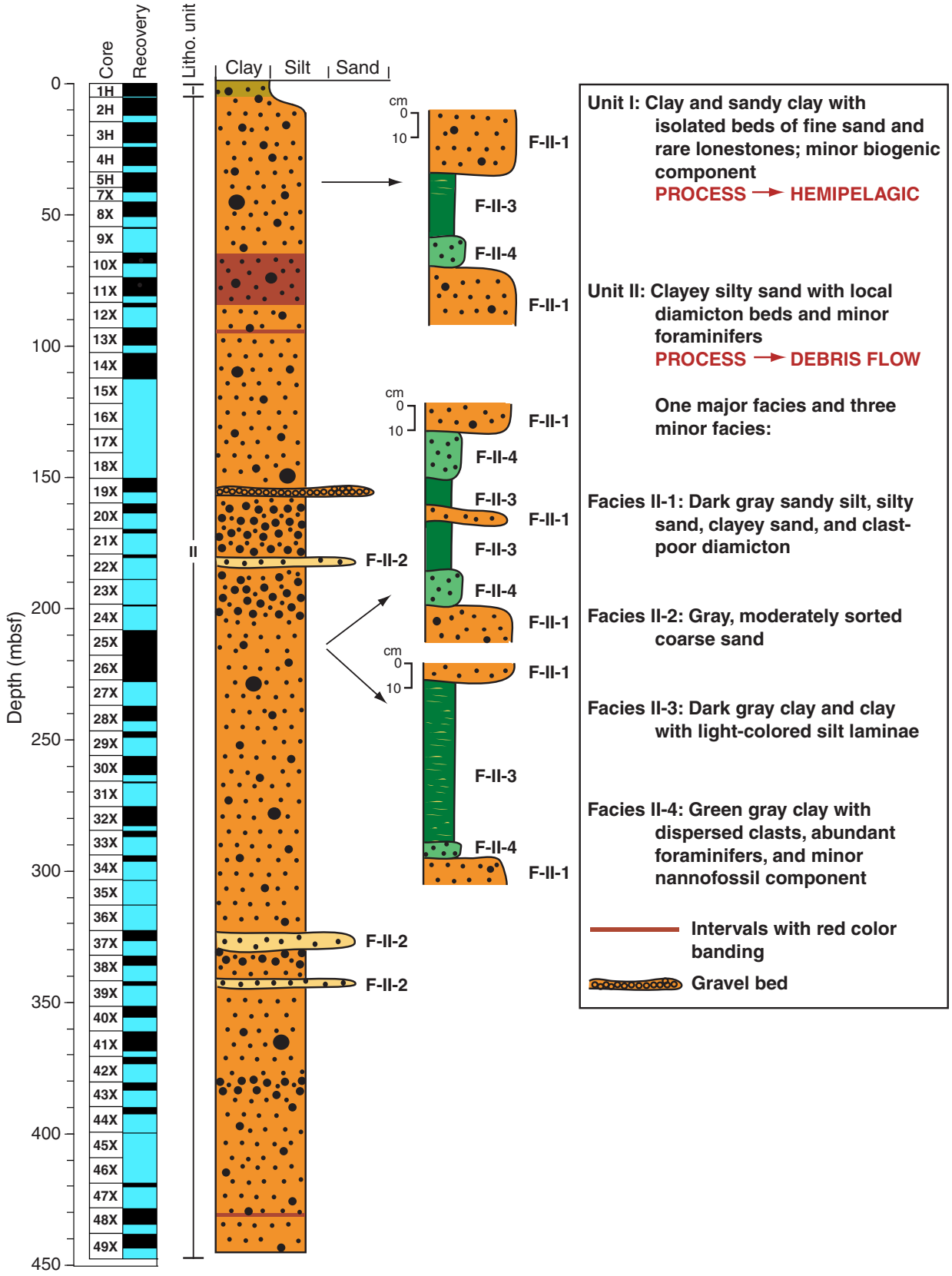

Figure F19. Distribution and frequency of sandstone vs. granite/igneous lonestones in Hole 1167A. A shift from largely sandstone clasts to granite clasts occurs uphole at ~200 mbsf.

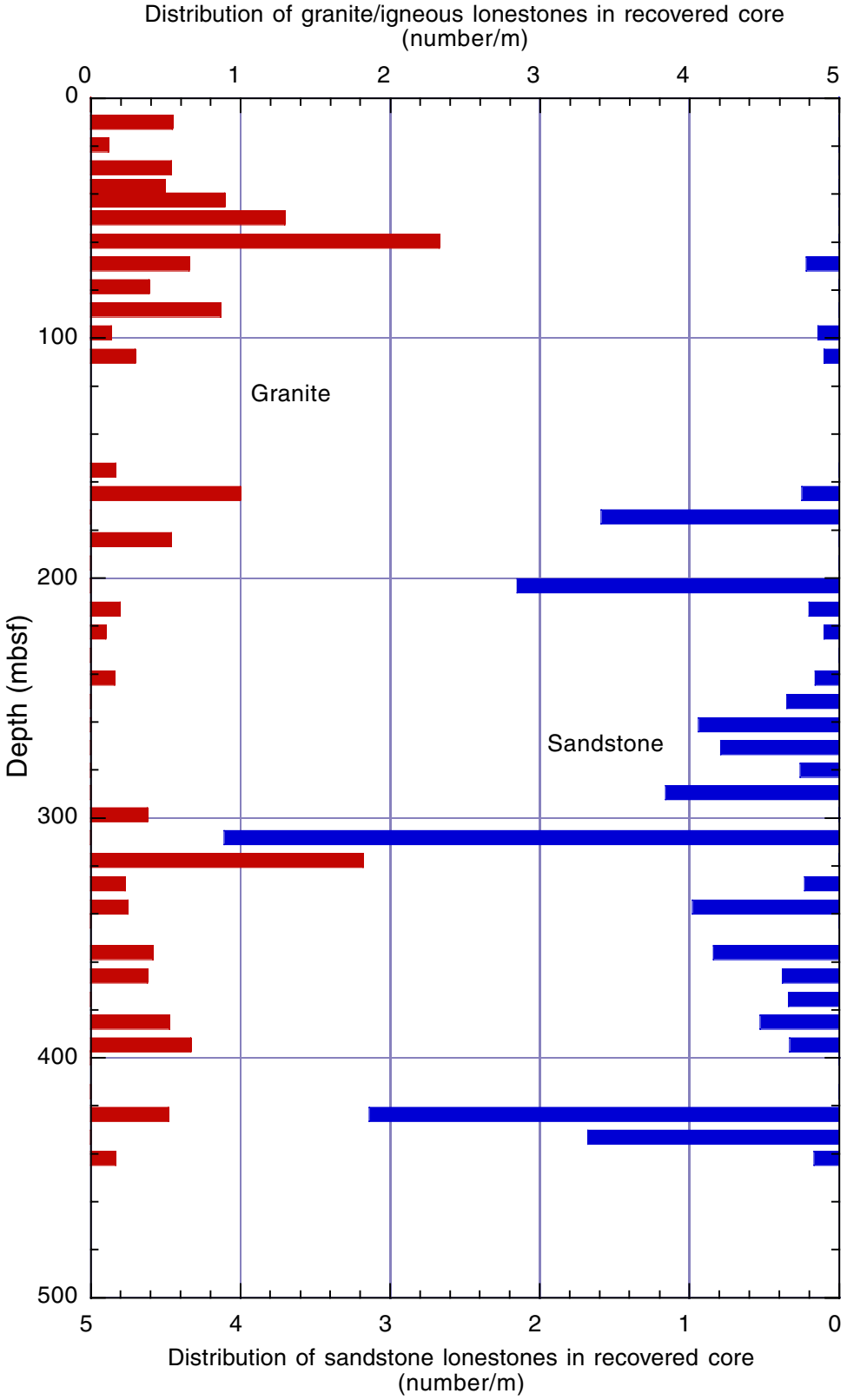

Figure F20. Plots showing magnetostratigraphy, magnetic susceptibility, and the ratio of anhysteretic and isothermal remanent magnetization (ARM/IRM) for Site 1167. The inclinations from split cores are compared with inclinations from stepwise-demagnetized discrete samples (solid squares). The horizontal lines and the labels on the magnetic susceptibility plot indicate intervals with different magnetic properties. (**Figure shown on next page.**)

Figure F20 (continued). (Caption shown on previous page.)

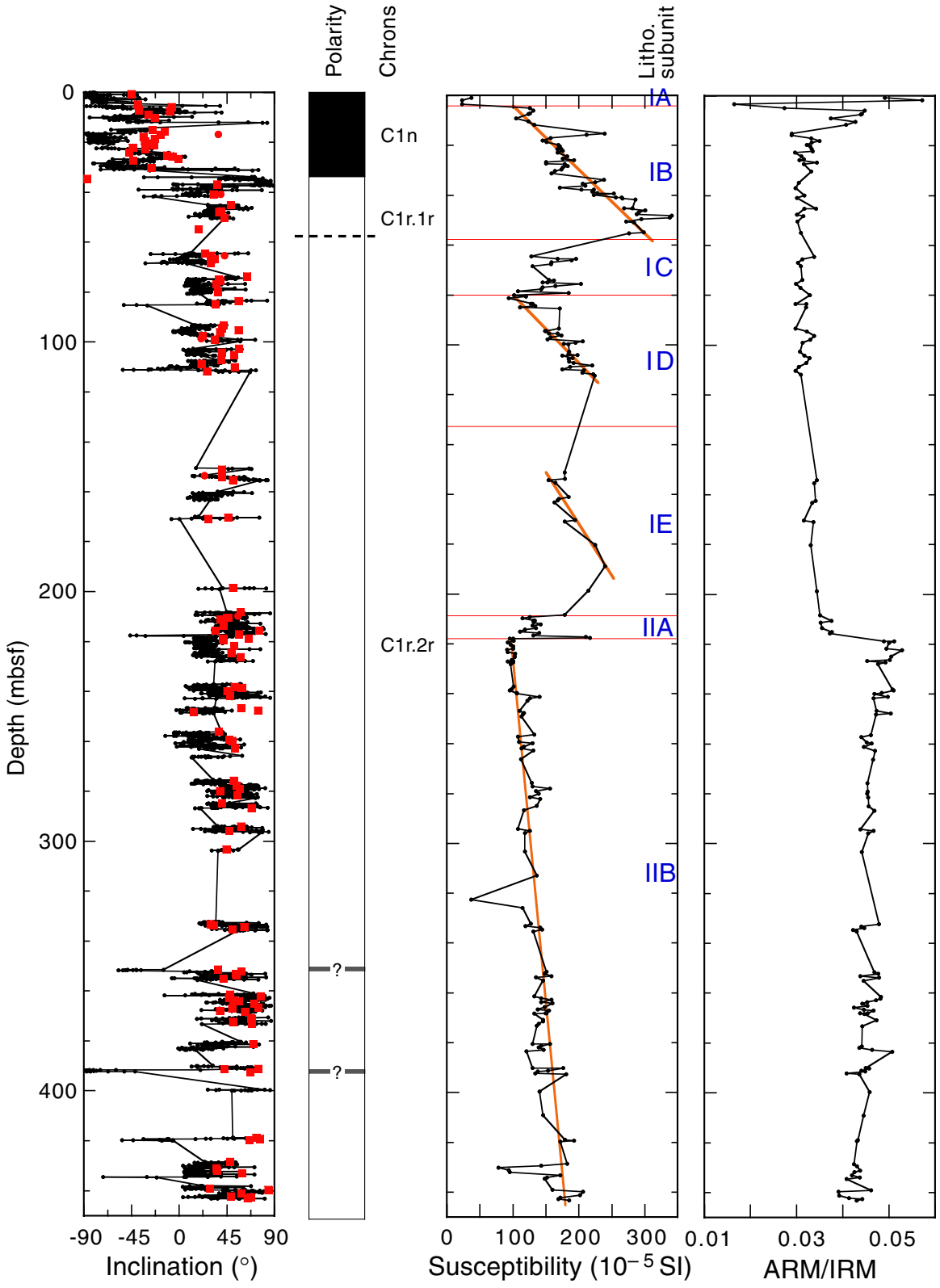

Figure F21. Plots of chloride and sulfate interstitial water values vs. depth at Site 1167.

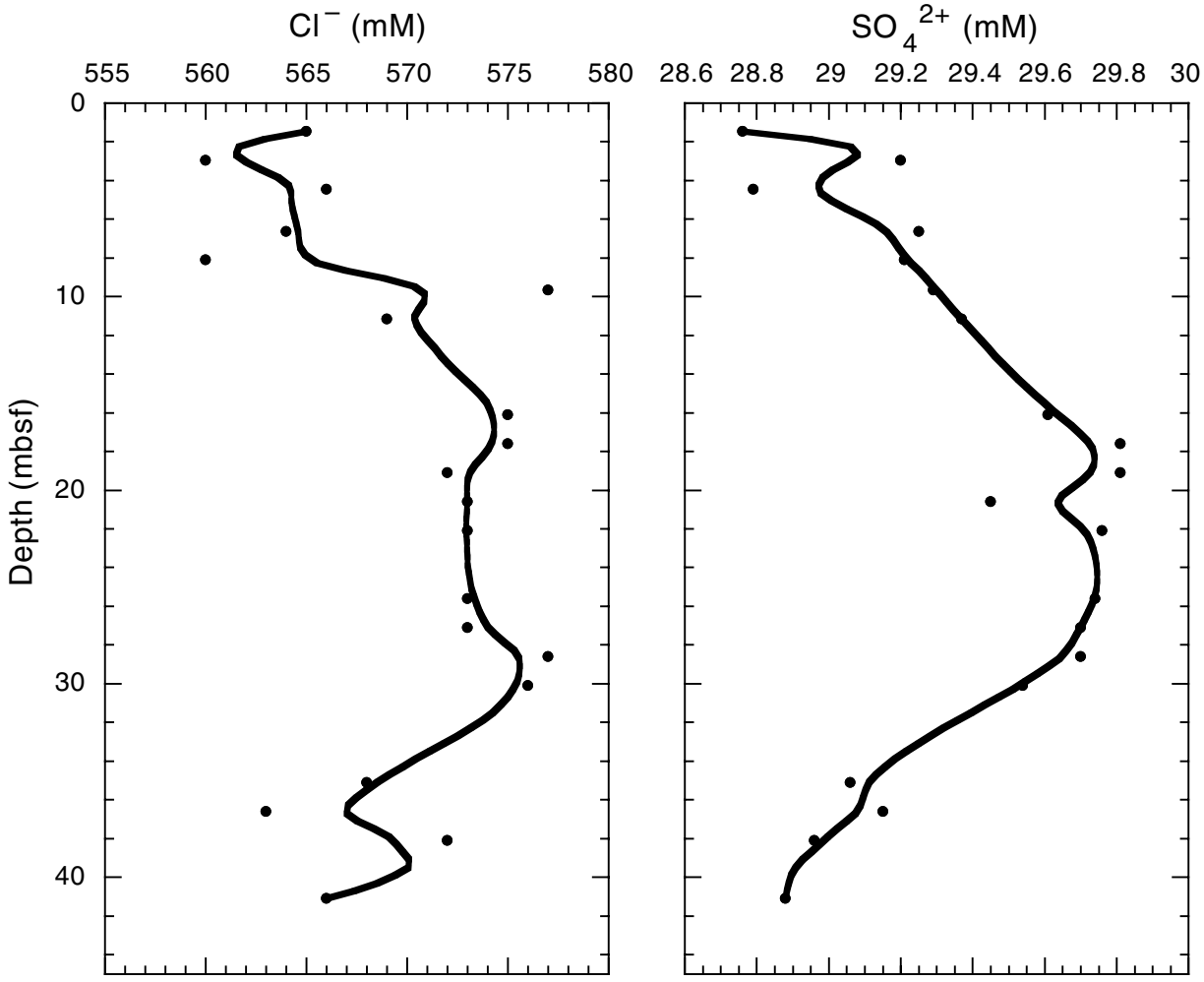

Figure F22. Seismic reflection profiles across Site 1165. **A.** Regional profile across the Wild Drift. The regional horizon PP12 can be traced beneath the continental slope and is the base of the Prydz Bay Trough Mouth Fan. (Continued on next page.)

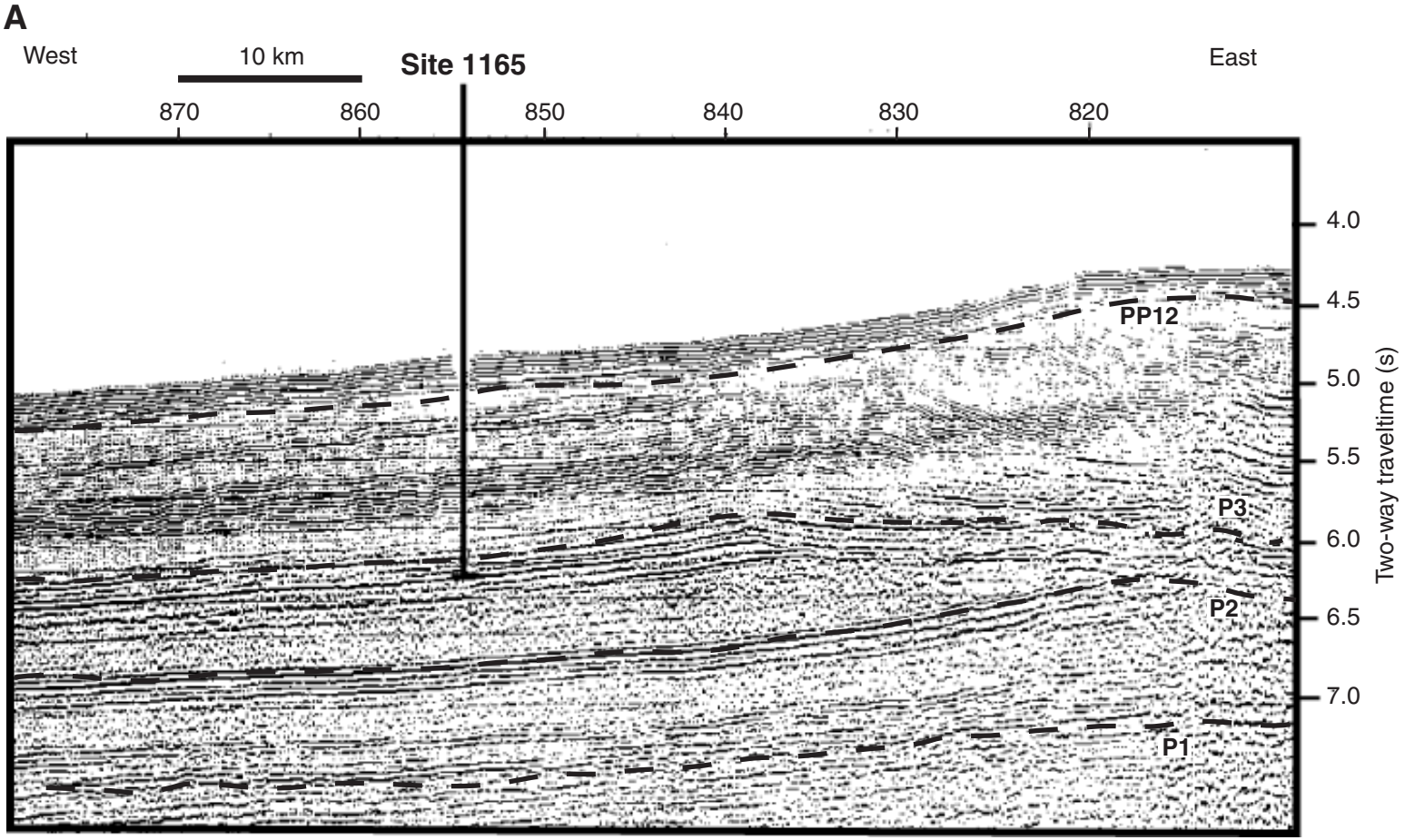

Figure F22 (continued). B. Profile recorded over the drill site by the *JOIDES Resolution*'s water gun seismic system upon approach to the site. Lithostratigraphic units and lithology are also shown.

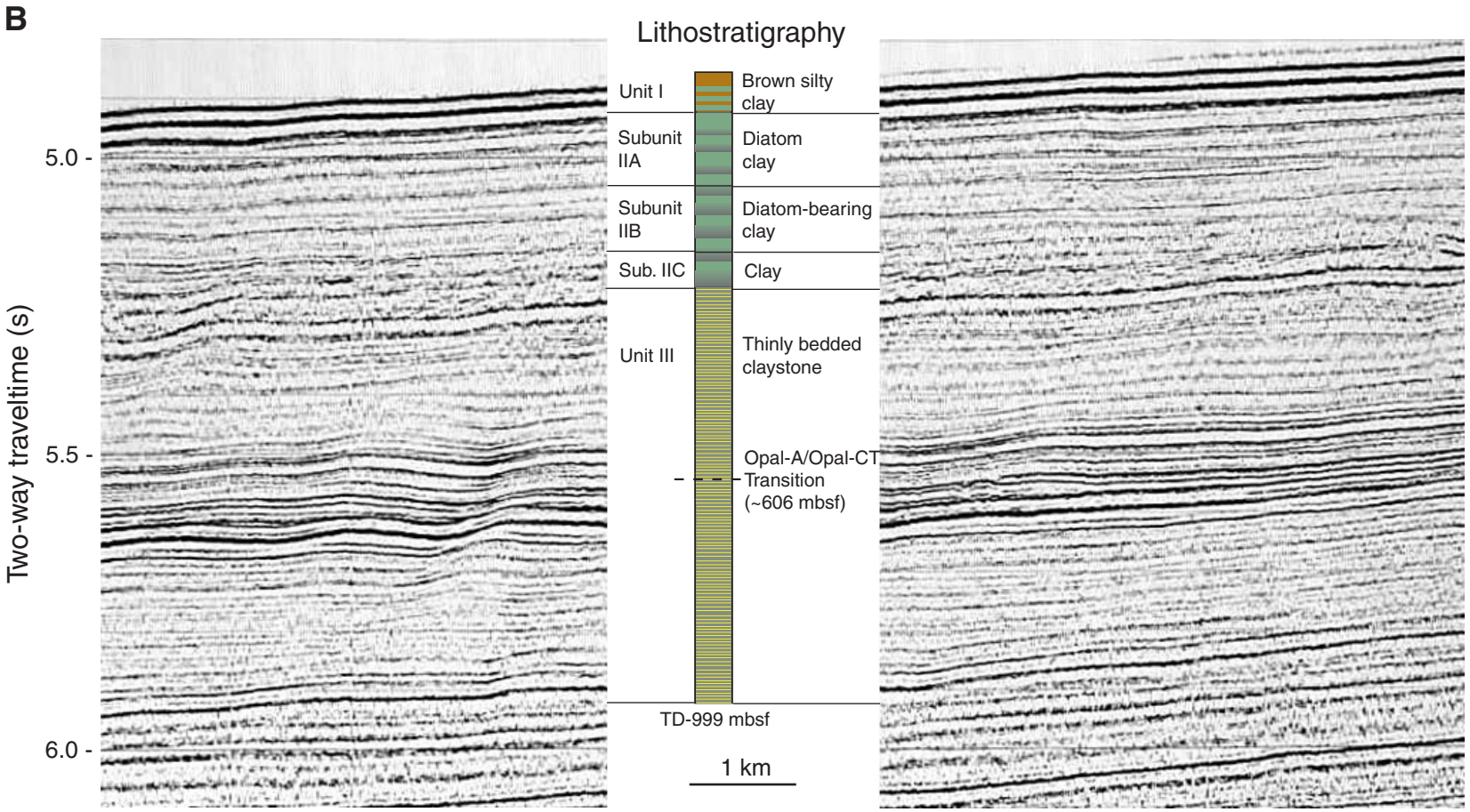

Figure F23. Composite stratigraphic section for Site 1165 showing core recovery, a simplified summary of lithology, lithostratigraphic unit boundaries, and age. Also shown are the distribution of lonestones and dispersed clasts, mineral abundances identified by XRD, the percentage of diatoms and sponge spicules from smear slides, and color reflectance. See Figure F12, p. 41, for lithology and mineral legends. The bar graph shows the distribution of isolated lonestones (>5 mm) downhole. The vertical bars on the right side of the column show the distribution of dispersed grains and granules (<5 mm). X-ray diffraction shows the percentage of most abundant minerals. This graph was plotted using the methods of Forsberg et al. (1999). In the smear-slide graph, solid line = diatoms and dashed line = sponge spicules. The thin line in the color reflectance plot shows the reflectance percent downhole. The thick line is a 200-point moving average. (**Figure shown on next two pages.**)

Figure F23 (continued). (Caption shown on previous page.)

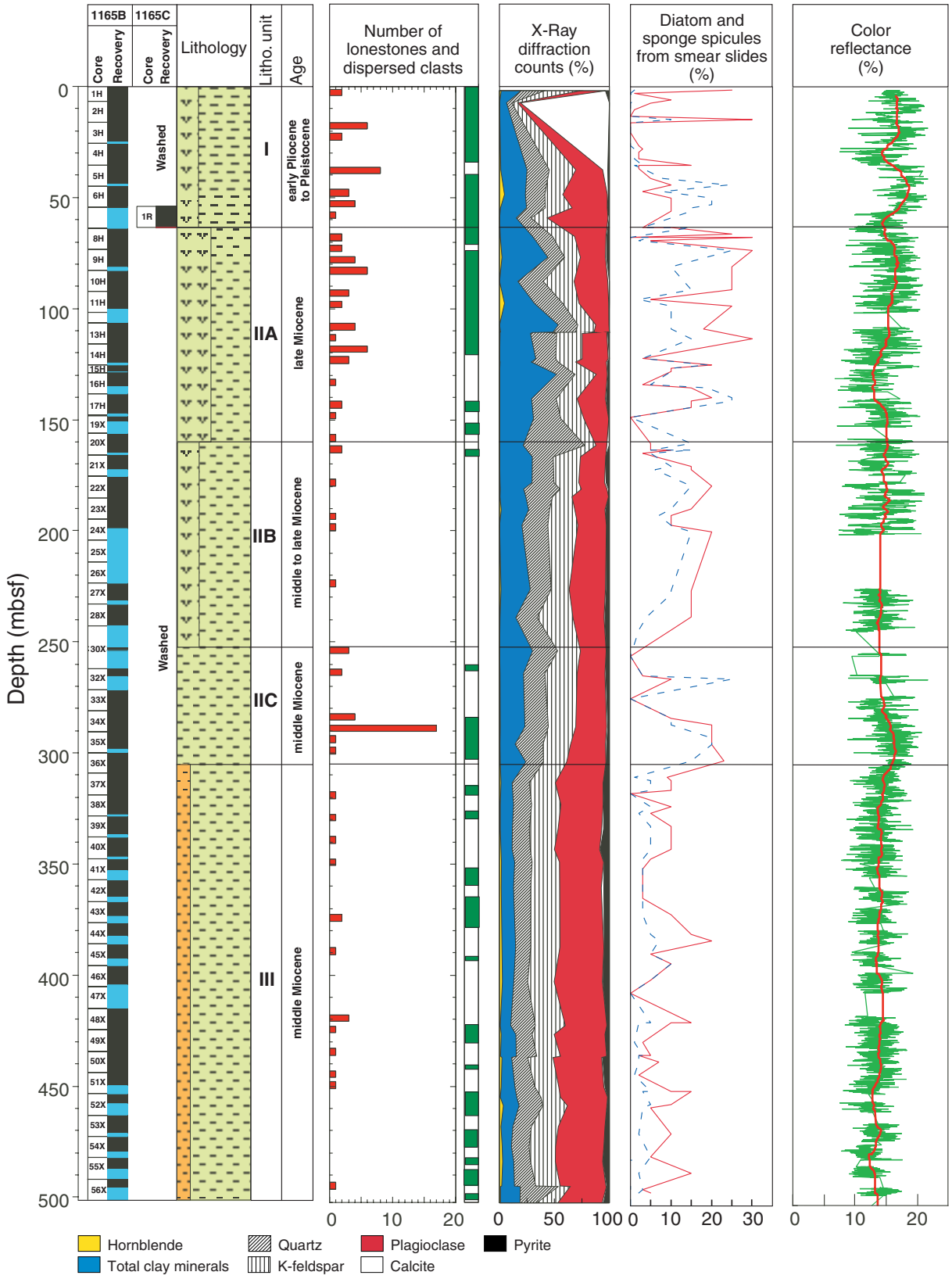

Figure F23 (continued).

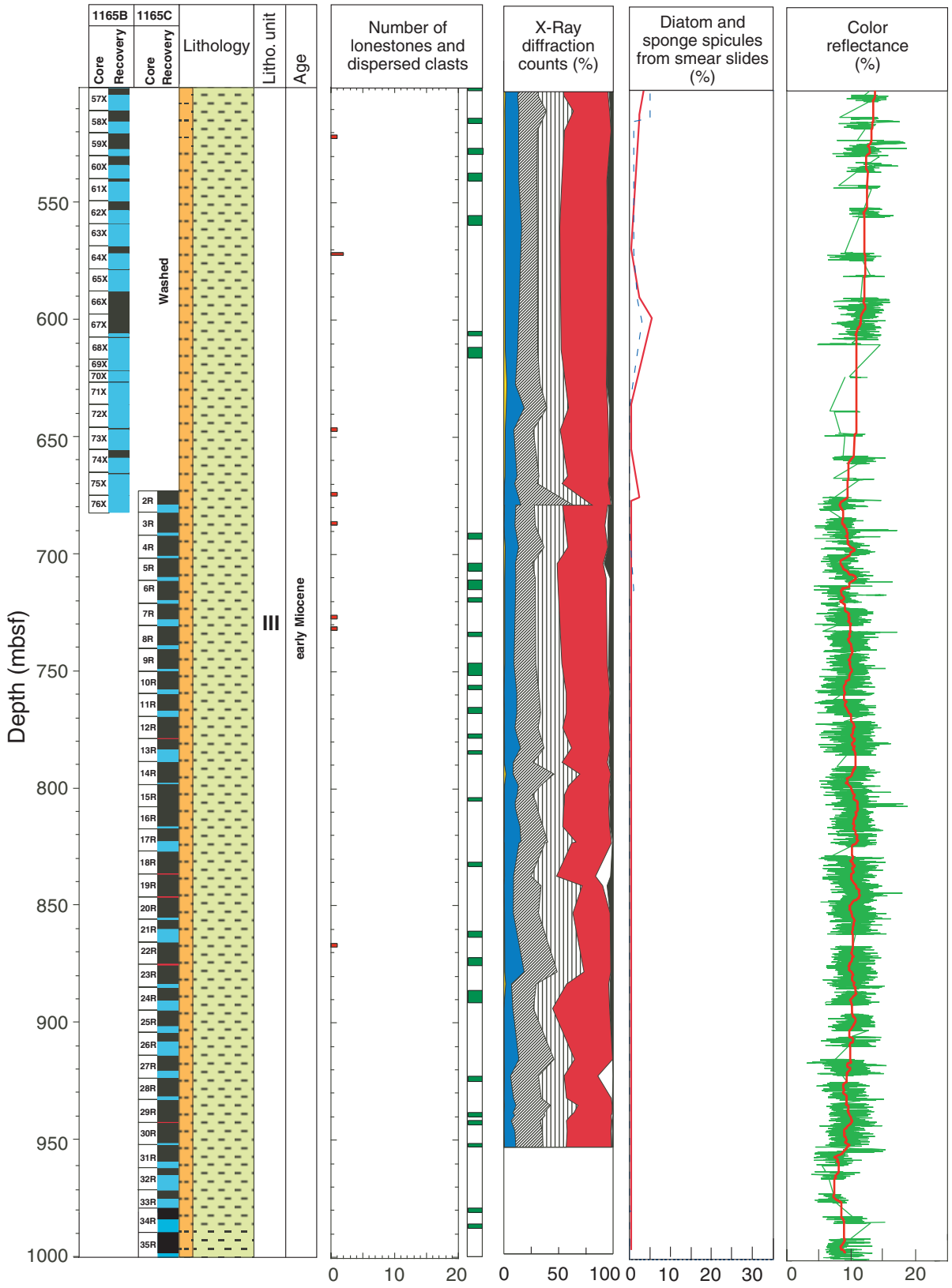

Figure F24. Magnetostratigraphy for Site 1165.

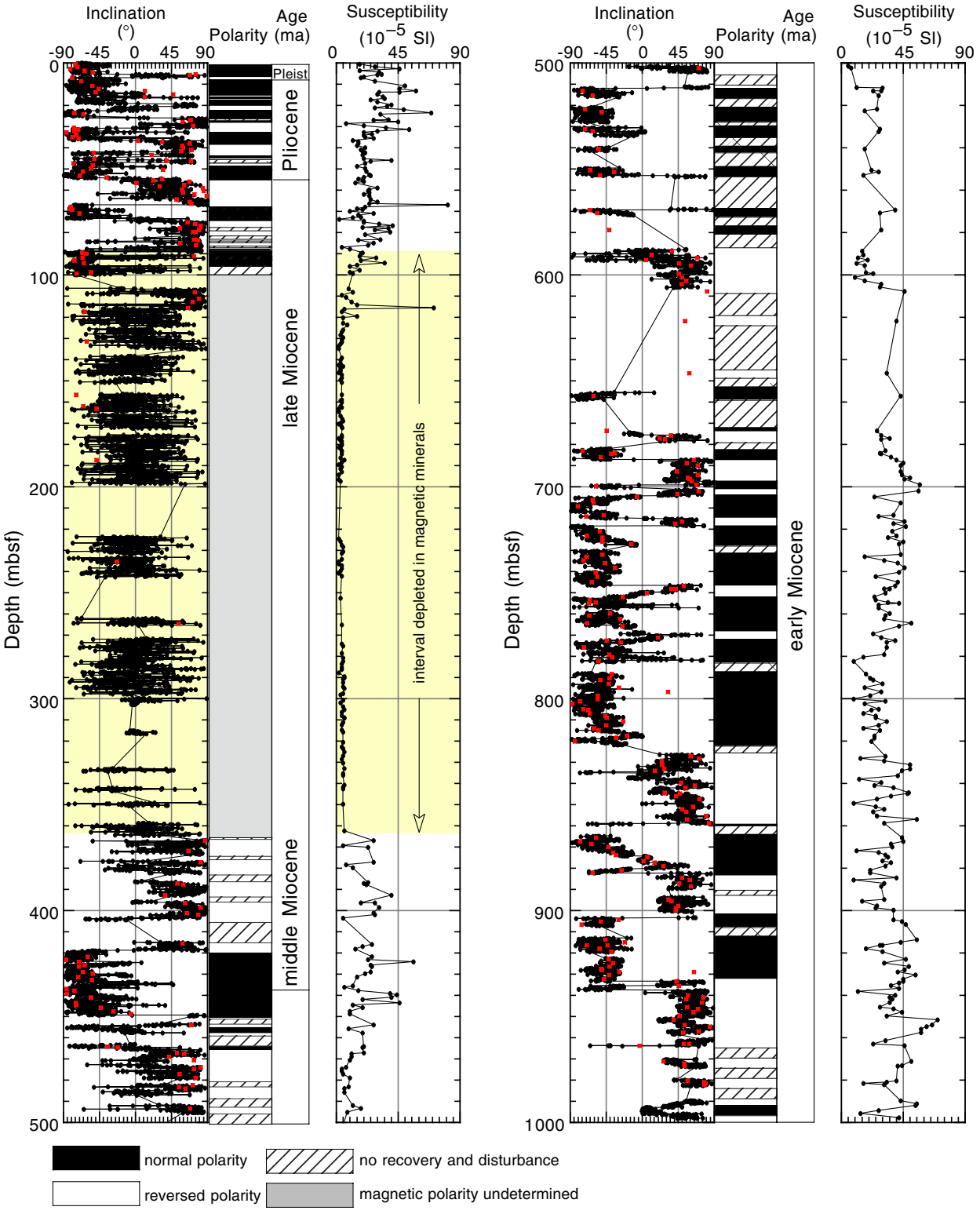

Figure F25. Age-depth plot for Site 1165 based on biostratigraphy and magnetostratigraphy. FO = first occurrence and LO = last occurrence.

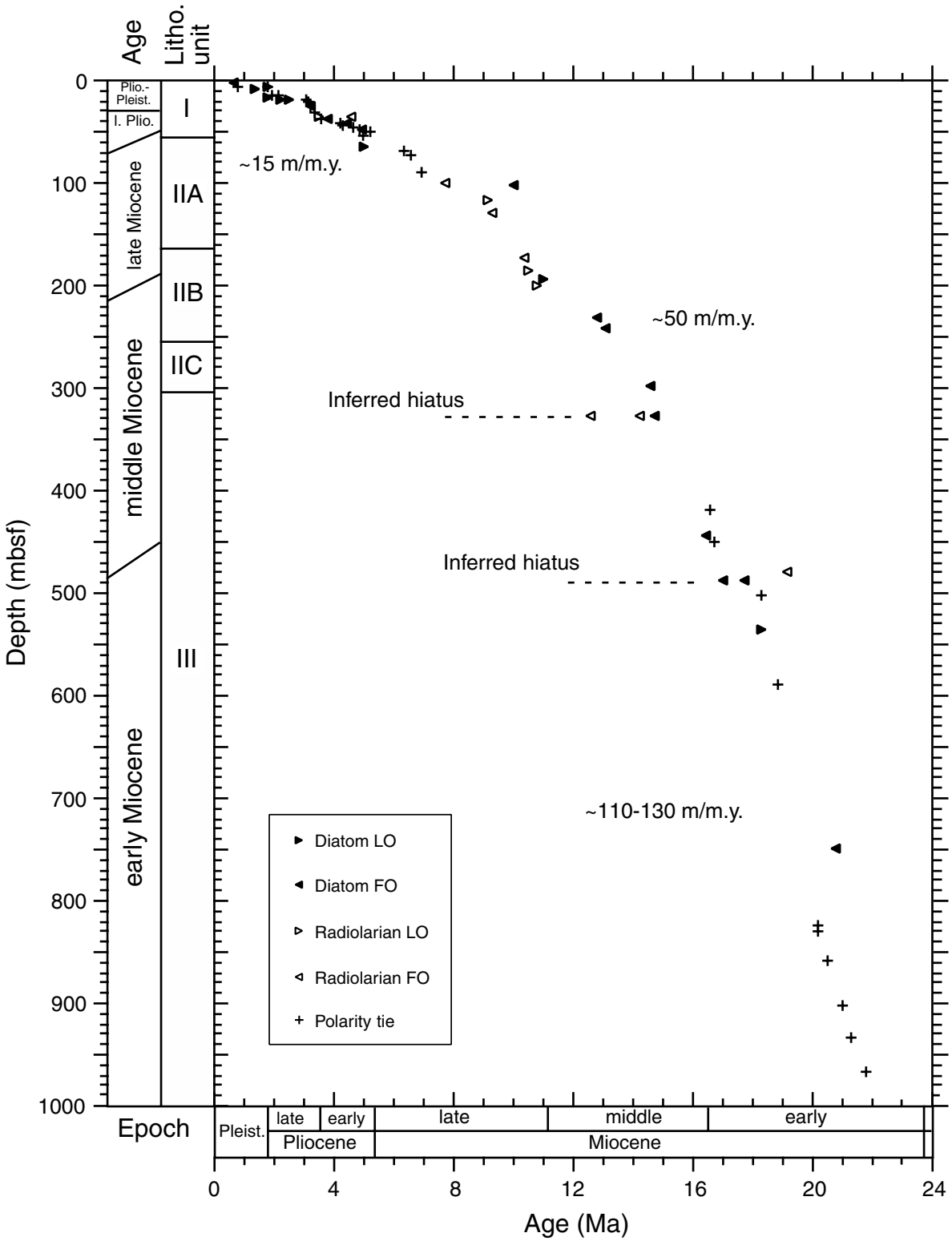

Figure F26. Organic gases and carbon in Holes 1165B (open symbols) and 1165C (solid symbols). **A.** Concentrations of methane (C_1), ethane (C_2), and propane (C_3) gases with depth. **B.** Percentage of organic carbon with depth.

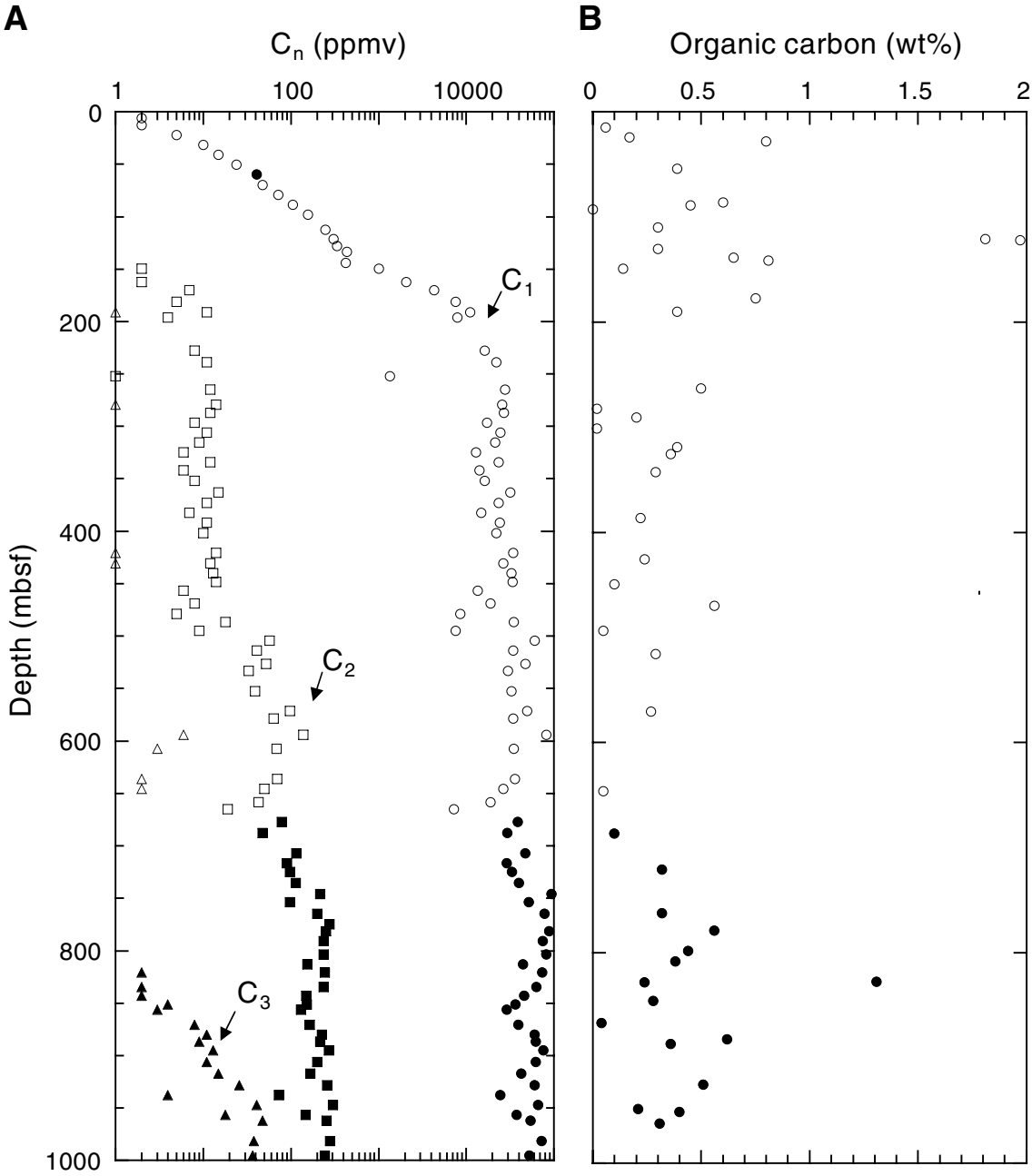

Figure F27. Example of the cyclicity (at Milankovitch periodicities; see "Site 1165," p. 19) observed in Site 1165 cores, with spectra of spectrophotometer-lightness and gamma-ray (GRA) bulk-density values. **A.** Three sections for Core 188-1165B-14H with core photo (left), model (center), and lightness curve. **B.** Lightness and bulk-density values, with maximum entropy spectra showing peaks (in depth) at periods of 4.27, 1.55, 0.95, and 0.72 m, equivalent to approximate time intervals of 93.7, 41.5, 20.8, and 18.2 k.y., respectively, at a sedimentation rate of 3.8 to 4.1 cm/k.y. CI = confidence interval. (**Figure shown on next page.**)

Figure F27 (continued). (Caption shown on previous page.)

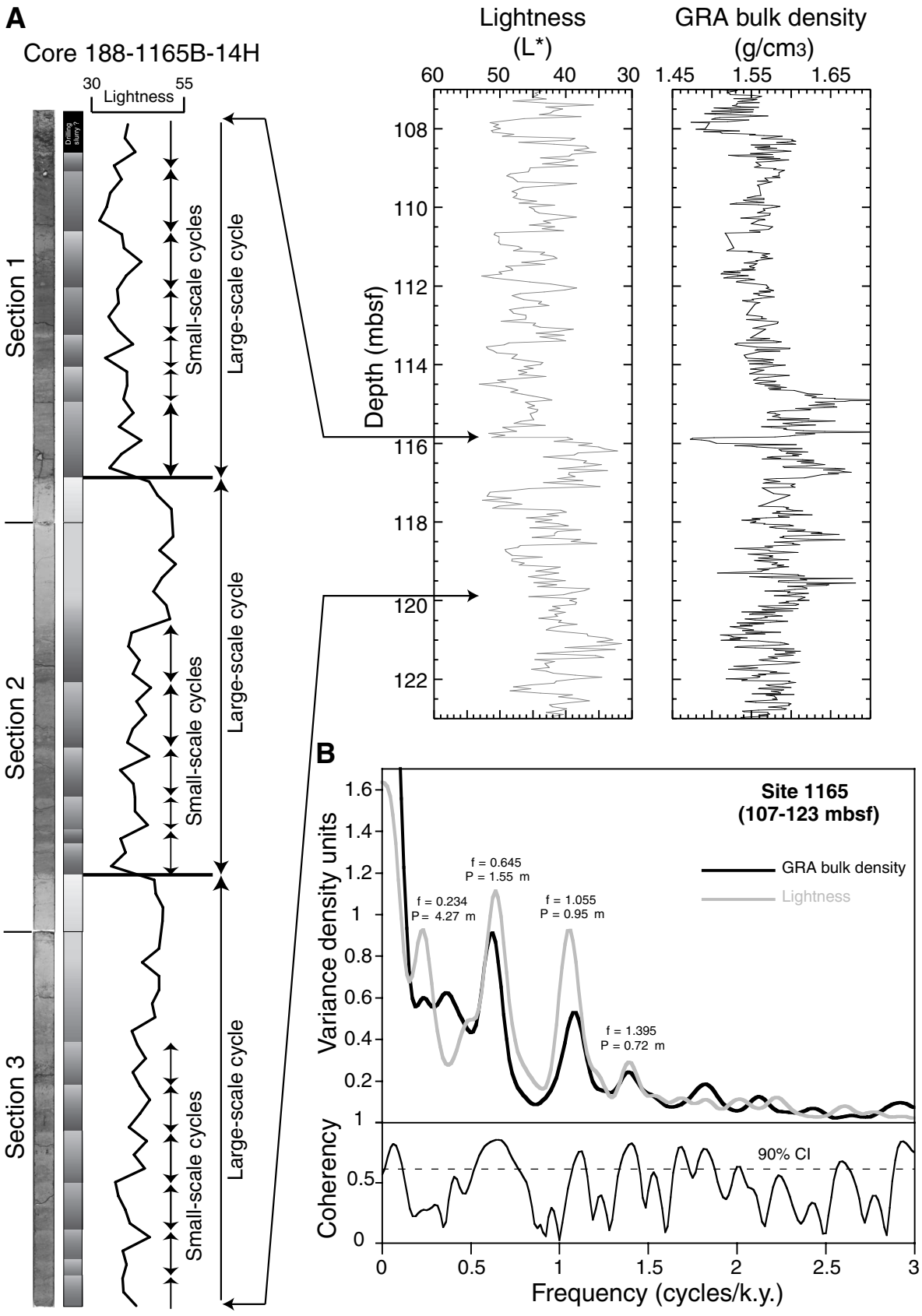

Figure F28. Conceptual diagrams showing the changes in glacial erosion and sedimentation on the Antarctic continental margin accompanying the change from temperate to cold polar conditions. 1. Glacial onset (middle–late Eocene). Small glaciers fed meltwater and detritus to shelf basins. Coastal plains were vegetated. 2. Small continental glaciers (Oligocene?–early Miocene) fed abundant meltwater and detritus from the central part of the continent to shelf basins and the continental rise. 3. Early advance onto the shelf (middle Miocene). Glaciers start to erode shelf basins, feeding recycled detritus to the continental slope and rise. 4. Shelf overdeepening (late Miocene–Pleistocene glacial episodes). The inner shelf is deeply eroded and detritus is delivered to the shelf, slope, and rise. The extent of the ice sheet determines the relative amounts of basement- and shelf basin–derived detritus provided to the slope and rise. 5. Interglacial episodes (late Miocene–Present). Ice is grounded far from the shelf edge. Slope and rise receive biogenic and hemipelagic sediments and IRD. (**Figure shown on next page.**)

Figure F28 (continued). (Caption shown on previous page.)

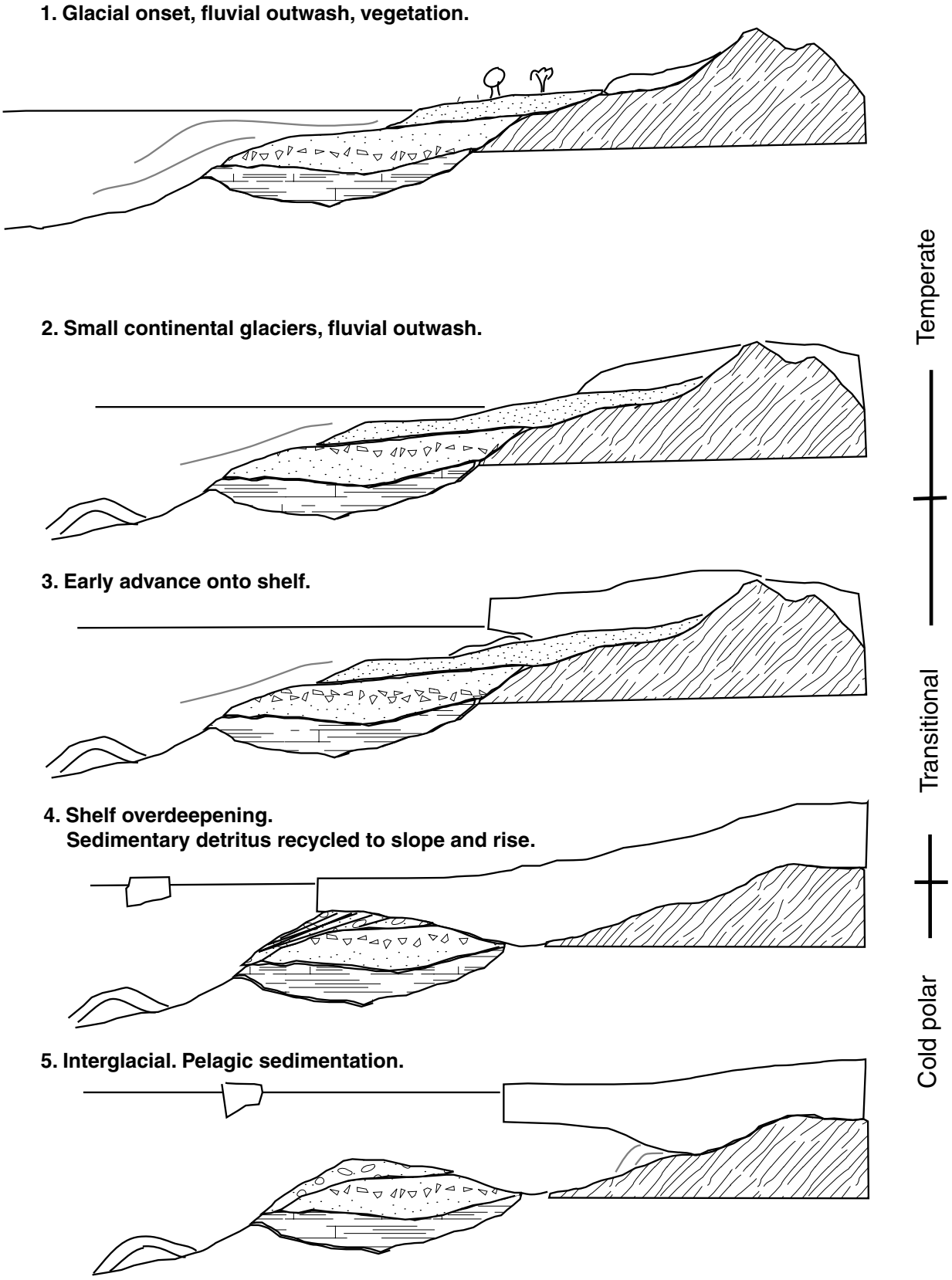

Table T1. Leg 188 site summary.

Hole	Latitude	Longitude	Water depth (m)	Number of cores	Interval cored (m)	Core recovered (m)	Recovered (%)	Drilled (m)	Maximum penetration (m)	Total drilled (m)	Time on hole (hr)
1165A	64°22.8´S	67°13.1´E	3537.0	1	5.4	5.43	100.6	0	5.4	5.4	14.25
1165B	64°22.8´S	67°13.1´E	3537.6	76	682.2	434.04	63.6	0	682.2	682.2	144.25
1165C	64°22.8´S	67°13.1´E	3537.5	35	335.7	269.27	80.2	663.4	999.1	999.1	255.00
Site 1165 summary	64°22.8´S	67°13.1´E	3537.4	112	1023.3	708.74	69.3	663.4	999.1	1686.7	413.50
1166A	67°41.8´S	74°47.2´E	475.4	40	381.3	71.25	18.7	0	381.3	381.3	134.50
1166B	67°41.8´S	74°47.3´E	475.4	0	0	0	0	42.5	42.5	42.5	21.50
Site 1166 summary	67°41.8´S	74°47.2´E	475.4	40	381.3	71.25	18.7	42.5	381.3	423.8	156.00
1167A	66°24.0´S	72°17.1´E	1639.9	49	447.5	191.33	42.8	0	447.5	447.5	130.42
1167B	66°24.0´S	72°17.0´E	1639.9	0	0	0	0	261.8	261.8	261.8	33.08
Site 1167 summary	66°24.0´S	72°17.0´E	1639.9	49	447.5	191.33	42.8	261.8	447.5	709.3	163.50
Totals:	65°54.3´S	70°49.7´E	2120.4	201	1852.1	971.32	52.4	967.7	999.1	2819.8	733.00